Damage Mechanics Modeling Using Eshelby Inclusions

A Thesis
Submitted to the
Faculty of Engineering Shoubra, Benha University
In Partial Fulfillment of the Requirements for the
Degree of Doctor of Philosophy
in
Engineering Mathematics

by

Mohamed Ahmed Kamal Abd-EL-Khalik Ahmed Soliman

Teaching assistant in Engineering Mathematics and Physics Department
Faculty of Engineering at Shoubra, Benha University

Faculty of Engineering-Shoubra
Benha University
2021

Damage Mechanics Modeling Using Eshelby Inclusions

by

Mohamed Ahmed Kamal Abd-EL-Khalik Ahmed Soliman

Teaching assistant in Engineering Mathematics and Physics Department
Faculty of Engineering at Shoubra, Benha University

A thesis submitted in partial fulfillment of the requirements for the degree of
Doctor of Philosophy in Engineering Mathematics

Under supervision of

Prof. Dr. Abd-Elrahman Ali Saad
(may God bless his soul)
Professor of Engineering Mathematics
Eng. Mathematics and Physics Dept.
Faculty of Engineering – Shoubra
Benha University

Prof. Dr. Youssef Fawzy Rashed
Professor of Structural Analysis and Mechanics
Structural Eng. Department
Faculty of Engineering
Cairo University

Dr. Taha Hussien Abd-Allah Abu Al-Naga
Lecturer in Eng. Mathematics and Physics Dept.
Faculty of Engineering – Shoubra
Benha University

Dr. Ahmed Fady Mahmoud Farid
Lecturer in Structural Eng. Department
Faculty of Engineering
Cairo University

Faculty of Engineering-Shoubra
Benha University
2021

APPROVAL COMMITTEE

The Committee on Final Examination recommends that the thesis by

Mohamed Ahmed Kamal Abd-El-Khalik Ahmed Soliman

entitled

Damage Mechanics Modeling Using Eshelby Inclusions

be accepted in partial fulfillment of the requirements for the degree of
Doctor of Philosophy in Engineering Mathematics

EXAMINERS COMMITTEE:

Prof. Dr. Mohamed Saad Matbuly ……

Professor of Engineering Mathematics — External Examiner
Eng. Mathematics and Physics Departement
Vice Dean of the Post graduate affairs
Faculty of Engineering
Zagazig University

Prof. Dr. Mostafa Ahmed Moawad Abdeen ……...

Professor of Engineering Mechanics — External Examiner
Head of Departement of Eng. Mathematics and Physics
Faculty of Engineering
Cairo University

Prof. Dr. Youssef Fawzy Rashed ……

Professor of Structural Analysis and Mechanics — Supervisor
Structural Eng. Department
Faculty of Engineering
Cairo University

Date: ……

DEDICATION

To my father,

my mother,

my brother,

and my little nephew Youssef.

ACKNOWLEDGEMENT

First of all, due thanks go to **God** the most merciful and most graceful, who without his guidance and inspiration nothing could have been accomplished.

I would like also to thank my professors in my college for the advices and support. I would like to express my gratitude to everyone who contributed, in different ways, to completion of this work. Inevitably some names will be missing here.

I wish to express my great appreciation and thanks to **Prof. Dr. Abd-Elrahman Saad (may God bless his soul)**, Professor of Engineering Mechanics, Engineering Mathematics and Physics Departement, Faculty of Engineering Shoubra, Benha University, for his kind guidance, valuable advice, sincere fatherhood, and continuous caring during this research.

I also wish to express my deep indebtedness to **Prof. Dr. Youssef Fawzy Rashed,** Professor of Structural Analysis and Mechanics, Structural Engineering Department, Faculty of Engineering, Cairo University, for his generous guidance and encouraging, sincere help, valuable suggestions, and precise advice through all stages of this research work.

Sincere thanks go to my friends **Dr. Taha Hussien**, Lecturer in Engineering Mathematics and Physics Departement , Faculty of Engineering - Shoubra, Benha University, and **Dr. Ahmed Fady** Lecturer in Structural Engineering Departement, Faculty of Engineering, Cairo University for their guidance and advice in my research.

Also, I would like to thank all my colleagues in the research group **CUFEBE** (Cairo university- Faculty of Engineering – Boundary elements) for their support and assistant.

Abstract

This Thesis consists of three parts:

In the first part of the thesis, the idea of the Eshelby equivalent inclusion theory is coupled with the Fictitious stress method (FSM) as a meshless technique to model inhomogeneity problems. The FSM is regarded herein as an indirect boundary element formulation. The problem is divided into complementary and particular parts. The particular solution is obtained using Eshelby theory. Hence the complementary solution could be obtained using the FSM. Analytical solutions are used to model circular inclusions. In this approach there is no meshing on the boundary or inside the domain. The problem is solved by distributing points on the boundary and inserting points at the center of the inhomogeneities. Although the fictitious stresses on the boundary is assumed constant and also the eigenstrain inside the inclusion is assumed uniform the results are in good agreement with the direct boundary integral equation method and the finite element method as will be shown in chapter 3.

In the second part of the thesis, a new simulation of damage in the direct boundary element formulation is presented. The Eshelby equivalent inclusion theory is coupled with the direct boundary integral equation to model the change in the elastic properties due to damage. A finite element-like stiffness matrix is formed for the damaged domain, where the problem stiffness matrix is obtained directly on the boundary (in condensed form). The developed method is a boundary-only method although the domain contains damaged parts. A system of nonlinear equation is then solved using a load control approach (secant method). Both local and non-local damage models are considered. Several examples are presented to demonstrate the validity and the accuracy of the proposed formulation as will be shown in chapter 4.

In the third part, the application of the damage modelling within the finite element method is reviewed. Hence the basic theory of the variational boundary integral equations (VBIE) is discussed, where a finite element-like

stiffness matrix obtained using VBIE is used to model the damage. The VBIE gives the ability to use large dimensions compared to the conventional finite element. Although using coarse mesh the results as will be shown in chapter 5 are in good agreement with the conventional finite element.

Table of Contents

LIST OF FIGURES

LIST OF SYMBOLS AND ABREVIATIONS

σ_{ij}, ε_{kl} , C_{ijkl}	Stress, Strain and elasticity tensor
E, G, ν	Young`s modulus, shear modulus, Poisson`s ratio
x, ξ	Field point and source point position vector
r	Position vector
R	Characteristic length
U_{ij}^{*}, T_{ij}^{*}, σ_{ijk}^{*}	The fundamental solution for displacement, traction, and stress
ε_{jk}^{o} , σ_{jk}^{o}	Eigenstrain and eigenstress
D	Scalar Damage variable
FEM	Finite element method
BEM	Boundary element method
BIE	Boundary integral equation
FSM	Fictitious stress method
VBIE	Variational boundary integral equation

Chapter 1: Introduction

1.1 Problem statement and background

Inhomogeneity problems have important applications in engineering. For example, modelling composite materials, damage, cracks and dislocations could be considered as inhomogeneities [63].

The inhomogeneity problem has been modelled using the direct boundary integral equation method (DBIEM) in several researches [19-21,61], but no research has been reported to use meshless methods for such a problem.

Meshless methods are very attractive as they get rid of the meshing problem (recall Belytschko *et al.* [4]). The method of fundamental solution (MFS) [10] is regarded, in the literature, as the only meshless method based on the indirect boundary element method. Alternatively, the fictitious stress method (FSM) [8,9,12,60], the displacement discontinuity method (DDM) [8], the non-singular method of fundamental solution (NMFS) [28,32,33,36] and the boundary node method (BNM) [30,41,62] could be also regarded as meshless methods as only points are presented to describe the problem boundary. All relevant integrals are performed analytically; i.e. no numerical integration is employed. In the MFS sources are placed outside the boundary of the problem on a fictitious boundary (to avoid singularities), where the solution is formed as the superposition of several states employing relevant fundamental solutions. Its main problem is the location of the fictitious boundary which makes the solution not unique [10]. In the NMFS the sources are distributed over circular disks whose centers are on the boundary. Employing this trick the singularity problem is avoided and in the same time the method still gains the advantage of being a meshless method. Despite they were developed prior to the NMFS, the FSM and the DDM, in that sense, also could be regarded as meshless techniques as they integrate the relevant fundamental solutions over

lines (instead of disks in the NMFS) which also could be located on the problem boundary. Therefore, such methods are even more powerful compared to the NMFS, as the later accuracy is still dependent on the size of the chosen disk. It has to be noted that the advantage of FSM, DDM and NMFS over BNM (which also uses analytical integration) is that there is no interchange between influence matrices columns in case of different prescribed boundary conditions.

Carpinteri *et.al* [8] used the FSM and DDM to model microcracks propagation in brittle materials subjected to compression. Also, Carpenteri and Yang [9] used the FSM to study microcracks propagation and intersection by superposition, where the FSM was first used to calculate the internal stresses in absence of microcracks then their effects were added. Liu and Sarler [33] used NMFS to study bi-material problems where they discretized the interface and solved the problem.

The study of damage mechanics is important in engineering as it predicts the structure's failure load, so it can be used in repair problems to interpret the origin of the occurred damage. The continuum damage mechanics is the approach to study the degradation of the medium properties due to damage. There are two approaches to deal with damage the first is from the phenomenological point of view where the damage is described by changing of the material properties according to Kachanouv [43], the second is from the micromechanical point of view. Here the first approach is used.

When dealing with quasi-brittle materials due to strain softening the problem becomes ill-conditioned and mesh dependent [1,2,25,26,49]. So, a localization limiter is needed to overcome this problem [26]. One of the localization limiters is the nonlocal damage theory. Where a chosen variable is replaced by its weighted average in a relevant nonlocal integral type [2,25,26,49] or incorporating higher order gradients in the constitutive model in the nonlocal differential type [44].

Simulating damage using the finite element method (FEM) [25,26,13] is carried out in an explicit procedure, where in each damaged element, a

damaged material property is directly assigned. As in FEM, Zihua Zhang et al. [64] modeled the nonlocal damage using the scaled boundary finite element method (SBFEM). The problem domain is discretized into cells where each cell is assigned with different material properties according to the damage level. This formulation suffers the same disadvantage as that of the FEM in terms of the need to discretize the whole domain, which loses the advantage of the SBFEM.

Silva and Castro [52-56] have simulated the damage using non-conventional finite elements, hybrid mixed [52,53,56] and the hybrid Trefftz [54]. In the hybrid mixed the stress and the displacement are approximated inside the domain using Legendre polynomial and on the boundary the displacement is approximated using the usual shape function. In the hybrid Trefftz the displacement only is approximated inside the domain using Trefftz function and on the boundary the displacement is approximated using the usual shape functions.

In the boundary element method (BEM) [7], where the discretization is carried only on the boundary, the change in material properties due to domain damage was modeled by one of three approaches. The first approach is to apply initial strain or initial stress to the homogeneous problem. The second approach is to discretize the domain with subregions and change the overall property of each subregion according to the damage level. The third approach is to couple the BEM with the FEM to use the advantage of the FEM in explicitly modeling damage.

The first approach was considered in the work of Rajgelj *et al*. [51] and Herding and Kuhn [22], where local damage is modeled by discretizing the domain into cells. It has to be noted that [51] considered quasi-brittle materials and [22] elastoplastic materials. Both [51] and [22] applied the continuum damage mechanics (CDM) approach [43] in their formulation. Lin et al. [31] simulated the nonlocal damage for quasi-brittle materials using initial stress. The plasticity damage model with yield degradation was considered in [31]. Sladek *et al.* [57] used the first approach to model elastoplastic materials. Botta

et al. [5,6] and Mallardo [35] applied initial stress to model nonlocal damage. In [35] the CDM approach in [11] was used to model the damage and the arc length technique [34] was used to solve the nonlinear equations. Peixoto *et al*. [45] applied initial strain with the nonlocal damage (using CDM approach). In reference [45], the variation in strain is decomposed into strain due to the external applied load and another strain due to residual load. This decomposition made it easy to use several control methods in their algorithm with application to the elastoplastic materials and materials with degrading elasticity. Peixoto *et al.* [47] applied also initial strain with nonlocal damage (using CDM approach) as in [45], but with different numerical integration procedure for the calculation of the averaged variable. Peixoto *et al.* [46] used the first approach coupled with the strong discontinuity analysis to model the strain softening to overcome the size effect due to localization.

Considering the second approach: Garcia *et al*. [17] modeled the nonlocal damage using CDM approach. The grid method [15] is used for the nonlocal approach, so the subregion dimensions are assigned equal to the interaction radius (which is obtained from experimental results). The average of the strain is carried out over each subregion. The disadvantage of this simulation is the domain discretization which makes the BEM lose its main advantage of discretizing the problem boundary only.

Considering the third approach Mobasher and Waisman [40] studied the damage problem by coupling the BEM and the FEM (nonlocal damage is used). The damaged part is modeled using the FEM and the rest of the problem, which is linear, is modeled using the BEM. The main disadvantage of this model is the need to prior knowledge of the locations of the damaged parts in the problem before the analysis, which of course is not known in the practical problems. In chapter 5 and 6, it will be demonstrated that the BEM can model damage without coupling with the FEM.

Eshelby [15] in 1957 setup a theory to solve inhomogeneous problems in elasticity where the problem can be solved as a homogeneous problem with a prescribed strain (eigenstrain) at the locations of inhomogeneities. This theory

is suitable to be coupled with the boundary element method where no domain discretization is required.

1.2 Thesis objectives

The object of this research is:

1. Using the Variational formulation in BEM to model damage in 2D elasticity problems.
2. Coupling indirect boundary integral equation as a meshless technique with Eshelby's theory to model 2D elasticity problems with inhomogeneities.
3. Introducing a new damage modeling using Eshelby's theory of equivalent inclusions coupled with direct boundary integral equation for 2D elasticity problems.

1.3 Thesis organization

This thesis consists of six chapters after this chapter. These chapters contain the followings:

Chapter 2: Theoretical background.

Chapter 3: Indirect BIE with inhomogeneities.

Chapter 4: Damage simulation in Direct BIE.

Chapter 5: Damage simulation in Variational BIE.

Chapter 6: Conclusion.

Chapter 2: Theoretical background

2.1. Introduction

In this chapter a theoretical background is introduced for different approaches for the boundary element method, direct, indirect boundary integral equations and the boundary integral equation based on the variational principle. Also, in this chapter Eshelby's theory for equivalent inclusions is introduced and how it is coupled with the direct boundary integral equation to solve problem with inhomogeneities.

2.2. Governing equations of 2D Elasticity

Consider a 2D elasticity problem as shown in Fig.(2.1) the governing system of equations (in the absence of body load) are [7]:

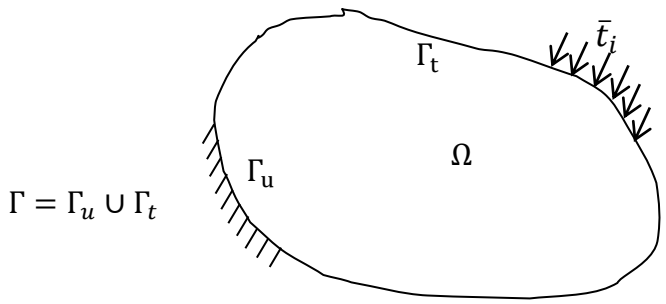

Fig.(2.1): 2D Elasticity problem

$$\sigma_{ij,j} = 0 \tag{2.1}$$

$$u_i = \bar{u}_i \text{ on } \Gamma_u \tag{2.2}$$

$$\bar{t}_i = \sigma_{ij} n_j \text{ on } \Gamma_t \tag{2.3}$$

$$\sigma_{ij} = C_{ijkl}\varepsilon_{kl} \tag{2.4}$$

$$\varepsilon_{ij} = \frac{1}{2}\left(u_{i,j} + u_{j,i}\right) \tag{2.5}$$

Where, σ_{ij}, ε_{kl} and C_{ijkl} are the stress, strain and elasticity tensor. u_i is the displacement vector on the boundary, $\bar{u}_i$ and $\bar{t}_i$ are the vectors of known

displacements and tractions on the boundary. n_j is the outward normal to the boundary.

$$C_{ijkl} = \frac{2G\nu}{(1-2\nu)}\delta_{ij}\delta_{kl} + G\left(\delta_{ik}\delta_{jl} + \delta_{il}\delta_{jk}\right) \tag{2.6}$$

$$G = \frac{E}{2(1+\nu)} \tag{2.7}$$

Where G, E and ν are the shear modulus, Young's modulus and Poisson's ratio, respectively.

2.3. Fundamental solutions for 2D Elasticity

The fundamental solution is the solution of the problem in infinite domain due to a unit load.

$$U_{ij}^{*}(\xi, x) = \frac{-1}{8\pi(1-\nu)G}\left[(3-4\nu)ln(r)\delta_{ji} - r_{,i}r_{,j}\right] \tag{2.8}$$

$$\begin{aligned} T_{ij}^{*}(\xi, x) = \frac{-1}{4\pi(1-\nu)r}\Big[r_{,n}\Big((1-2\nu)\delta_{ji} + 2r_{,i}r_{,j}\Big) \\ -(1-2\nu)\big(r_{,i}n_j - r_{,j}n_i\big)\Big] \end{aligned} \tag{2.9}$$

$$\sigma_{ijk}^{*}(\xi, x) = \frac{-1}{4\pi(1-\nu)r}\left[(1-2\nu)\left[\left(r_{,k}\delta_{ji} + r_{,j}\delta_{ik} - r_{,i}\delta_{jk}\right) + 2r_{,i}r_{,j}r_{,k}\right]\right. \tag{2.10}$$

$U_{ij}^{*}(\xi, x)$and $T_{ij}^{*}(\xi, x)$ are the fundamental solutions of displacement and traction [7] in j direction at field point x due to unit load in i direction at source point ξ. $\sigma_{ijk}^{*}(\xi, x)$ is the fundamental solution of stress [7] in j direction acting upon plane whose normal is in k direction due to a unit load in *i* direction.

2.4. Boundary element method

The boundary element method (BEM) is a semi-analytical method, where only the boundary is discretized. The method is divided into three main methods:

1. Direct boundary integral equation method
2. Indirect boundary element method
3. Variational boundary integral equation method

2.4.1.Direct Boundary integral equation method

In this method the governing differential equation Eq.(2.1) is converted to integral equation using Green's identity [7] as follows:

$$c_{ij}(\xi)u_j(\xi) = \int_{\Gamma} U^*_{ij}(\xi,\mathrm{x})t_j(\mathrm{x})d\Gamma(\mathrm{x}) - \int_{\Gamma} T^*_{ij}(\xi,\mathrm{x})u_j(\mathrm{x})d\Gamma(\mathrm{x}) \tag{2.11}$$

$$c_{ij}(\xi) = \begin{cases} 0 & \xi \; outside \; the \; domain \\ 1 & \xi \; inside \; the \; domain \\ Get \; it \; using \; rigid \; body \; consideration & \xi \; on \; the \; boundary \end{cases} \tag{2.12}$$

Where, $u_j(\mathrm{x})$ and $t_j(\mathrm{x})$ are the displacements and tractions at the field point x in j direction. Eq.(2.11) represents the boundary integral equation for displacement.

In Eq.(2.11) the integrals are on the boundary of the problem, and there is no domain integral. So, for any problem the boundary is only discretized. The discretization of the boundary is only needed to solve the integrals, unlike the finite element method where the domain discretization is needed to approximate the governing equations. Equation (2.11) is an exact form of Eq.(2.1).

The matrix form of Eq.(2.11) is [7]:

$$[H]_{2N\times 2N}\{u\}_{2N\times 1} = [G]_{2N\times 6NE}\{t\}_{6NE\times 1} \tag{2.13}$$

Where, *NE* is the number of elements used to discretize the boundary and *N* is the number of nodes.

Solving Eq.(2.13) the displacements and tractions at the boundary are known. To get the internal displacement substitute in Eq.(2.11). To get the internal strain differentiate Eq(2.11) with respect to the source point ξ which gives:

$$\varepsilon_{im}(\xi) = \int_{\Gamma} U^*_{ijm}(\xi,\mathrm{x})t_j(\mathrm{x})d\Gamma(\mathrm{x}) - \int_{\Gamma} T^*_{ijm}(\xi,\mathrm{x})u_j(\mathrm{x})d\Gamma(\mathrm{x}) \tag{2.14}$$

Where,

$$U^*_{ijm}(\xi,x)=\frac{1}{8\pi(1-\nu)Gr}\left[(1-2\nu)\left(r_{,m}\delta_{ji}+r_{,i}\delta_{jm}\right)-r_{,j}\delta_{im}+2r_{,m}r_{,i}r_{,j}\right] \tag{2.15}$$

$$\begin{aligned}T^*_{ijm}(\xi,x)=\frac{-1}{4\pi(1-\nu)r^2}\Big[&2r_{,n}\left(-\nu\left(r_{,m}\delta_{ji}+r_{,i}\delta_{jm}\right)-r_{,j}\delta_{im}\right.\\&\left.+4r_{,m}r_{,i}r_{,j}\right)-2(1-2\nu)r_{,i}n_jr_{,m}\\&-2\nu r_{,j}\left(n_ir_{,m}+n_mr_{,i}\right)\\&-(1-2\nu)\left(n_m\delta_{ji}+n_i\delta_{jm}\right)+(1-2\nu)n_j\delta_{im}\Big]\end{aligned} \tag{2.16}$$

2.4.2.Indirect Boundary element method

In this method instead of solving the real problem, an infinite domain is solved subjected to unknown forces P_i in order to make its boundary condition the same as the real problem Fig.(2.2) [12,32].

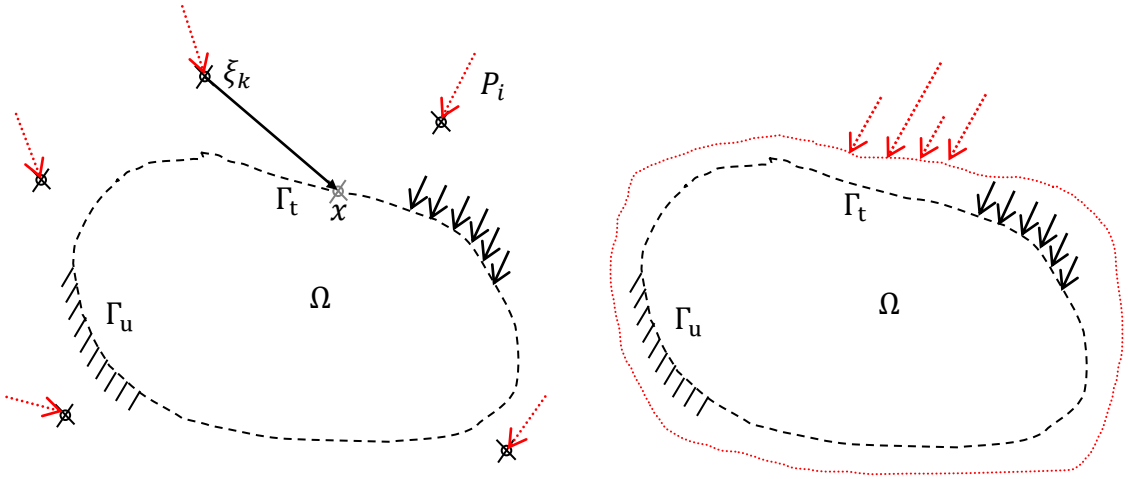

(a) Discrete Source points (b) Distributed sources

Fig.(2.2): Source points

From Fig.(2.2a)

$$u_j(x)=\sum_{k=1}^{k=N}U^*_{ij}(x,\xi_k)P_i \tag{2.17}$$

$$t_j(x) = \sum_{k=1}^{k=N} T_{ij}^*(x, \xi_k) P_i \tag{2.18}$$

The unknown forces are placed at the source points ξ_k. If the source points are placed outside the problem domain as in Fig.(2.2) then Eqs.(2.17) and (2.18) are regular (not singular) but the problem solution will depend on the distance at which the source points are placed, i.e. the solution is not unique.

In order to overcome the problem of singularity of the above equations distributed sources Fig.(2.2b) are used so that the 2 above equations can be written as follows:

$$u_j(x) = \sum_{k=1}^{k=N} \int_{\Gamma_k} U_{ij}^*(x, \xi) P_i(\xi) d\Gamma(\xi) \tag{2.19}$$

$$t_j(x) = \sum_{k=1}^{k=N} \int_{\Gamma_k} T_{ij}^*(x, \xi) P_i(\xi) d\Gamma(\xi) \tag{2.20}$$

2.4.3.Variational Boundary integral equation method

In this method the principle of minimum total potential energy is used to construct the boundary integral equation to solve the 2D elasticity problem.

The total potential energy Π (with the absence of body load) can be written as follows [14]:

$$\Pi(u_i) = \int_{\Omega} \frac{1}{2} \sigma_{ij}(y) \varepsilon_{ij}(y) d\Omega(y) - \int_{\Gamma_t} \bar{t}_i(x) u_i(x) d\Gamma(x) \tag{2.21}$$

with boundary conditions

$$u_i = \bar{u}_i \text{ on } \Gamma_u \tag{2.22}$$

$$t_i = \bar{t}_i \text{ on } \Gamma_t \tag{2.23}$$

Using Lagrange's multiplier and let:

$$u_i = \tilde{u}_i \text{ on } \Gamma \tag{2.24}$$

Therefore, Eq.(2.21) can be written as:

$$\begin{aligned}\Pi(u_i, \tilde{u}_i, \lambda_i) = & \int_{\Omega} \frac{1}{2}\sigma_{ij}(y)\varepsilon_{ij}(y)d\Omega(y) \\ & + \int_{\Gamma} \lambda_i(x)\big(\tilde{u}_i(x) - u_i(x)\big)d\Gamma(x) \\ & - \int_{\Gamma_t} \bar{t}_i(x)\tilde{u}_i(x)d\Gamma(x)\end{aligned} \tag{2.25}$$

With boundary conditions

$$u_i = \bar{u}_i \text{ on } \Gamma_u \tag{2.26}$$

Minimizing Eq.(2.25), it is found that Lagrange's multiplier must be equal to the traction on the boundary $\tilde{t}_i$ i.e.:

$$\lambda_i = \tilde{t}_i \text{ on } \Gamma_u \tag{2.27}$$

So, Eq.(2.25) can be written as follows:

$$\begin{aligned}\Pi(u_i, \tilde{u}_i, \tilde{t}_i) = & \int_{\Gamma} \frac{1}{2} t_i(x)u_i(x)d\Gamma(x) \\ & + \int_{\Gamma} \tilde{t}_i(x)\big(\tilde{u}_i(x) - u_i(x)\big)d\Gamma(x) \\ & - \int_{\Gamma_t} \bar{t}_i(x)\tilde{u}_i(x)d\Gamma(x) - \int_{\Omega} \frac{1}{2}\sigma_{ij,j}(y)u_i(y)d\Omega(y)\end{aligned} \tag{2.28}$$

With boundary conditions

$$u_i = \bar{u}_i \text{ on } \Gamma_u \tag{2.29}$$

So, minimizing Eq.(2.28) the problem is solved.

Now to minimize Eq.(2.28) , approximate the displacement and traction in the domain and on the boundary as follows:

In the domain:

$$u_j(y) = \sum_{k=1}^{k=N} U_{ij}^*(y, \xi_k)\psi_i(\xi_k) \tag{2.30}$$

$$t_j(y) = \sum_{k=1}^{k=N} T_{ij}^*(y, \xi_k)\psi_i(\xi_k) \tag{2.31}$$

On the boundary the same approximation is used as in the direct boundary integral equation.

Substitute by these approximations in Eq.(2.28) the following equation is obtained:

$$\begin{aligned}\Pi(u_i, \tilde{u}_i, \tilde{t}_i) = &\frac{1}{2}\{\psi(\xi)\}^T[Q(x,\xi)]\{\psi(\xi)\} \\ &- \{t(x)\}^T[G_i(x,\xi)]^T\{u(x)\} + \{t(x)\}^T[L(x)]\{u(x)\} \\ &- \{u(x)\}^T\{\bar{T}(x)\}\end{aligned} \tag{2.32}$$

Where;

$$[Q(x,\xi)]_{2N\times 2N} = \int_\Gamma \left[U_{ij}^*(x,\xi)\right]\left[T_{ij}(x,\xi)\right]^T d\Gamma(x) \tag{2.33}$$

$$[G_i(x,\xi)]_{2N\times 2N} = \int_\Gamma \left[U_{ij}^*(x,\xi)\right]\left[\phi_j(x)\right]^T d\Gamma(x) \tag{2.34}$$

$$\left[L_{ij}(x)\right]_{2N\times 2N} = \int_\Gamma [\phi_i(x)]\left[\phi_j(x)\right]^T d\Gamma(x) \tag{2.35}$$

$$\left\{\bar{T}_j(x)\right\}_{2N\times 2N} = \int_\Gamma \left[\phi_j(x)\right]\{\bar{t}_i(x)\}d\Gamma(x) \tag{2.36}$$

Where, ϕ_i is a set of relevant shape functions.

Minimizing Eq.(2.32) and rearranging, the following system of equations is obtained:

$$\{F(x)\} = [K(x,\xi)]\{u(x)\} \tag{2.37}$$

Where;

$$[K(x,\xi)]_{2N\times 2N} = \left[R_{ij}^{*}(x,\xi)\right]^{T}\left[Q_{ij}^{*}(x,\xi)\right]\left[R_{ij}^{*}(x,\xi)\right] \tag{2.38}$$

$$[R(x,\xi)]_{2N\times 2N} = \left(\left[G_{ij}^{*}(x,\xi)\right]^{T}\right)^{-1}[L(x)] \tag{2.39}$$

$$\{F(x)\} = \{\bar{T}(x)\} \tag{2.40}$$

And,

$$\{\psi(\xi)\}_{2N\times 1} = \left(\left[G_{ij}^{*}(x,\xi)\right]^{T}\right)^{-1}[L(x)]\{u(x)\} \tag{2.41}$$

$$\{t\} = \left[G_{ij}^{*}(x,\xi)\right]^{-1}\left[Q_{ij}^{*}(x,\xi)\right]\left(\left[G_{ij}^{*}(x,\xi)\right]^{T}\right)^{-1}[L(x)]\{u(x)\} \tag{2.42}$$

Where, $[K(x,\xi)]$ represents the stiffness of the domain, which is symmetric, unlike the stiffness obtained from the direct or indirect boundary elements which is unsymmetric. $\{F(x)\}$ is the nodal force vector.

Now on solving Eq.(2.37) the displacement and the nodal force and also the traction on the boundary is obtained.

2.5. Eshelby equivalent inclusion theory

Eshelby equivalent inclusion theory [16,42] is used to solve problems with inhomogeneities Fig.(2.3). In this theory the real problem is replaced by a homogeneous problem and at the location of inhomogeneities a prescribed strain (eigenstrain ε_{jk}^{o}) is applied to take the effect of the difference in properties. The location at which the eigenstrain is applied is called equivalent inclusion.

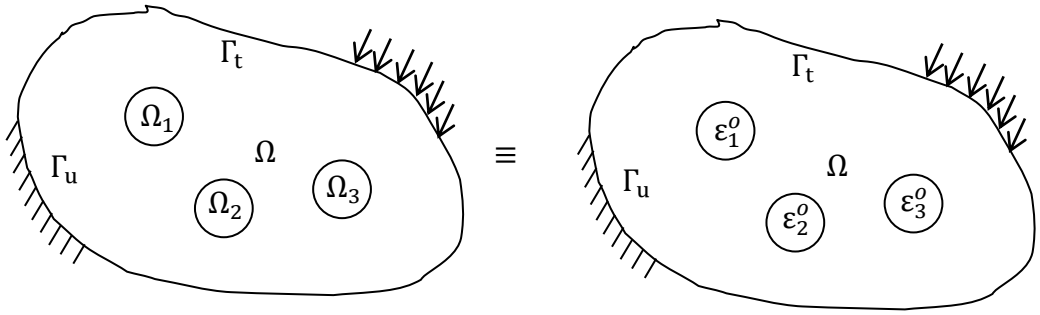

Fig.(2.3): Inhomogeneity and its equivalent inclusion problem

According to this theory the disturbance in strain due to the difference in properties (which is called constraint strain ε_{im}^{CO}) at inclusion number I is calculated as follows [16,42]:

$$\varepsilon_{im}^{CO^I} = S_{imjk}{}^{IJ}\varepsilon_{jk}^{o\ J} \tag{2.43}$$

Where, $S_{imjk}{}^{IJ}$ is the Eshelby tensor relating the constrain strain at inclusion number I with the eigenstrains at the other inclusions around it. Eshelby tensor depends on the inclusion geometry and the problem elastic constants.

To get the eigenstrain, the stresses inside the inhomogeneity and inside the equivalent inclusion are equated as follows [15]:

$$C'_{ijkl}\left(\varepsilon_{kl}^{applied} + \varepsilon_{kl}^{CO^I}\right) = C_{ijkl}\left(\varepsilon_{kl}^{applied} + \varepsilon_{kl}^{CO^I} - \varepsilon_{kl}^{o\ I}\right) \tag{2.44}$$

Where, C'_{ijkl} is the elasticity tensor for the inhomogeneous part, and $\varepsilon_{kl}^{applied}$ is the strain due to the applied load.

Substituting Eq.(2.43) into Eq.(2.44) the following relation can be obtained:

$$\varepsilon_{ij}^{applied^I} = -S_{ijkl}{}^{IJ}\varepsilon_{kl}^{o\ J} + (C_1 + C_2)\varepsilon_{ij}^{o\ I} - C_2\varepsilon_{mm}^{o}{}^{I}\delta_{ij} \tag{2.45}$$

$$C_1 = \frac{A + (1 + C)B}{B(2A + B)} \tag{2.46}$$

$$C_2 = \frac{A - CB}{B(2A + B)} \tag{2.47}$$

$$B = 1 - \frac{E_I}{E} \tag{2.48}$$

$$A = C - \frac{E_I}{E}\left(\frac{\nu_I}{1-2\nu_I}\right) \tag{2.49}$$

$$C = \frac{\nu}{1-2\nu} \tag{2.50}$$

Where, E_I and ν_I are the material Young's modulus and Poisson's ratio of inclusion number *I*.

The matrix form of Eq. (2.45) could be written as follows:

$$\{\varepsilon^{applied}\}_{3NOI\times 1} = [ek]_{3NOI\times 3NOI}\{\varepsilon^{o}\}_{3NOI\times 1} \tag{2.51}$$

Where, *NOI* is the number of equivalent inclusions in the problem.

The constraint displacement and strain from Eshelby theory is as follows:

$$u_i(x) = \sum_{I=1}^{I=NOI} \varepsilon_{jk}^{o\ I} \int_{\Omega_I} \sigma_{ijk}(x,\xi)\, d\Omega_I(\xi) \tag{2.52}$$

$$\varepsilon_{im}(x) = \begin{cases} \sum_{I=1}^{I=NOI} \varepsilon_{jk}^{o\ I} \int_{\Omega_I} O_{ijkm}(x,\xi)\, d\Omega_I(\xi) & x \neq \xi \\ \frac{1}{8(1-\upsilon)}\left[(6-8\upsilon)\varepsilon_{im}^{o} - (1-4\upsilon)\varepsilon_{ll}^{o}\delta_{im}\right] & x = \xi \end{cases} \tag{2.53}$$

$$\begin{aligned} O_{ijmk}(\xi,x) = \frac{1}{4\pi(1-\nu)r^2}\big[&2\upsilon\left(r_{,k}r_{,m}\delta_{ij} + r_{,j}r_{,m}\delta_{ik} + r_{,i}r_{,j}\delta_{km}\right. \\ &\left. + r_{,i}r_{,k}\delta_{jm}\right) + 2(1-2\nu)r_{,i}r_{,m}\delta_{jk} + 2r_{,j}r_{,k}\delta_{im} \\ &- 8r_{,i}r_{,j}r_{,k}r_{,m} \\ &+ (1-2\nu)\left(\delta_{ij}\delta_{km} + \delta_{ik}\delta_{jm} - \delta_{jk}\delta_{im}\right)\big] \end{aligned} \tag{2.54}$$

ε_{jk}^{o} is assumed here to be constant inside the inclusion.

2.6. Continuum Damage Mechanics

Continuum Damage Mechanics CDM is the science which studies the deterioration of the material under the action of loads until fracture occurs.

Unlike Fracture Mechanics which study the material with the presence of a crack.

In CDM the material deterioration is studied by decreasing the elastic tensor of the material by Damage variable (D) which depends on the material behavior. In this thesis the damage is considered isotropic, so D is a scalar quantity (D=0 for undamaged material and 1 for fully damage material). According to the CDM the stress strain relation becomes [43]:

$$\sigma_{ij} = (1 - D)C_{ijkl}\varepsilon_{kl} \tag{2.55}$$

The damage growth is governed by the following activation function [25]:

$$f(\varepsilon^*) = \varepsilon^*(\varepsilon) - \varepsilon^*_{max} \tag{2.56}$$

Such that, $f(\varepsilon^*) \leq 0$ and $\dot{\varepsilon}^*_{max} \geq 0$ and,

$$\varepsilon^* = \sqrt{\langle\varepsilon_1\rangle^2 + \langle\varepsilon_2\rangle^2} \tag{2.57}$$

where, ε^*_{max} is the maximum effective strain measured in the medium, ε^* is the effective strain and $\dot{(\ )}$ is a time derivative. ε_1 and ε_2 are the principle strains, and $\langle\varepsilon_i\rangle$ denotes the positive values of the strain.

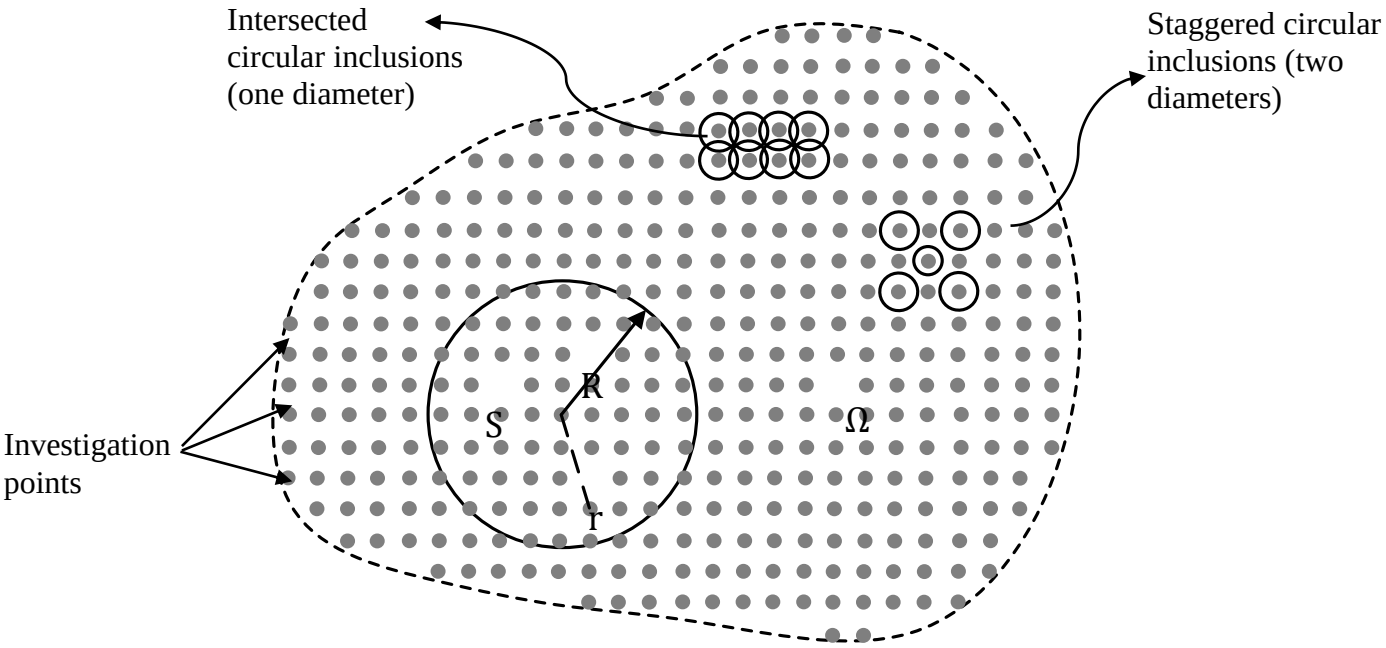

Fig.(2.4): Different inclusion patterns and the interaction radius.

The above damage approach is called the local damage approach. To extend such an approach to the nonlocal approach (the integral type), a certain variable $f(X)$ is replaced by its nonlocal counterpart $f_{nl}(X_p)$ [27]. In this thesis two approaches are used for the nonlocal integral type, the first one is averaging the strain [25], and the second one is averaging the damage [49]. The averaging is done as follows:

$$f_{nl}(X_p) = \int_S \alpha(r) f(X) dS \Big/ \int_S \alpha(r) dS \tag{2.58}$$

in which $\alpha(r)$ is the weight function, where it is chosen here to be the bell-shape function as follows:

$$\alpha(r) = \begin{cases} \left(1 - \dfrac{r^2}{R^2}\right)^2 & 0 \le r \le R \\ 0 & r > R \end{cases} \tag{2.59}$$

where, X_p is the coordinate of the investigation point, at which the nonlocal strain or nonlocal damage is calculated and X is the coordinate of any arbitrary

point inside a circle of radius R (the interaction radius, which is a material property) as given in Fig.(2.4).

The integration in Eq.(2.36) is approximated as follows:

$$f_{nl}(X_p) = \sum_{i=0}^{NC} \alpha(r_i) f(X_i) \Big/ \sum_{i=0}^{NC} \alpha(r_i) \tag{2.60}$$

where *NC* is the number of points inside the circle as shown in Fig.(2.4).

2.7. Coupling Eshelby theory with DBIEM

In order to solve a problem with inhomogeneities using the BEM the problem domain needs to be discrteized to define different elastic properties. This approach makes the BEM losses its main advantage of boundary only discretization. In 2008 Hang *et.al* [19-21] coupled the DBIE Eq.(2.11) and Eq.(2.14) with Eshelby equivalent inclusion theory Eq.(2.52) and Eq.(2.53) to get the following:

$$\begin{aligned} c_{ij}(\xi)u_j(\xi) = &\int_{\Gamma} U^*_{ij}(\xi, x)t_j(\mathrm{x})d\Gamma(\mathrm{x}) - \int_{\Gamma} T^*_{ij}(\xi, \mathrm{x})u_j(\mathrm{x})d\Gamma(\mathrm{x}) \\ &+ \sum_{\mathrm{I}=1}^{\mathrm{I}=NOI} \varepsilon^o_{jk}(\mathrm{x}_I) \int_{\Omega_\mathrm{I}} \sigma^*_{ijk}(\xi, \mathrm{x}_I)\mathrm{d}\Omega_\mathrm{I}(\mathrm{x}_I) \end{aligned} \tag{2.61}$$

$$\begin{aligned} \varepsilon_{im}(\xi) = &\int_{\Gamma} U^*_{ijm}(\xi, \mathrm{x})t_j(\mathrm{x})d\Gamma(\mathrm{x}) - \int_{\Gamma} T^*_{ijm}(\xi, \mathrm{x})u_j(\mathrm{x})d\Gamma(\mathrm{x}) + \\ &\begin{cases} \sum_{I=1}^{I=NOI} \varepsilon^{o\ I}_{jk} \int_{\Omega_I} O_{ijkm}(x, \xi)d\Omega_I(\xi) & x \neq \xi \\ \frac{1}{8(1-\nu)}[(6-8\upsilon)\varepsilon^o_{im} - (1-4\upsilon)\varepsilon^o_{ll}\delta_{im}] & x = \xi \end{cases} \end{aligned} \tag{2.62}$$

$$[G_{ij}]\{t_j\} - [H_{ij}]\{u_j\} + [B_{ijk}]\{\varepsilon^o_{jk}\} = \{0\} \tag{2.63}$$

$$\{\varepsilon_{im}\} = [\bar{G}_{ijm}]\{t_j\} - [\bar{H}_{ijm}]\{u_j\} + [\bar{B}_{ijkm}]\{\varepsilon^o_{jk}\} \quad (2.64)$$

To Solve Eq.(2.63) the eigenstrain is needed first which can be obtained using Eq.(2.45) and Eq.(2.14). These equations can be solved iteratively as in [19-21] or directly as in [55]. The advantage of this approach is that the system of equations is decreased.

2.8. Conclusions

In this chapter a brief introduction to different approaches in the boundary element method (Direct, indirect and variational boundary integral equations), which will be used in the three coming chapters to solve problems of inhomogeneities and damage. Also, Eshelby's theory is discussed and how it is coupled with the direct boundary integral equation to solve problems with inhomogeneities. It will be shown in the following chapter how Eshelby theory can also be coupled with the indirect BIE to solve problems with inhomogeneities.

Chapter 3: Indirect BIE with inhomogeneities

3.1. Introduction

In this chapter Eshelby equivalent inclusion theory is coupled with the FSM, where the advantage of no meshing on the boundary or inside the domain is gained. The Eshelby theory is being coupled as a set of particular solutions where analytical solutions are employed for circular inclusions [23,24,30,42], so there is no domain discretization and all involved integrations are carried out analytically and closed form solutions are employed. Finally, the solution algorithm is performed using two approaches i.e. the direct approach and the iterative approach.

3.2. Fictitious Stress Method

Consider a 2D elasticity problem, with *N* points are placed on the boundary (Fig.(3.1)). The distance between these points is defined as the point interval; along which the boundary normal and tangential directions are defined. The displacements and tractions on the boundary can be computed using the fictitious stress method, as follows [12]:

$$u_s{}^i = \frac{P_s{}^j}{2G}[(3-4\nu)cos\gamma\bar{F}_1 - \bar{y}(sin\gamma\bar{F}_2 - cos\gamma\bar{F}_3)] + \frac{P_n{}^j}{2G}[(3-4\nu)sin\gamma\bar{F}_1 - \bar{y}(cos\gamma\bar{F}_2 + sin\gamma\bar{F}_3)] \tag{3.1}$$

$$u_n{}^i = \frac{P_s{}^j}{2G}[-(3-4\nu)sin\gamma\bar{F}_1 - \bar{y}(cos\gamma\bar{F}_2 + sin\gamma\bar{F}_3)] + \frac{P_n{}^j}{2G}[(3-4\nu)cos\gamma\bar{F}_1 + \bar{y}(sin\gamma\bar{F}_2 - cos\gamma\bar{F}_3)] \tag{3.2}$$

$$t_s{}^i = \frac{P_s{}^j}{2G}[(3-4\nu)cos\gamma\bar{F}_1 - \bar{y}(sin\gamma\bar{F}_2 - cos\gamma\bar{F}_3)] + \frac{P_n{}^j}{2G}[(3-4\nu)sin\gamma\bar{F}_1 - \bar{y}(cos\gamma\bar{F}_2 + sin\gamma\bar{F}_3)] \tag{3.3}$$

$$
\begin{aligned}
{t_n}^i = \frac{{P_s}^j}{2G}[&\bar{F}_2 - 2(1-\nu)(cos2\gamma\bar{F}_2 + sin2\gamma\bar{F}_3) \\
&- \bar{y}(cos2\gamma\bar{F}_4 - sin2\gamma\bar{F}_5)] \\
&+ \frac{{P_n}^j}{2G}[\bar{F}_3 - (1-2\nu)(sin2\gamma\bar{F}_2 - cos2\gamma\bar{F}_3) \\
&+ \bar{y}(sin2\gamma\bar{F}_4 + cos2\gamma\bar{F}_5)]
\end{aligned}
\tag{3.4}
$$

where, (recall Fig.(3.1)) u_s^i , u_n^i and t_s^i , t_n^i are the displacements and tractions at point *i* in direction s^i and normal direction n^i. u_s^i , u_n^i and t_s^i , t_n^i are due to fictitious stress ${P_s}^j$ and ${P_n}^j$ distributed on the interval at point *j* in the direction s^j and normal direction n^j. $\bar{y}$ is the y-coordinate of point *i* with respect to point *j* mesured in the local direction of the interval at point *j*, and $\gamma = \beta^i - \beta^j$, where, β^i and β^j are the inclination angle of s^i and $s^j$to the horizontal. The terms $\bar{F}_1$ to $\bar{F}_5$ are given as follows [12]:

$$
\begin{aligned}
\bar{F}_1 = -M\Bigg[&\bar{y}\left(tan^{-1}\left(\frac{\bar{y}}{\bar{x}-a}\right) - tan^{-1}\left(\frac{\bar{y}}{\bar{x}+a}\right)\right) \\
&-\frac{1}{2}(\bar{x}-a)ln((\bar{x}-a)^2+\bar{y}^2) + \frac{1}{2}(\bar{x}+a)ln((\bar{x}+a)^2+\bar{y}^2)\Bigg]
\end{aligned}
\tag{3.5}
$$

$$
\bar{F}_2 = \frac{1}{2}M[ln((\bar{x}-a)^2+\bar{y}^2) - (\bar{x}+a)ln((\bar{x}+a)^2+\bar{y}^2)] \tag{3.6}
$$

$$
\bar{F}_3 = -M\left[tan^{-1}\left(\frac{\bar{y}}{\bar{x}-a}\right) - tan^{-1}\left(\frac{\bar{y}}{\bar{x}+a}\right)\right] \tag{3.7}
$$

$$
\bar{F}_4 = M\left[\frac{\bar{y}}{(\bar{x}-a)^2+\bar{y}^2} - \frac{\bar{y}}{(\bar{x}+a)^2+\bar{y}^2}\right] \tag{3.8}
$$

$$
\bar{F}_5 = M\left[\frac{\bar{x}-a}{(\bar{x}-a)^2+\bar{y}^2} - \frac{\bar{x}+a}{(\bar{x}+a)^2+\bar{y}^2}\right] \tag{3.9}
$$

where,

$$
M = \frac{1}{4\pi(1-\nu)} \tag{3.10}
$$

In which, $\bar{x}$ is the x-coordinate of point *i* with respect to the point *j* mesured in the local direction of the interval at point *j*, and *a* is half the length of the interval at point *j*. On suitable substitutions from Eqs.(3.5-3.10) into Eqs.(3.1-3.4), the boundary displacements and tractions can be rewritten as [12]:

$$u_s{}^i = \sum_{j=1}^{N} B_{ss}{}^{ij} P_s{}^j + \sum_{j=1}^{N} B_{sn}{}^{ij} P_n{}^j \tag{3.11}$$

$$u_n{}^i = \sum_{j=1}^{N} B_{ns}{}^{ij} P_s{}^j + \sum_{j=1}^{N} B_{nn}{}^{ij} P_n{}^j \tag{3.12}$$

$$t_s{}^i = \sum_{j=1}^{N} A_{ss}{}^{ij} P_s{}^j + \sum_{j=1}^{N} A_{sn}{}^{ij} P_n{}^j \tag{3.13}$$

$$t_n{}^i = \sum_{j=1}^{N} A_{ns}{}^{ij} P_s{}^j + \sum_{j=1}^{N} A_{nn}{}^{ij} P_n{}^j \tag{3.14}$$

where, $B_{ss}{}^{ij}$, $B_{sn}{}^{ij}$, $B_{ns}{}^{ij}$ and $B_{nn}{}^{ij}$ are the influence matrices obtained from Eqs.(3.1,3.2) for displacements, and $A_{ss}{}^{ij}$, $A_{sn}{}^{ij}$, $A_{ns}{}^{ij}$ and $A_{nn}{}^{ij}$ are the influence matrices obtained from Eqs.(3.3,3.4) for tractions.

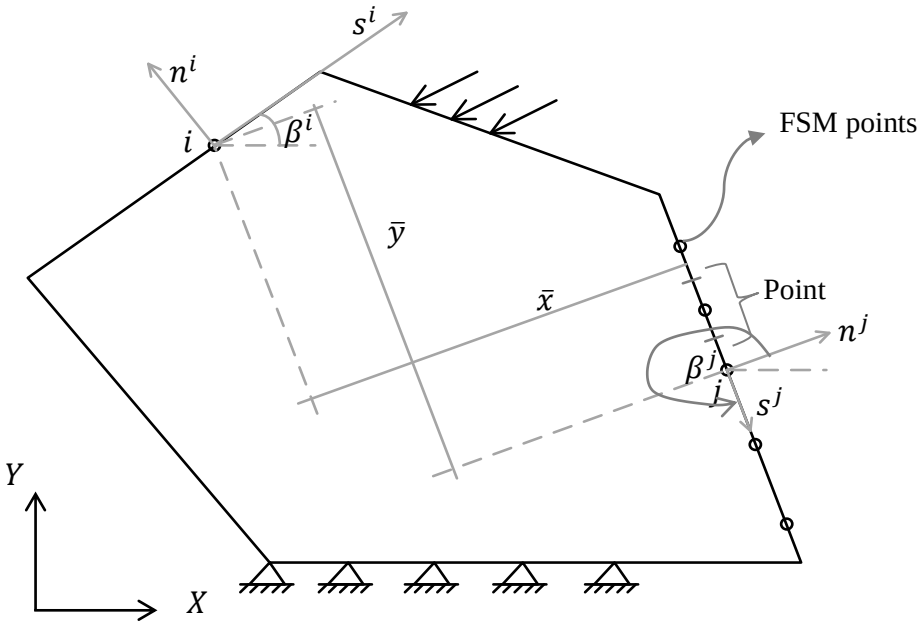

Fig.(3.1): A general problem with FSM points and associated intervals.

The matrix form of Eqs.(3.11-3.14) could be written as follows:

$$\begin{Bmatrix}\{u\}_{2N\times1}\\ \{t\}_{2N\times1}\end{Bmatrix}=\begin{bmatrix}[B]_{2N\times2N}\\ [A]_{2N\times2N}\end{bmatrix}\{P\}_{2N\times1} \tag{3.15}$$

Solving Eq.(3.15), the fictitious stress $\{P\}$ is computed, then one can substitute into Eqs.(3.11-3.14) to obtain the unknown boundary displacements and tractions. Also, internal displacements can be obtained from Eqs.(3.11,3.12), and the internal strains or stresses can be obtained by superposition after differentiation of Eqs.(3.11,3.12) as demonstrated in section 3.6.

3.3. The proposed FSM with inhomogeneities

In this chapter, Eshelby's equivalent inclusion theory is coupled with the FSM to model the inhomogeneity problems. The problem is solved by dividing the solution into complementary and particular solutions (Fig.(3.2)). The particular solution is obtained from Eshelby's theory in infinite domain. The complementary solution is computed as a later step using the FSM after modifying the relevant boundary conditions. Therefore, the problem final displacements and tractions could be written as follows:

$$u_m{}^i = u_m^{c\ i} + u_m^{p\ i} \tag{3.16}$$

$$t_m{}^i = t_m^{c\ i} + t_m^{p\ i} \tag{3.17}$$

where, $u_m^{c\ i}$ and $u_m^{p\ i}$ are the complementary and the particular solutions of displacements at point *i* in x and y directions, respectively. Also, $t_m^{c\ i}$ and $t_m^{p\ i}$ are the complementary and the particular solutions of tractions at point *i* in x and y directions, respectively. The particular solutions could be solved first as follows (assuming the eigenstrain to be constant inside the equivalent inclusion):

$$u_m^{p\ i} = \sum_{j=1}^{NOI} \int_{\Omega_j} \sigma_{mql}\, d\Omega\, \varepsilon_{ql}^{o\ j} \tag{3.18}$$

$$t_m^{p\,i} = \sum_{j=1}^{NOI} \int_{\Omega_j} \sigma_{mkql} n_k d\Omega\, \varepsilon_{ql}^{o\,j} \tag{3.19}$$

where, σ_{ijk} and σ_{ijkl} are defined in chapter 2. Without losing the generality in this thesis, the equivalent inclusion shape is taken in this work to be circular. The integrals in Eqs. (3.18 and 3.19) are computed as follows:

$$u_m^{p\,i} = \sum_{j=1}^{NOI} Q_{mql}^{ij} \varepsilon_{ql}^{o\,j} \tag{3.20}$$

$$t_m^{p\,i} = \sum_{j=1}^{NOI} \bar{S}_{mkql}^{ij} n_k \varepsilon_{ql}^{o\,j} \tag{3.21}$$

The expressions of Q_{mql}^{ij} and $\bar{S}_{mkql}^{ij}$ are derived in analytical form [23,24,30,42] and is listed in Appendix A, besides Eshelby's tensor.
Combining Eqs. (3.11-3.14) and Eqs. (3.20 and 3.21) using Eqs. (3.16 and 3.17), the total displacements and total tractions could be written as follows:

$$u_m{}^i = \left(u_s^{c\,i}\cos(90(m-1)-\beta^i) + u_n^{c\,i}\sin(90(m-1)-\beta^i)\right) + \sum_{j=1}^{NOI} Q_{mql}^{ij} \varepsilon_{ql}^{o\,j} \tag{3.22}$$

$$t_m{}^i = \left(t_s^{c\,i}\cos(90(m-1)-\beta^i) + t_n^{c\,i}\sin(90(m-1)-\beta^i)\right) + \sum_{j=1}^{NOI} R_{mql}^{ij} \varepsilon_{ql}^{o\,j} \tag{3.23}$$

It should be noticed that Eqs.(3.11-3.14) are defined in the local direction of the interval at point *i*, therefore, Eqs.(3.11-3.14) must be multiplied by the transformation matrix for each interval to transform it in the global directions be for combining with Eqs. (3.20 and 3.21).

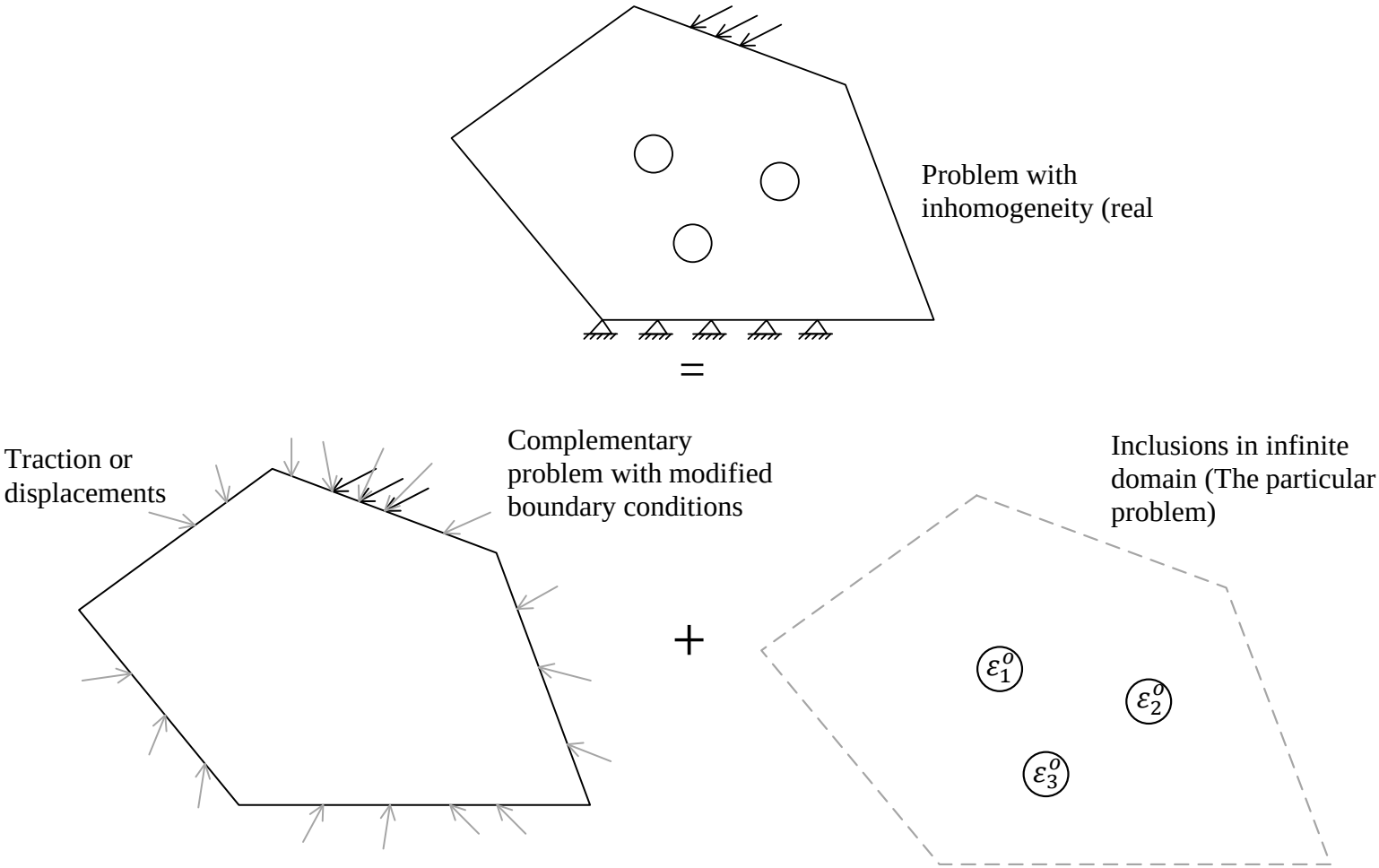

Fig.(3.2): The solution concept of dividing the problem into complementary and particular problems.

Equations (3.22 and 3.23) could be rewritten in a matrix form as follows:

$$\begin{Bmatrix}\{u\}_{2N\times1}\\ \{t\}_{2N\times1}\end{Bmatrix}=\begin{bmatrix}[\bar{B}]_{2N\times2N} & [Q]_{2N\times3NOI}\\ [\bar{A}]_{2N\times2N} & [R]_{2N\times3NOI}\end{bmatrix}\begin{Bmatrix}\{P\}_{2N\times1}\\ \{\varepsilon^{o}\}_{3NOI\times1}\end{Bmatrix} \tag{3.24}$$

$[\bar{B}]$ and $[\bar{A}]$ are the same as $[B]$ and $[A]$ but after multiplying the rows corresponding to each interval by the transformation matrix $[T^{i}]$, in which:

$$[T^{i}]=\begin{bmatrix}\cos\beta^{i} & -\sin\beta^{i}\\ \sin\beta^{i} & \cos\beta^{i}\end{bmatrix} \tag{3.25}$$

In order to solve Eq. (3.24) the eigenstrain should be obtained. This is carried out using Eq. (2.46), which needs first to obtain the applied strain. The applied strain at the inclusion center is obtained as follows:

$$\varepsilon_{ql}^{applied}=\frac{1}{E}\left[(1+\nu)\sigma_{ql}^{applied}-\nu(1+\nu)\sigma_{kk}^{applied}\delta_{ql}\right] \tag{3.26}$$

Where, the stress at the internal point *i* is calculated as follows [12]:

$$\begin{aligned}\sigma_{xx}{}^{i}=P_{s}{}^{j}[&\bar{F}_{2}+2(1-\nu)(\cos2\beta^{j}\bar{F}_{2}-\sin2\beta^{j}\bar{F}_{3})\\&+\bar{y}(\cos2\beta^{j}\bar{F}_{4}+\sin2\beta^{j}\bar{F}_{5})]\\+P_{n}{}^{j}[&\bar{F}_{3}-(1-2\nu)(\sin2\beta^{j}\bar{F}_{2}+\cos2\beta^{j}\bar{F}_{3})\\&+\bar{y}(\sin2\beta^{j}\bar{F}_{4}-\cos2\beta^{j}\bar{F}_{5})]\end{aligned} \tag{3.27}$$

$$\begin{aligned}\sigma_{xy}{}^{i}=P_{s}{}^{j}[&2(1-\nu)(\sin2\beta^{j}\bar{F}_{2}+\cos2\beta^{j}\bar{F}_{3})\\&+\bar{y}(\sin2\beta^{j}\bar{F}_{4}-\cos2\beta^{j}\bar{F}_{5})]\\+P_{n}{}^{j}[&(1-2\nu)(\cos2\beta^{j}\bar{F}_{2}-\sin2\beta^{j}\bar{F}_{3})-\bar{y}(\cos2\beta^{j}\bar{F}_{4}+\sin2\beta^{j}\bar{F}_{5})]\end{aligned} \tag{3.28}$$

$$\begin{aligned}\sigma_{yy}{}^{i}=P_{s}{}^{j}[&\bar{F}_{2}-2(1-\nu)(\cos2\beta^{j}\bar{F}_{2}-\sin2\beta^{j}\bar{F}_{3})\\&-\bar{y}(\cos2\beta^{j}\bar{F}_{4}+\sin2\beta^{j}\bar{F}_{5})]\\+P_{n}{}^{j}[&\bar{F}_{3}+(1-2\nu)(\sin2\beta^{j}\bar{F}_{2}+\cos2\beta^{j}\bar{F}_{3})\\&-\bar{y}(\sin2\beta^{j}\bar{F}_{4}-\cos2\beta^{j}\bar{F}_{5})]\end{aligned} \tag{3.29}$$

After substituting Eqs.(3.27-3.29) into Eq.(3.26), the latter system can be rewritten in a matrix form as follows :

$$\{\varepsilon^{applied}\}_{3NOI\times 1} = [Z]_{3NOI\times 2N}\{P\}_{2N\times 1} \tag{3.30}$$

In order to solve the inhomogeneity problem, Eq. (3.24) together with Eq. (3.30) and Eq. (2.52) is needed to be solved. In this chapter, two approaches are developed, i.e. the direct approach and the iterative approach.

3.4. The proposed iterative approach

In this approach the solution procedure is carried out in iterative way as follows:

1. Solve Eq. (3.15) to compute the fictitious stresses.
2. From Eq.(3.30), compute the strain at the center of the inhomogeneities.
3. From Eq.(2.51), compute the eigenstrain.
4. Substitute the computed eigenstrain into Eq.(3.24) then compute the new fictitious stress.
5. From Eq.(3.30), compute the updated applied strain at the equivalent inclusion center.
6. Repeat from step (3) and calculate the eigenstrain until the difference between two consecutive values of the eigenstrain is less than a prescribed *tolerance* as follows:

$$\{Error\} = \{\varepsilon^{o}\}^{i} - \{\varepsilon^{o}\}^{i-1} \tag{3.31}$$

$$max\{Error\} < tol, \text{ where} \tag{3.32}$$

i is the iteration number

Figure (3.3) summarizes the former steps in a flow diagram.

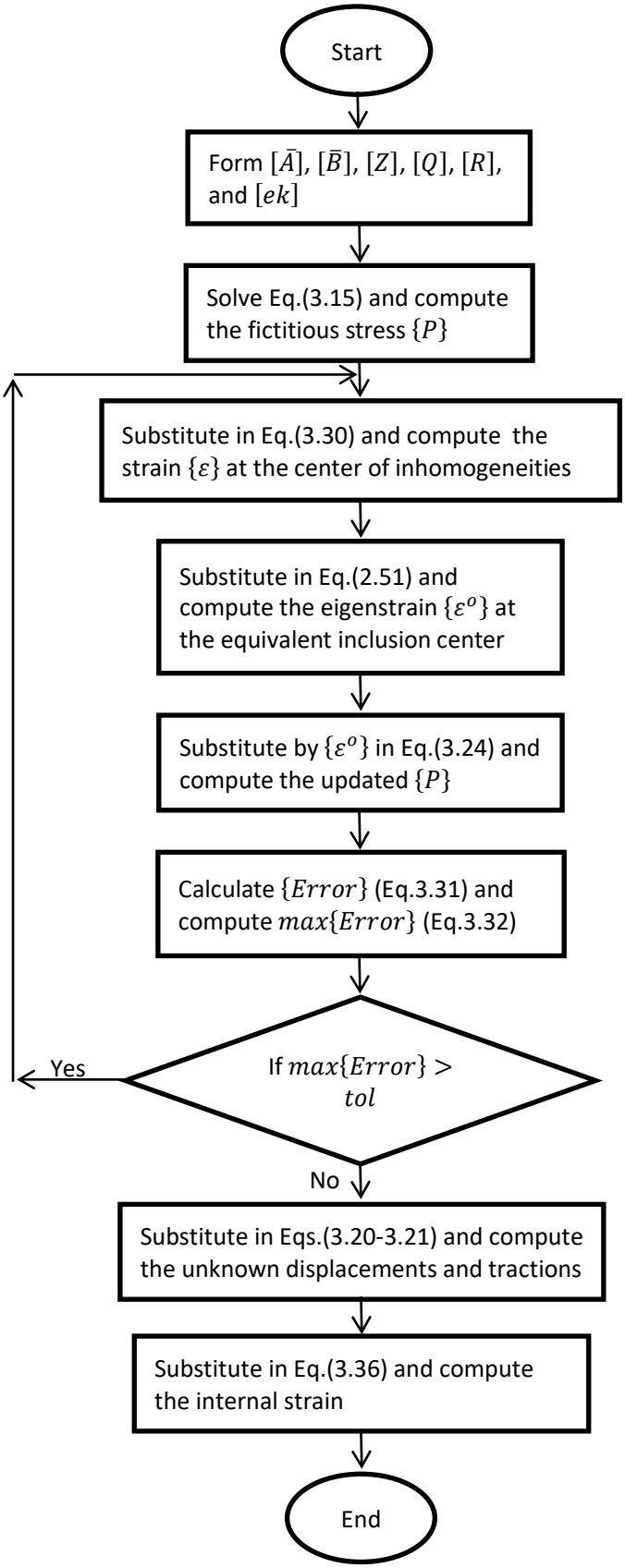

Fig.(3.3): A flow diagram of the proposed iterative approach.

3.5. The proposed direct approach

In this approach the eigenstrain values are obtained directly without iterations. From Eq.(2.45), and Eq.(3.26) the following relationships between the fictitious stress and the eigenstrain are obtained:

$$-S_{ijkl}{}^{IJ}\varepsilon_{kl}^{o\,J} + (C_1 + C_2)\varepsilon_{ij}^{o\,I} - C_2\varepsilon_{mm}^{o}{}^{I}\delta_{ij} = \frac{1}{E}\left[(1+\nu)\sigma_{ij}^{applied} - \nu(1+\nu)\sigma_{mm}^{applied}\delta_{ij}\right] \tag{3.33}$$

Eq.(3.33) is then rewritten in a matrix form as follows:

$$[ek]_{3NOI\times 3NOI}\{\varepsilon^o\}_{3NOI\times 1} = [Z]_{3NOI\times 2N}\{P\}_{2N\times 1} \tag{3.34}$$

From Eq.(3.24) and Eq.(3.34) the following matrix form could be written:

$$\begin{Bmatrix} \{u\}_{2N\times 1} \\ \{t\}_{2N\times 1} \\ \{0\}_{3NOI\times 1} \end{Bmatrix} = \begin{bmatrix} [\bar{B}]_{2N\times 2N} & [Q]_{2N\times 3NOI} \\ [\bar{A}]_{2N\times 2N} & [R]_{2N\times 3NOI} \\ [Z]_{3NOI\times 2N} & -[ek]_{3NOI\times 3NOI} \end{bmatrix} \begin{Bmatrix} \{P\} \\ \{\varepsilon^o\} \end{Bmatrix} \tag{3.35}$$

Solving Eq.(3.35), the fictitious stress and also the eigenstrain are obtained.

3.6. Post processing

After solving the problem by either of the above two approaches, substituting in Eqs.(3.22 and 3.23) the unknown displacements and tractions at the boundary are obtained.

The strain at the inclusion center could be computed as follows:

$$\varepsilon_{ql}{}^{i} = \varepsilon_{ql}^{c\,i} + \varepsilon_{ql}^{p\,i} \tag{3.36}$$

With the following particular part:

$$\varepsilon_{ql}^{p\,i} = \sum_{j=1}^{NOI} S_{qlkm}^{ij}\varepsilon_{km}^{o}{}^{j} \tag{3.37}$$

and the corresponding complementary part:

$$\varepsilon_{ql}^{c} = \frac{1}{E}\left[(1+\nu)\sigma_{ql}^{c} - \nu(1+\nu)\sigma_{kk}^{c}\delta_{ql}\right] \tag{3.38}$$

In which, σ_{ql}^{c} is the complementary part of stress from Eqs. (3.27-3.29).

3.7. Numerical examples

In this section five numerical examples are solved in order to demonstrate the accuracy and validity of the proposed formulations. FSM points are placed on the boundary of the problem and inclusion points are placed at the inhomogeneity center i.e. no boundary or domain discretization is required. For the first three examples direct approach is only used, and in the last two examples both the iterative and direct approaches are used for the purpose of comparison.

3.7.1.Kirsch problem

In this example, the well-known Kirsch problem (large plate with small circular void of radius *R*) as shown in Fig.(3.4) is solved. The analytical solution for stresses is given in Appendix C. The material properties used is E=1 N/m^2 and ν=0.3.

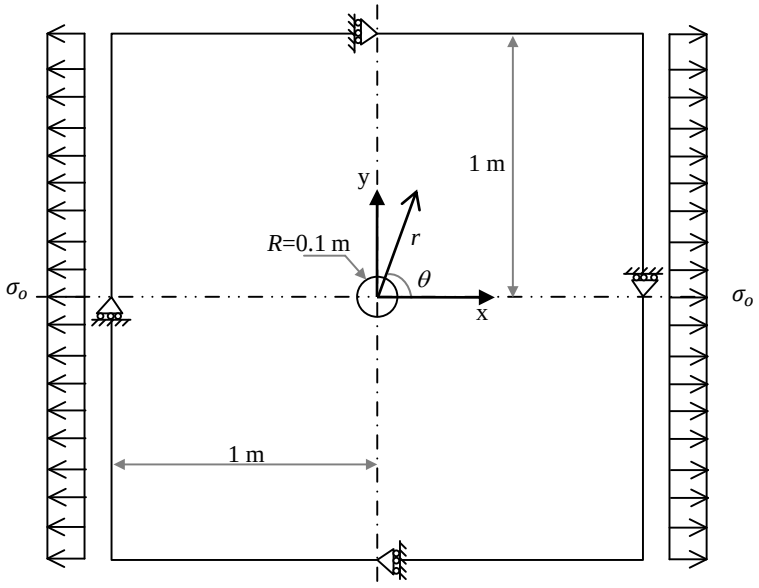

Fig.(3.4): Kirsch problem example 3.7.1

The problem is solved using 12,18,36 and 76 FSM points and one point at the void center. Figures (3.5,3.6) demonstrate the results of the stresses in x and y directions, respectively. It can be seen that good agreement between the present formulation solutions and the analytical solutions are obtained.

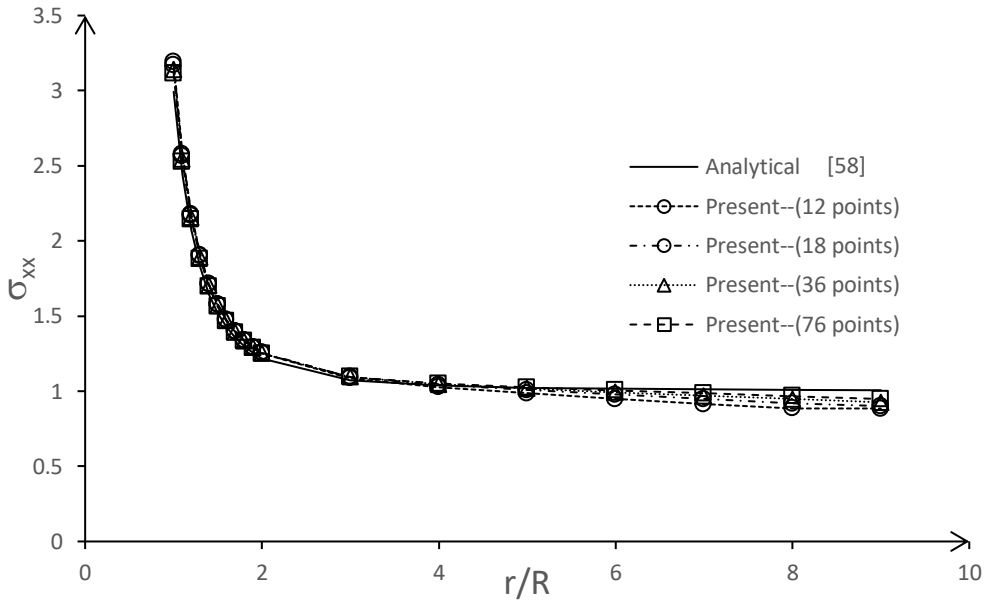

Fig.(3.5): Stresses in the x-direction in example 3.7.1

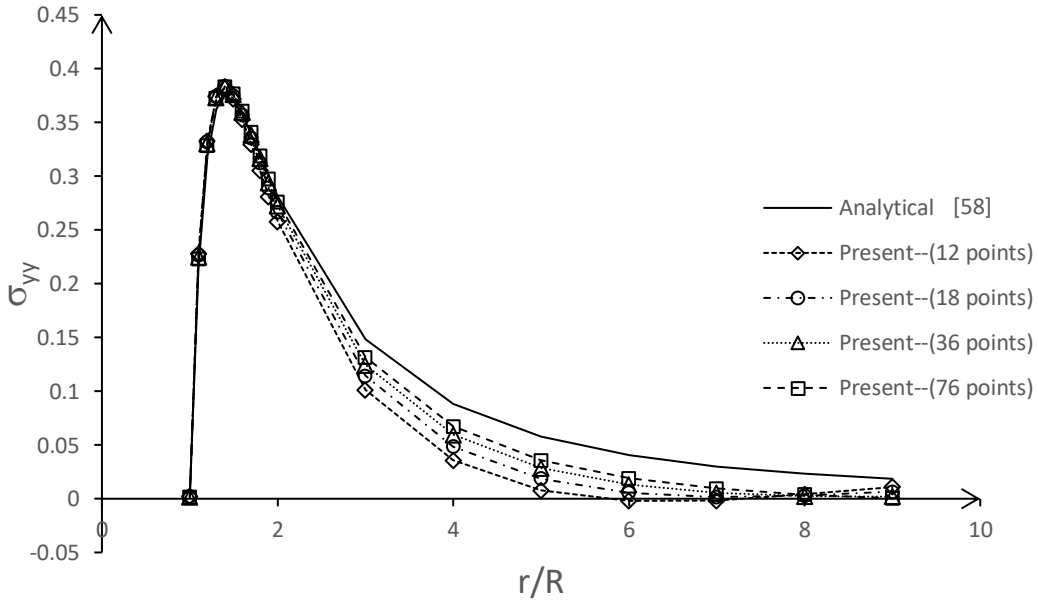

Fig.(3.6): Stress in the y-direction in example 3.7.1

3.7.2.Square plate with single inhomogeneity

The square plate shown in Fig.(3.7) is considered in this example. The plate is solved with different locations of inhomogeneity as shown in Fig.(3.7). Wu and Yin [61] previously solved this problem using the direct boundary element method, where quadratic boundary elements were used, and quadratic eigenstrain approximation was assumed. The material properties of the matrix are E=10^6 N/m^2 and v=0.25. Stiff and soft inhomogeneity are considered. The material properties of the stiff are E=2×10^6 N/m^2 and v=0.25 and for the soft one are E=10^5 N/m^2 and v=0.25. The problem is solved under vertical load t=10^4 N/m.

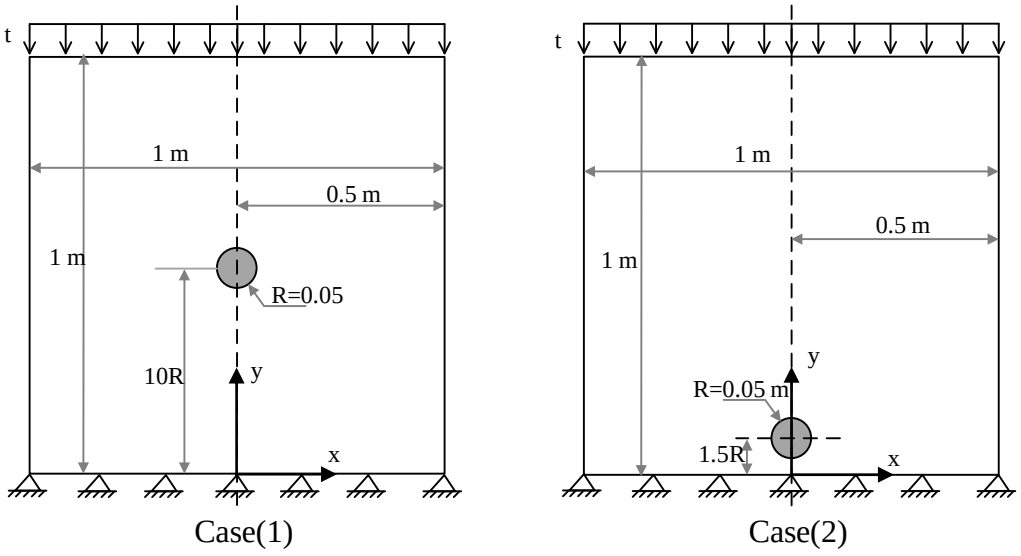

Fig.(3.7): Square plate with single inhomogeneity in example 3.7.2

The problem is discretized using different number of FSM points 20, 52, 100 and 200 (the points are uniformly distributed along the four sides). Cases (1) and (2) are solved with soft inhomogeneity. The stress σ_{yy} along the vertical dashed line is demonstrated in Figs.(3.8) for case(1) and stresses σ_{xx} and σ_{yy} are demonstrated in Figs.(3.9,3.10) for case(2). In these figures σ_{yy}^{H} denotes the stress in the homogeneous case.

Case (2) is solved again with stiff inhomogeneity. The stresses σ_{xx} and σ_{yy} along the vertical dashed line are demonstrated in Figs.(3.11,3.12). It is clear that there

is a good agreement of the present formulation results to those of reference [61] although in ref. [61] 200 quadratic boundary elements were used. It is clear from the figures that in case of soft inhomogeneity when it is away from the boundary, only 52 points is enough to capture reasonable accuracy but when the inhomogeneity is near the boundary more points should be used (100 points). In case of stiff inhomogeneity, the distance from the boundary has less influence than that of the soft one.

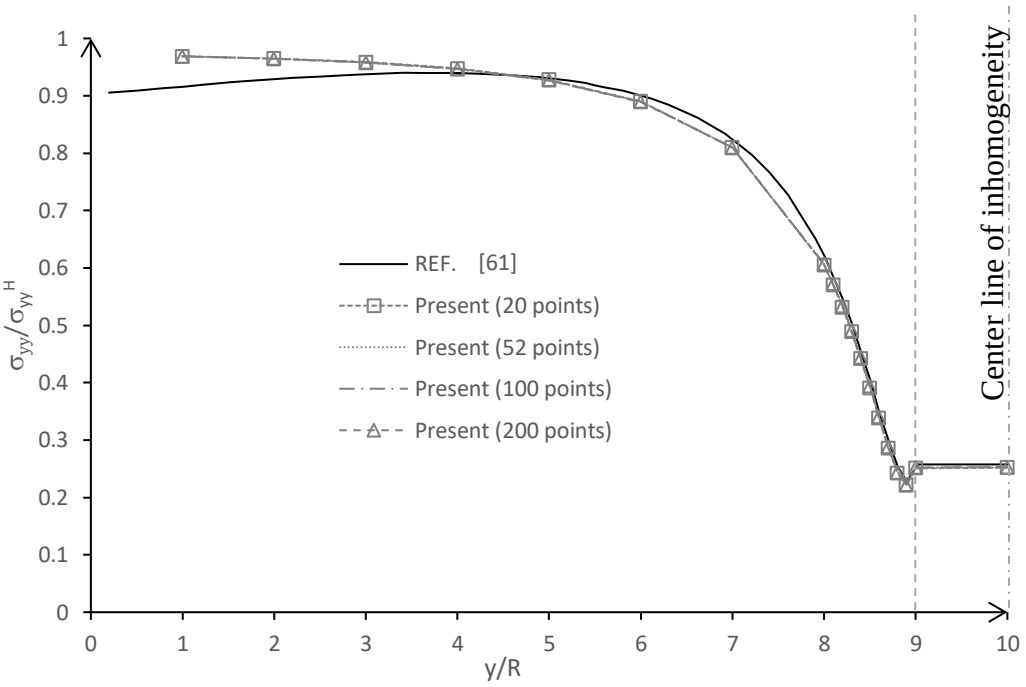

Fig.(3.8): Stress in the y-direction in example 3.7.2, case(1) (soft inhomogeneity).

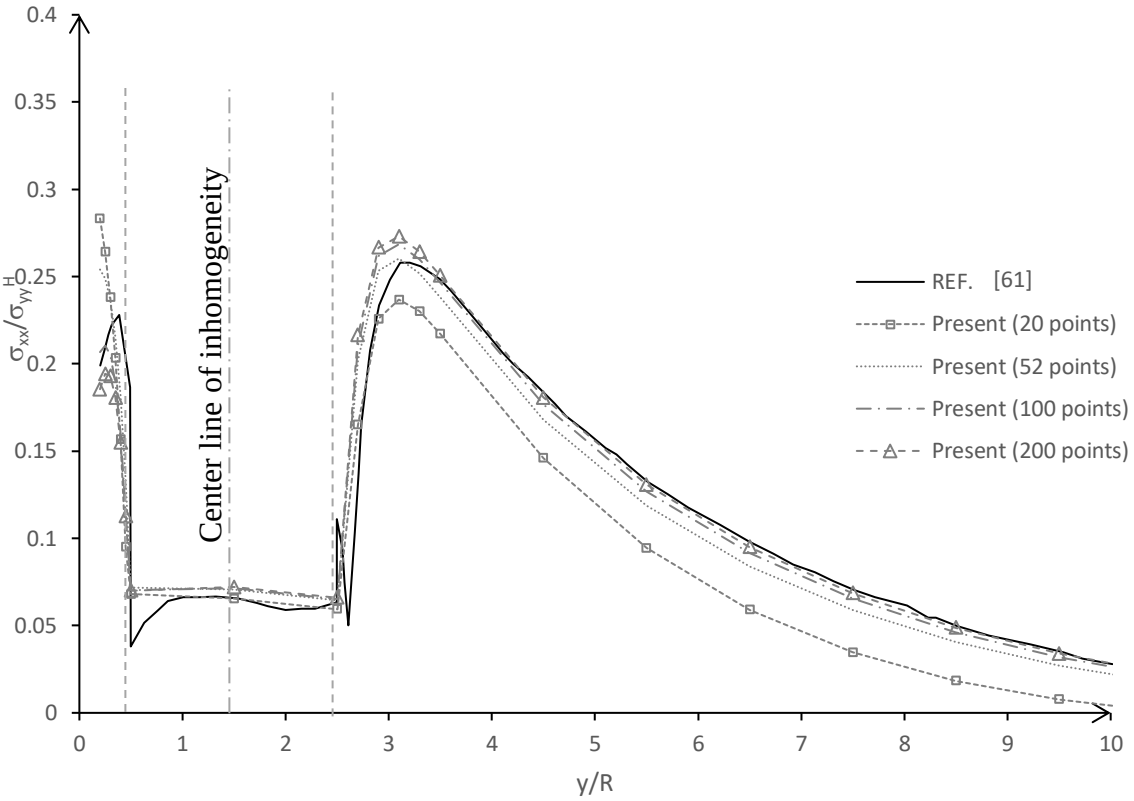

Fig.(3.9): Stress in the x-direction in example 3.7.2, case(2) (soft inhomogeneity).

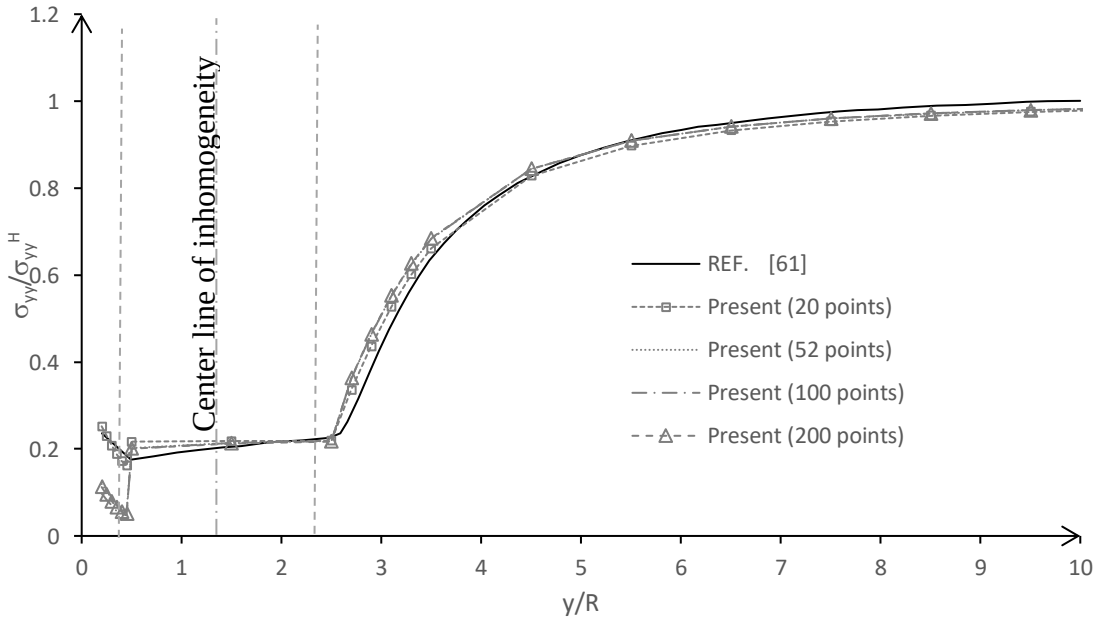

Fig.(3.10): Stress in the y-direction for example 3.7.2, case(2) (soft inhomogeneity).

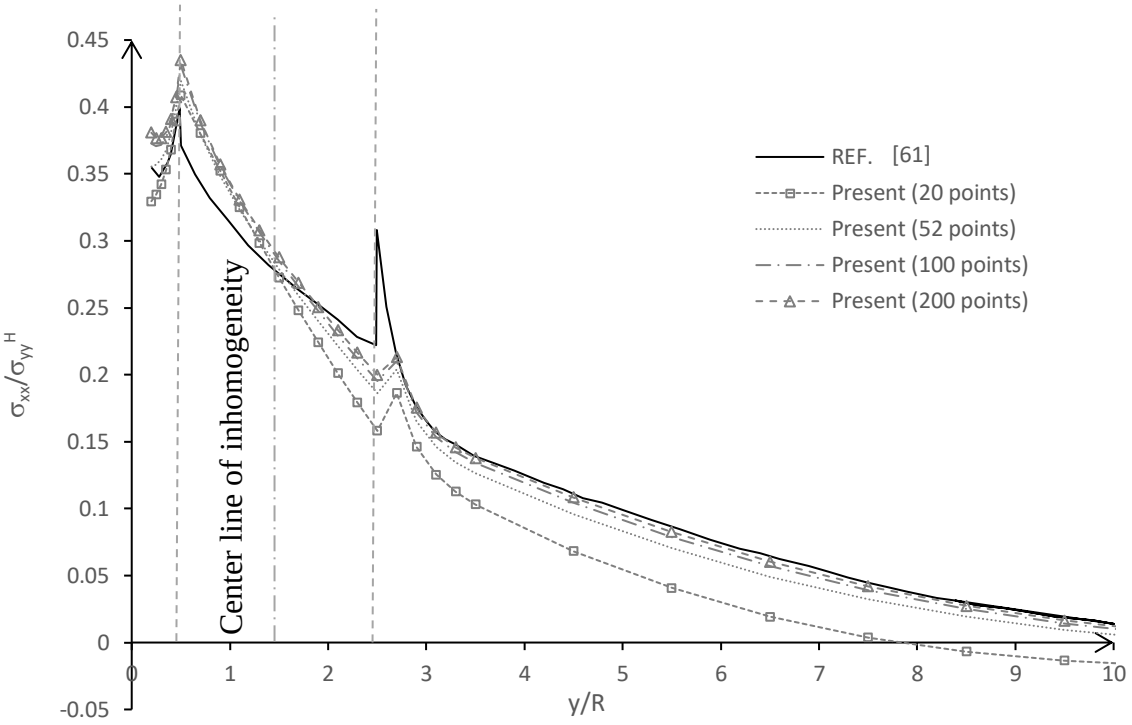

Fig.(3.11): Stress in the x-direction for example 3.7.2, case(2) (stiff inhomogeneity).

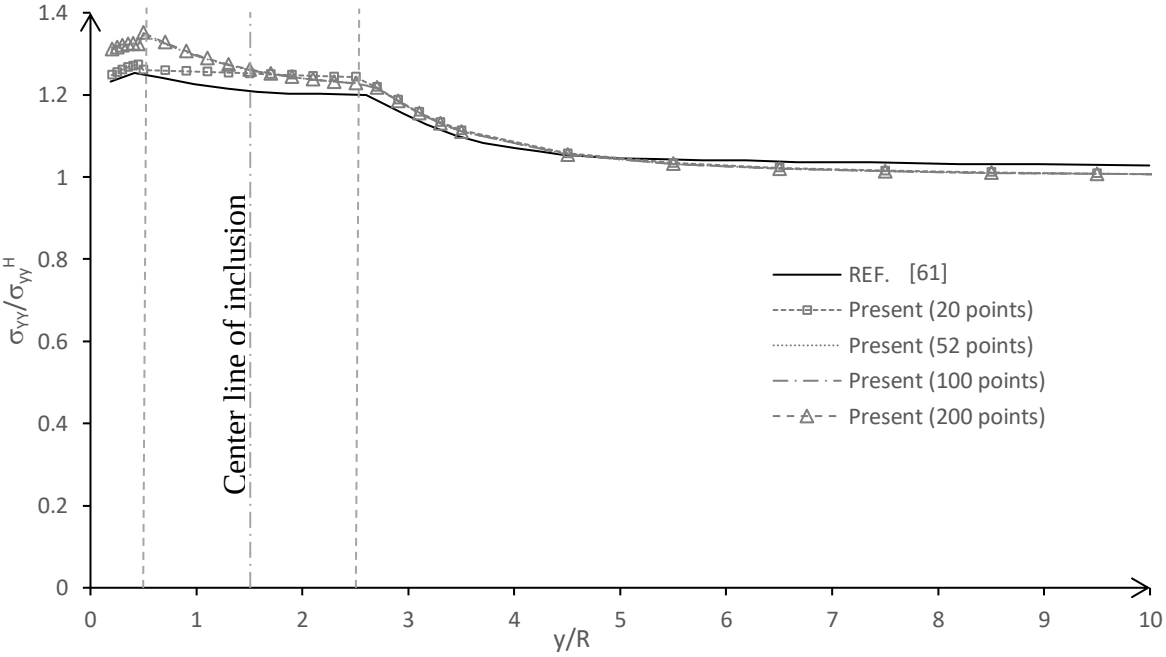

Fig.(3.12): Stress in the y-direction for example 3.7.2, case(2) (stiff inhomogeneity).

3.7.3.Square plate with two inhomogeneities

The square plate in example 3.7.2 is resolved herein with two inhomogeneities. These two inhomogeneities have the same radius as shown in Fig.(3.13) and has different radii as shown in Fig.(3.14).

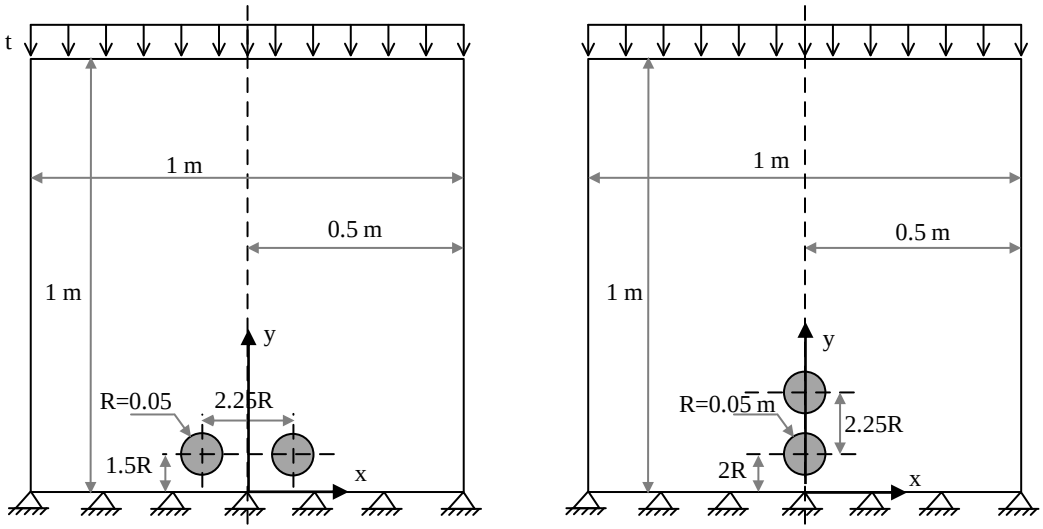

Fig.(3.13): Square plate with two equal diameter inhomogeneities in example 3.7.3.

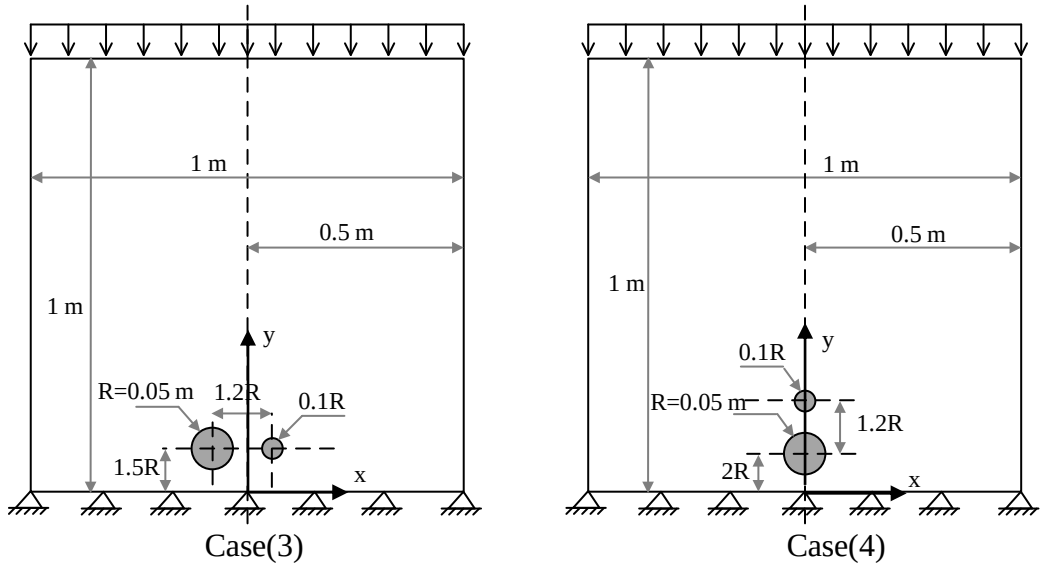

Fig.(3.14): Square plate with two unequal diameter inhomogeneities in example 3.7.3.

The same FSM points distributions in example 3.7.2 is reused herein. The problem is solved with the stiff inhomogeneity property, and the results are compared with those solved by Wu and Yin [61] using the DBIEM. Figures (3.15-3.26) demonstrate the stresses σ_{xx} and σ_{yy} for cases 1, 2, 3 and 4 (recall figures 3.13 and 3.14 for case definitions). It is clear from the figures that in case of equal diameter inhomogeneities, only 52 points is enough to capture good accuracy. In case of different diameters inhomogeneities, more points are needed (100 points) to reach a reasonable accuracy.

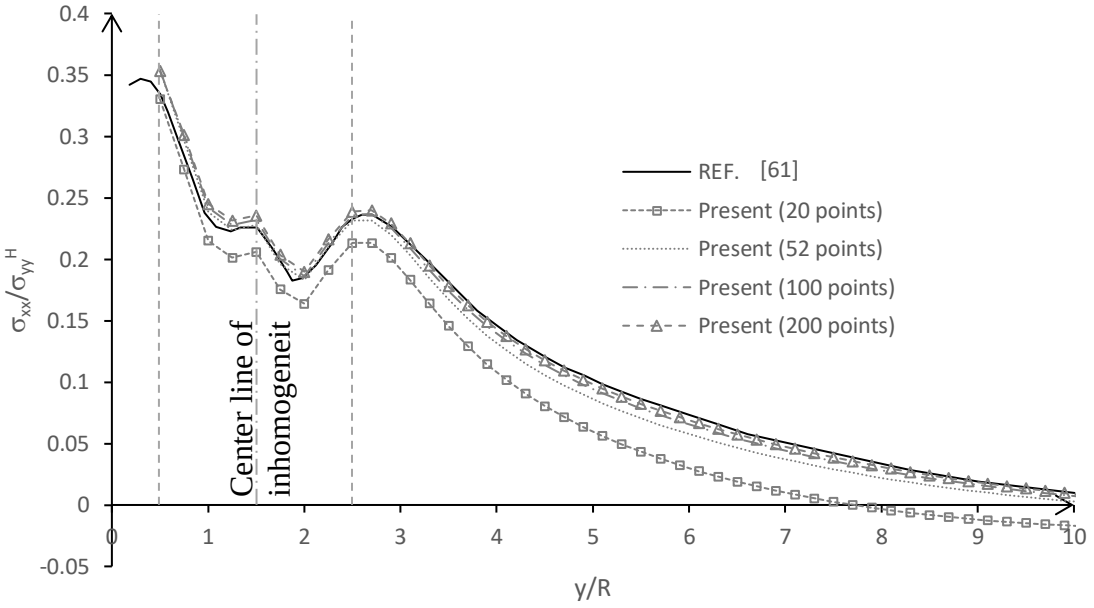

Fig.(3.15): Stress in the x-direction along the vertical dashed line (case 1) in example 3.7.3.

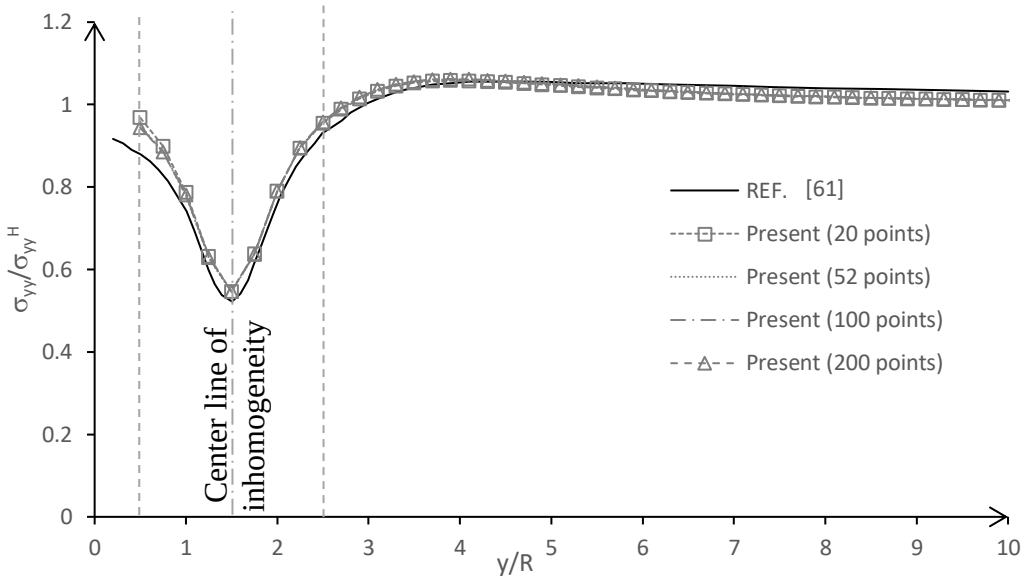

Fig.(3.16): Stress in the y-direction along the vertical dashed line (case 1) in example 3.7.3.

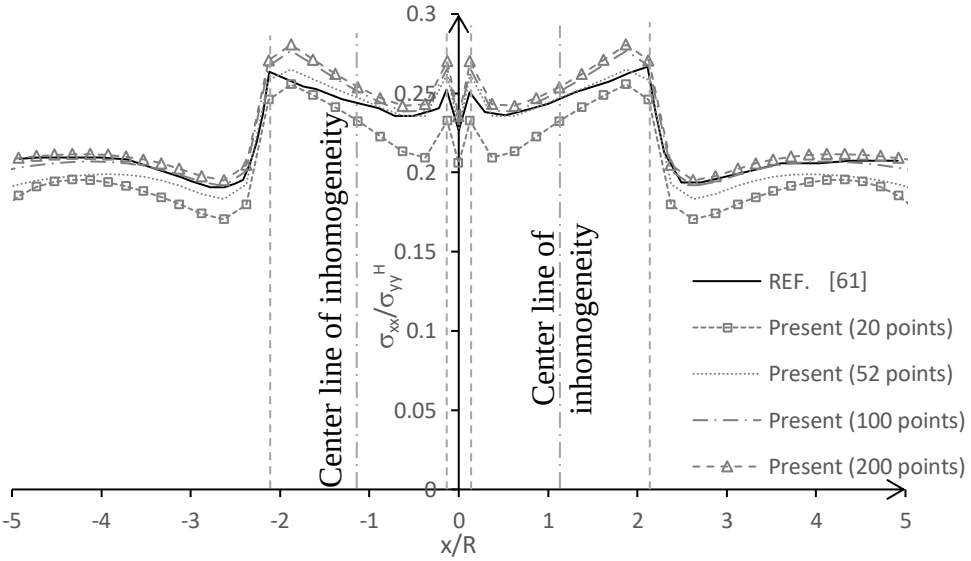

Fig.(3.17): Stress in the x-direction along the horizontal dashed line (case 1) in example 3.7.3.

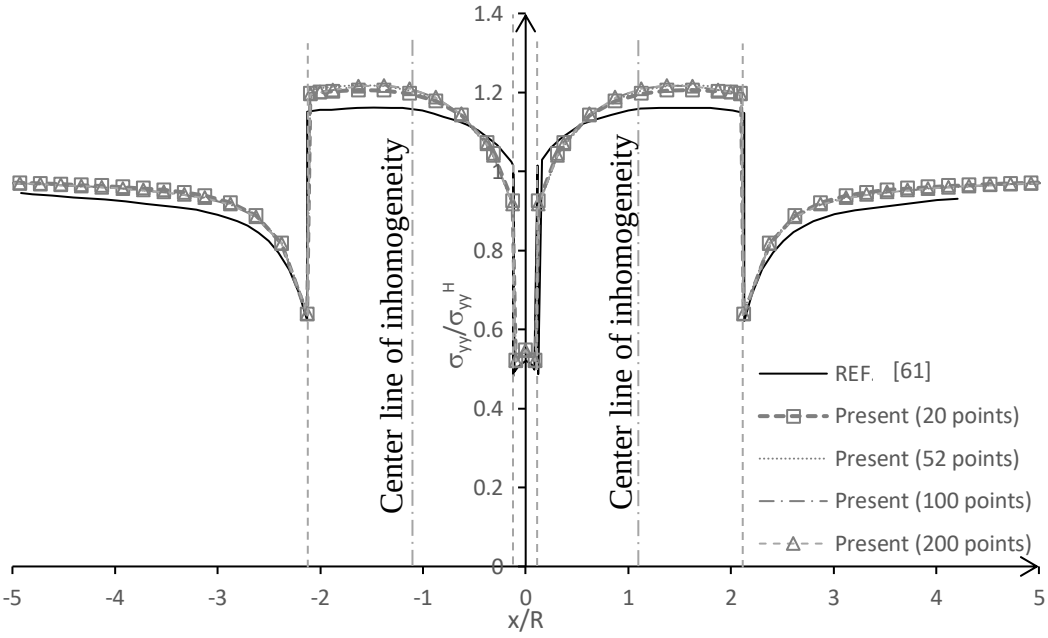

Fig.(3.18): Stress in the y-direction along the horizontal dashed line (case 1) in example 3.7.3.

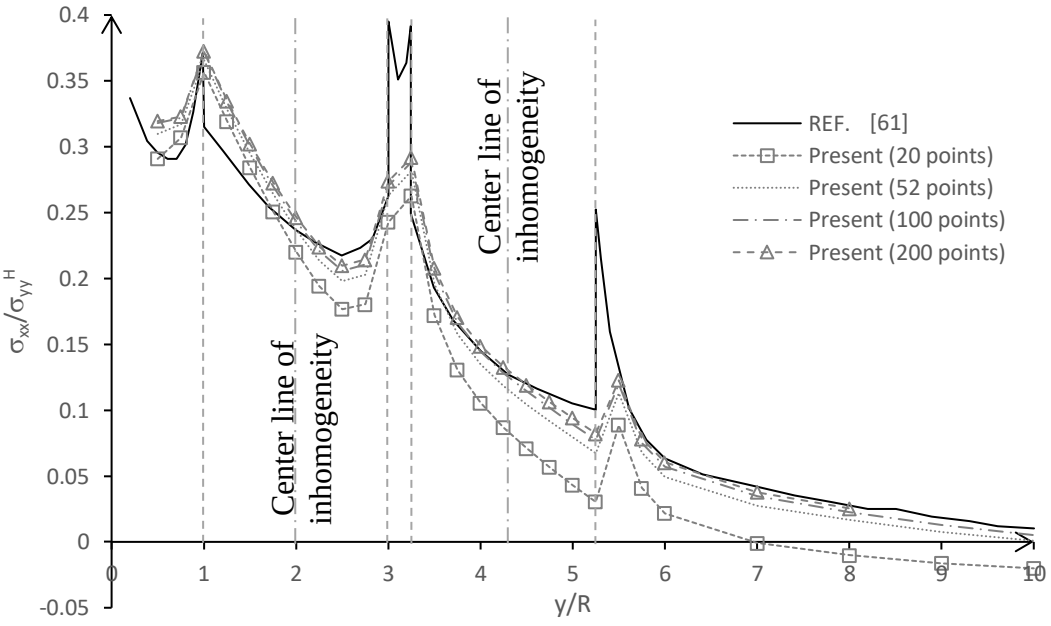

Fig.(3.19): Stress in the x-direction along the vertical dashed line (case 2) in example 3.7.3.

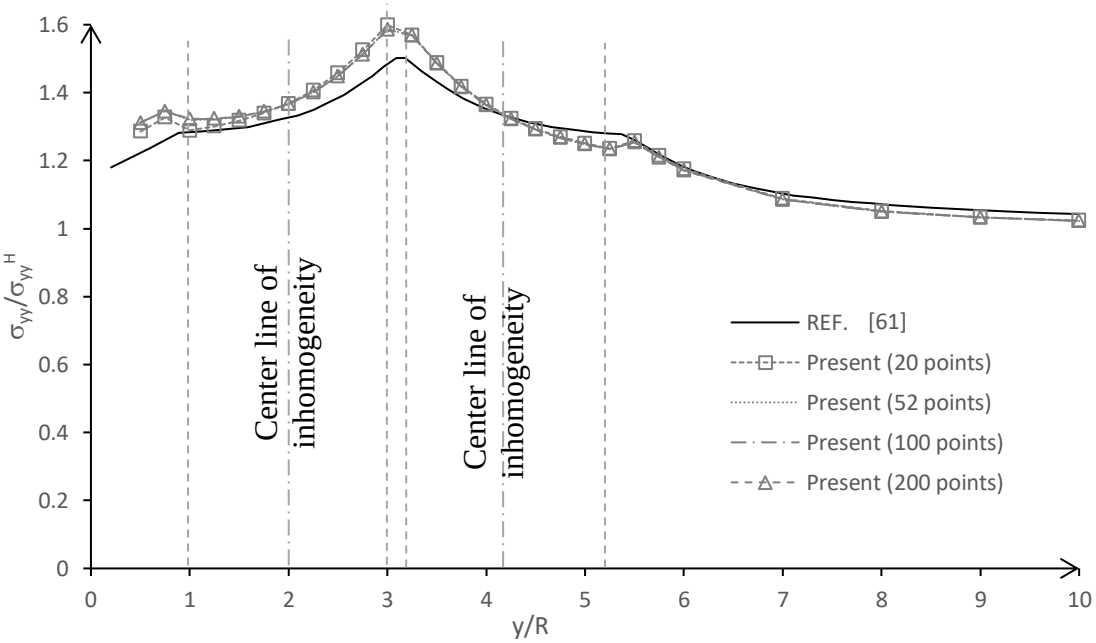

Fig.(3.20): Stress in the y-direction along the vertical dashed line (case 2) in example 3.7.3.

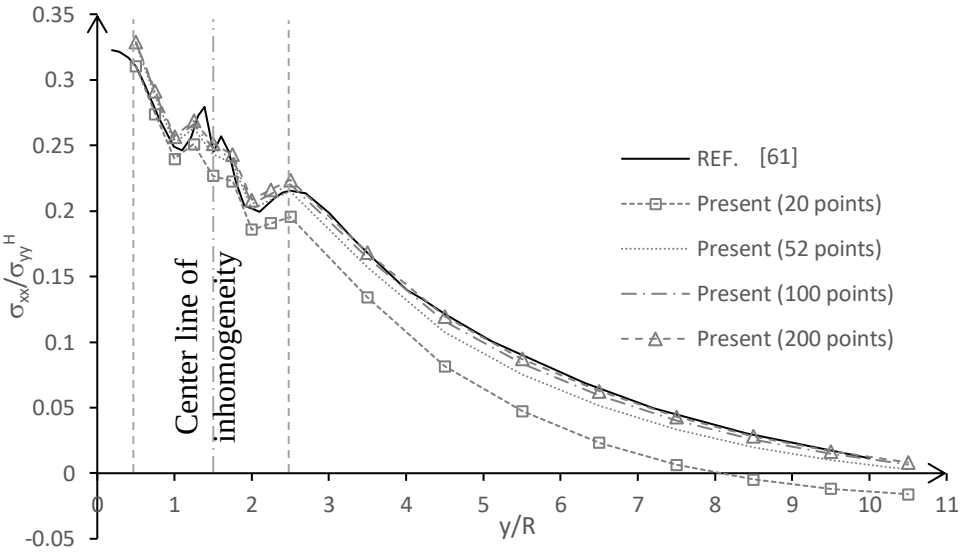

Fig.(3.21): Stress in the x-direction along the vertical dashed line (case 3) in example 3.7.3.

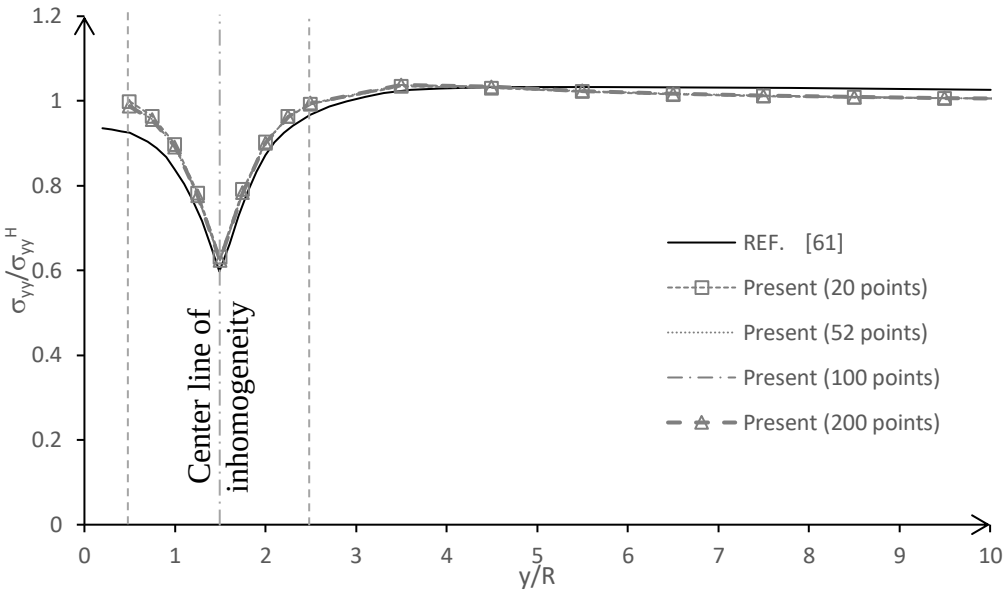

Fig.(3.22): Stress in the y-direction along the vertical dashed line (case 3) in example 3.7.3.

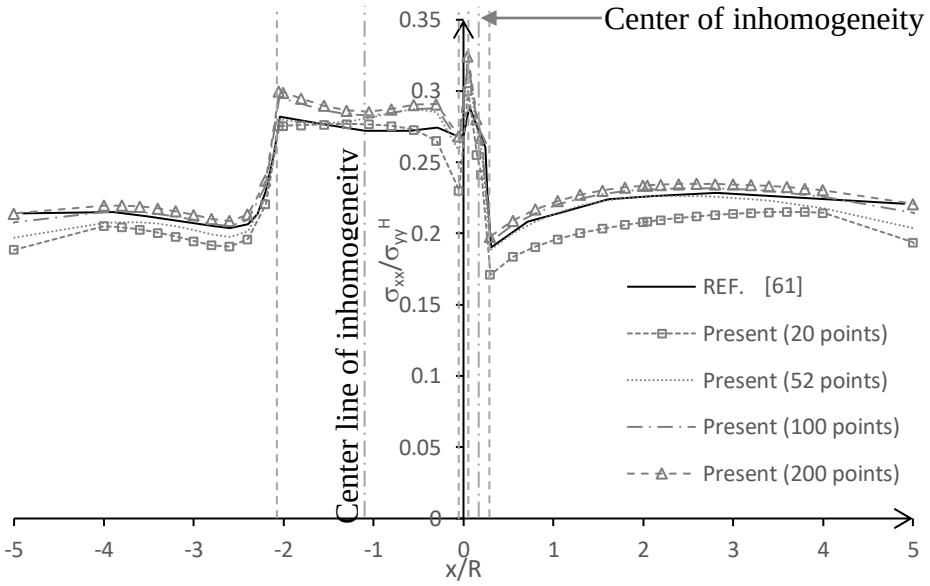

Fig.(3.23): Stress in the x-direction along the horizontal dashed line (case 3) in example 3.7.3.

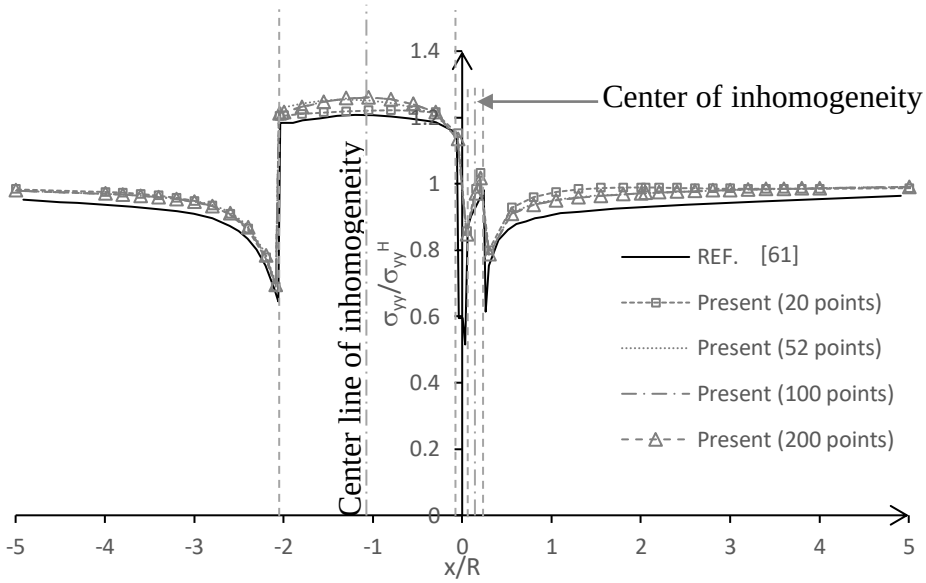

Fig.(3.24): Stress in the y-direction along the horizontal dashed line (case 3) in example 3.7.3.

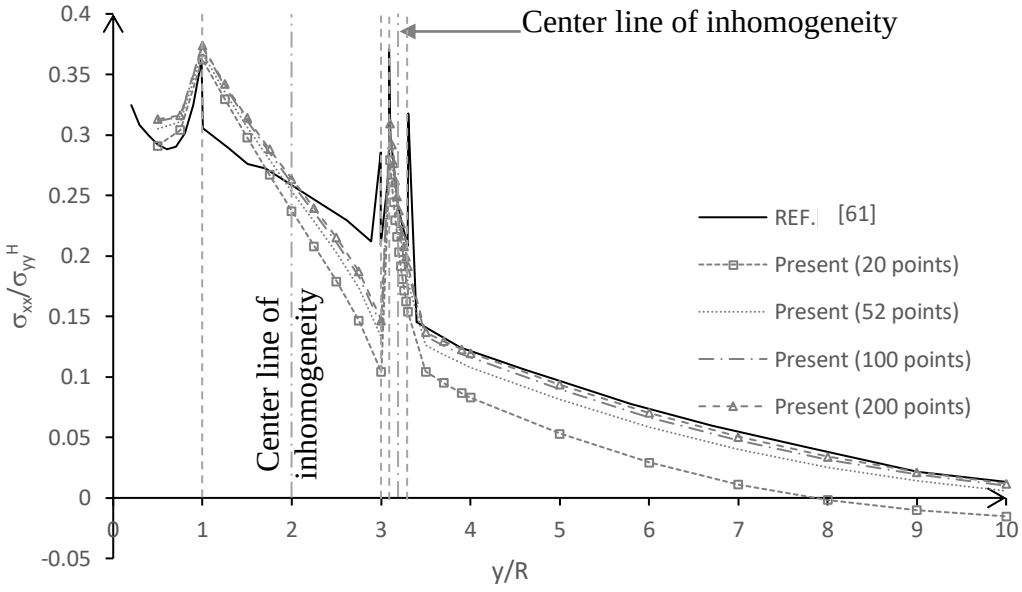

Fig.(3.25): Stress in the x-direction along the vertical dashed line (case 4) in example 3.7.3.

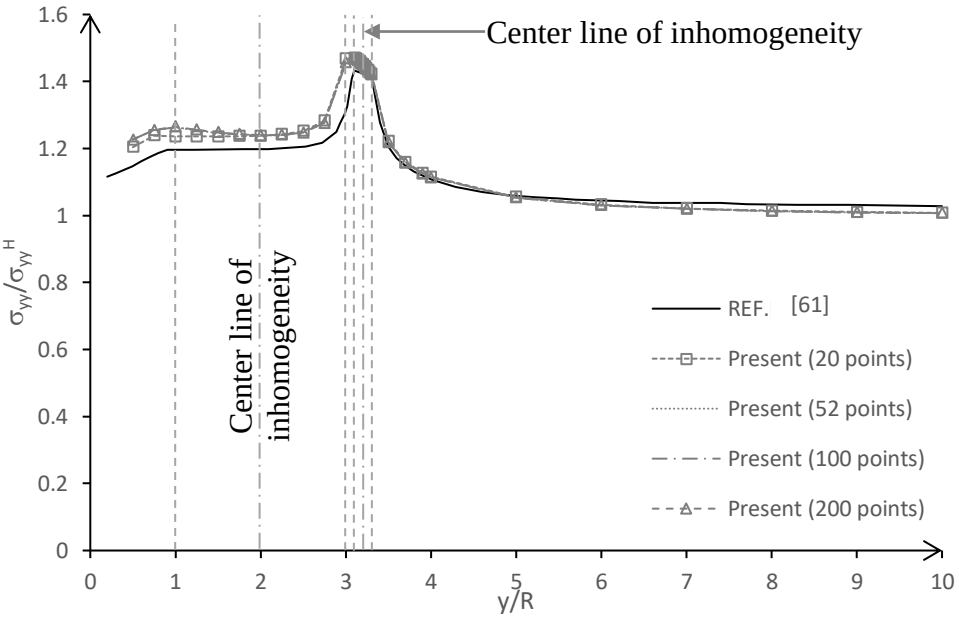

Fig.(3.26): Stress in the y-direction along the vertical dashed line (case 4) in example 3.7.3.

3.7.4.Tapered cantilever with voids

The tapered cantilever with voids shown in Fig.(3.27), is considered herein to test the ability of the proposed formulation to model several voids as inhomogeneities. In this example the present formulation results are compared to results of the FEM. Also, the two solution approaches (direct and iterative) are considered. The used material properties are E=10^6 N/m^2 and v=0.25.

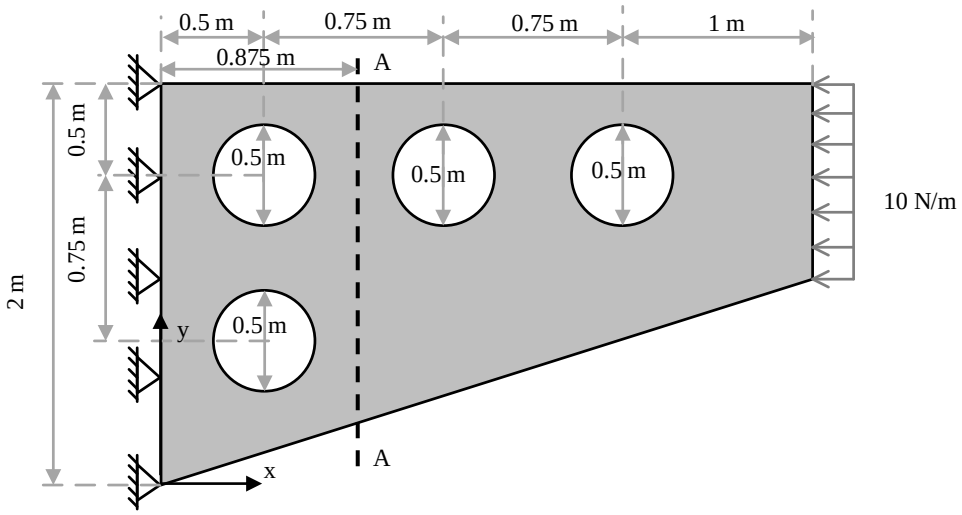

Fig.(3.27): The tapered cantilever in example 3.8.

Two sets of FSM points are used to simulate the problem, 391 and 782 FSM points, along the boundary of the problem (Fig.(3.28)). In the present analysis voids are treated as an equivalent inclusion with E=0. The problem is also solved also using FEM with two discretizations 932 and 4045 four-noded quadratic elements as shown in Fig.(3.29).

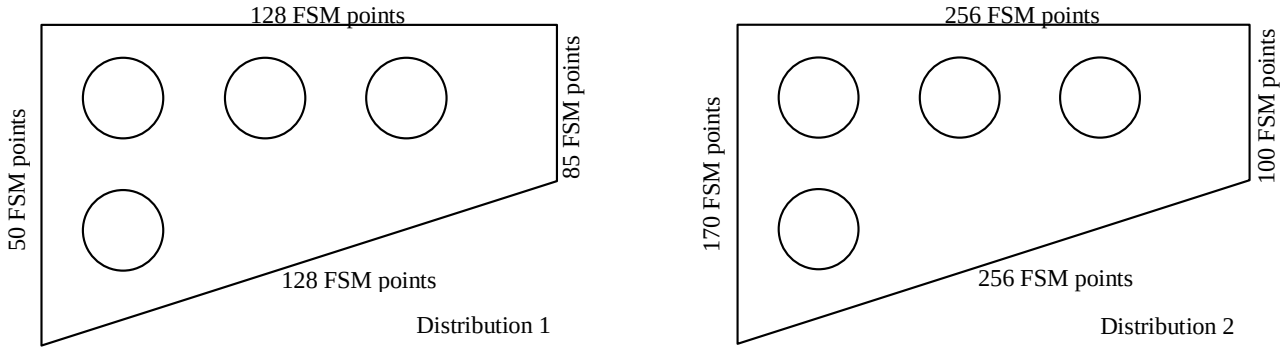

Fig.(3.28): The FSM points distribution in example 3.8.

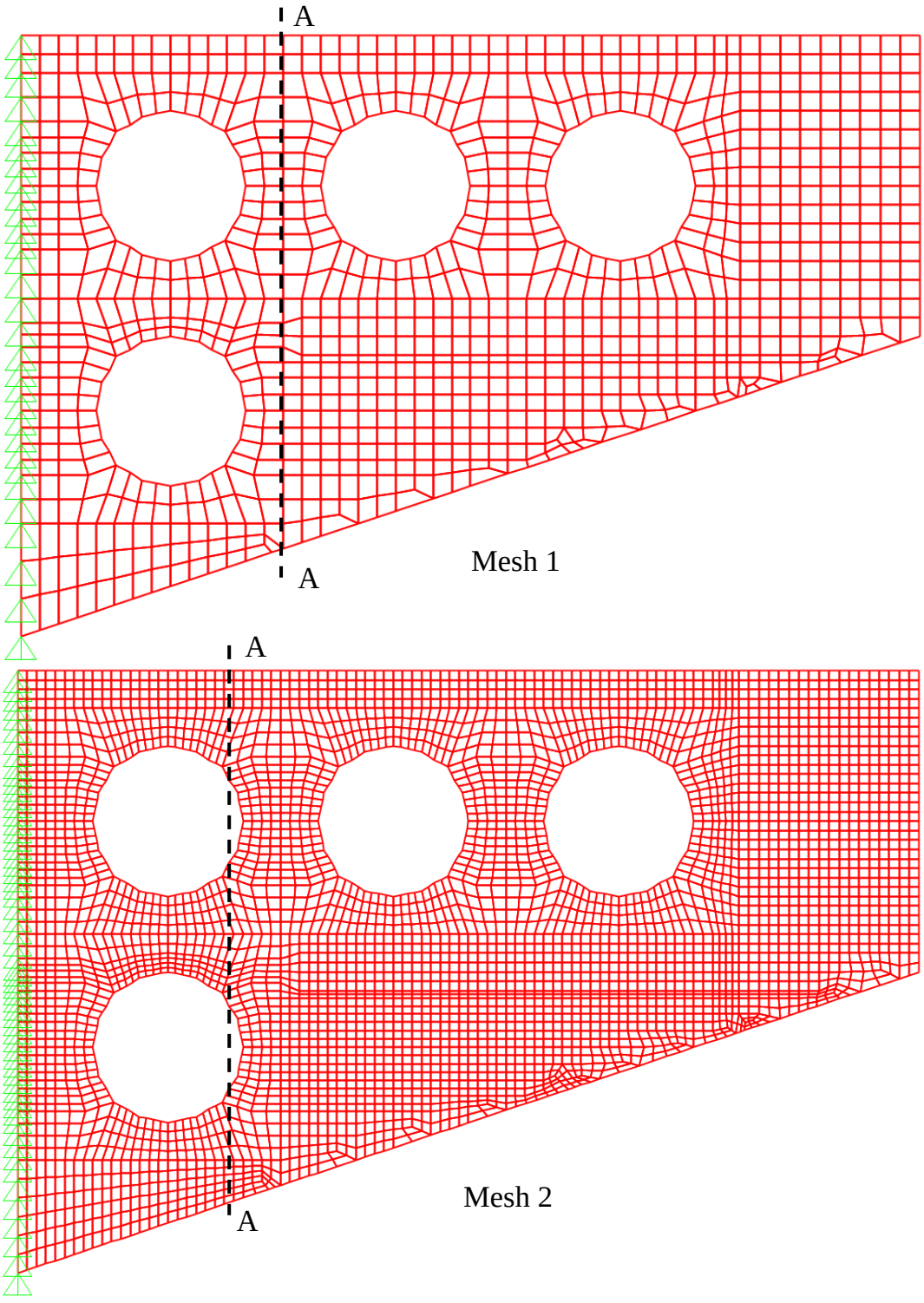

Fig.(3.29): The used FEM discretization in example 3.8.

Figures (3.30-3.32) demonstrate the stresses σ_{xx}, σ_{yy} and σ_{xy} at section A-A (recall Fig.(3.27)) for both approaches (direct and iterative) compared to that of the FEM. Excellent agreements between results are observed. The deformed shape is demonstrated in Fig.(3.33) compared to that of the FEM.

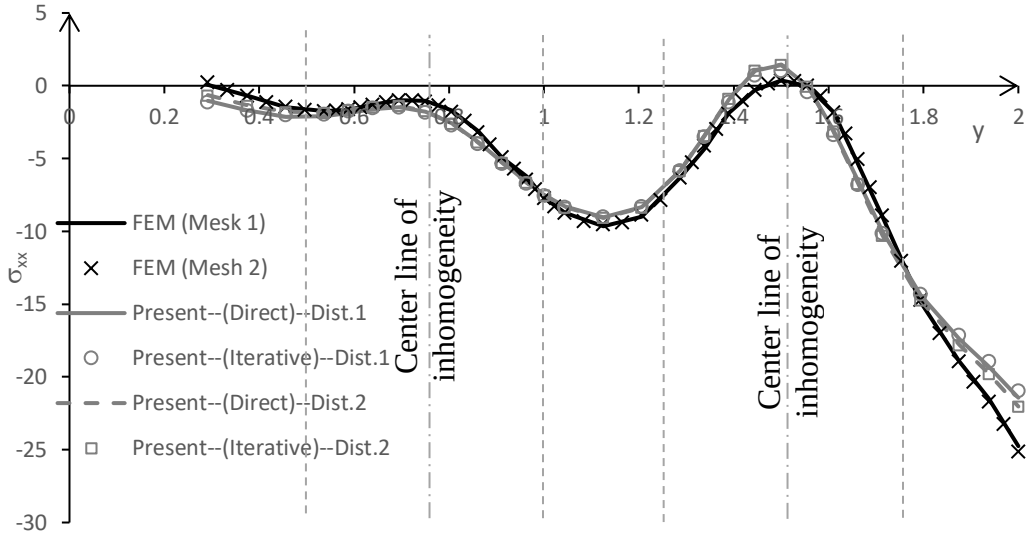

Fig.(3.30): Stresses in x-direction along section A-A in example 3.8.

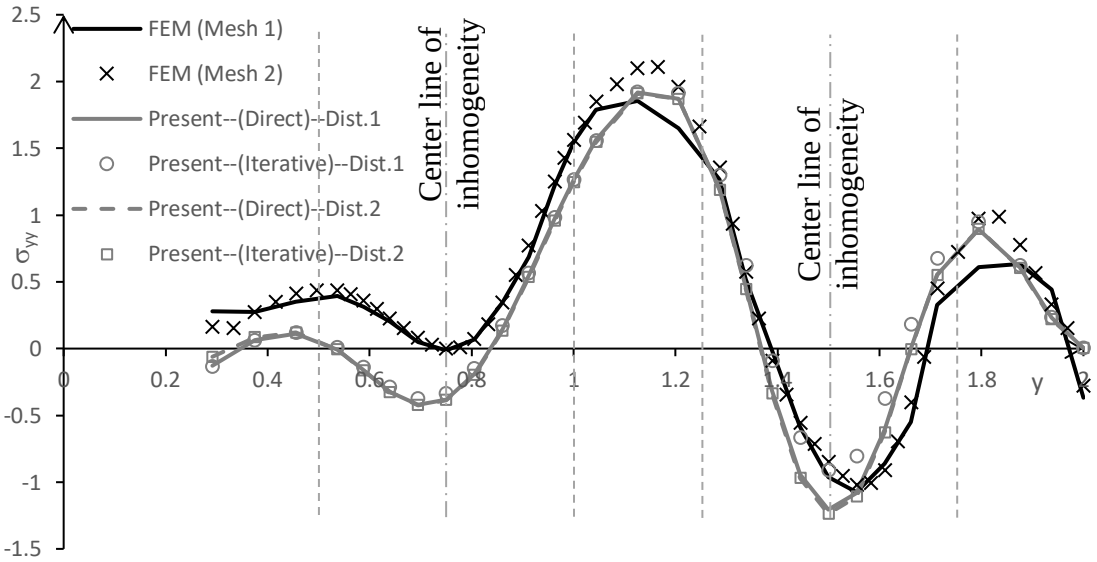

Fig.(3.31): Stresses in y-direction along section A-A for example 3.8.

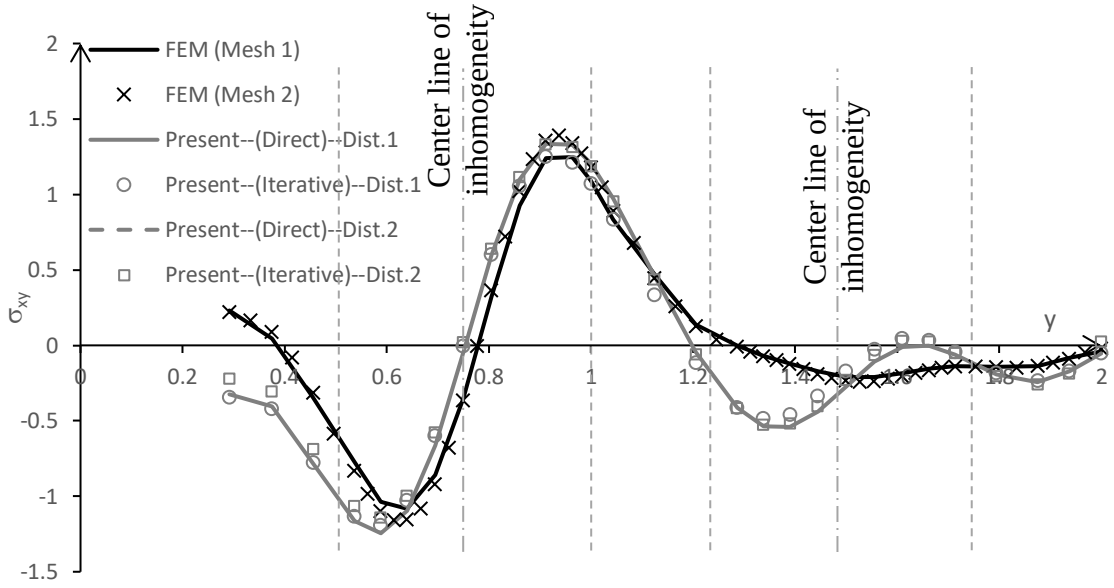

Fig.(3.32): Shear Stresses along section A-A for example 3.8.

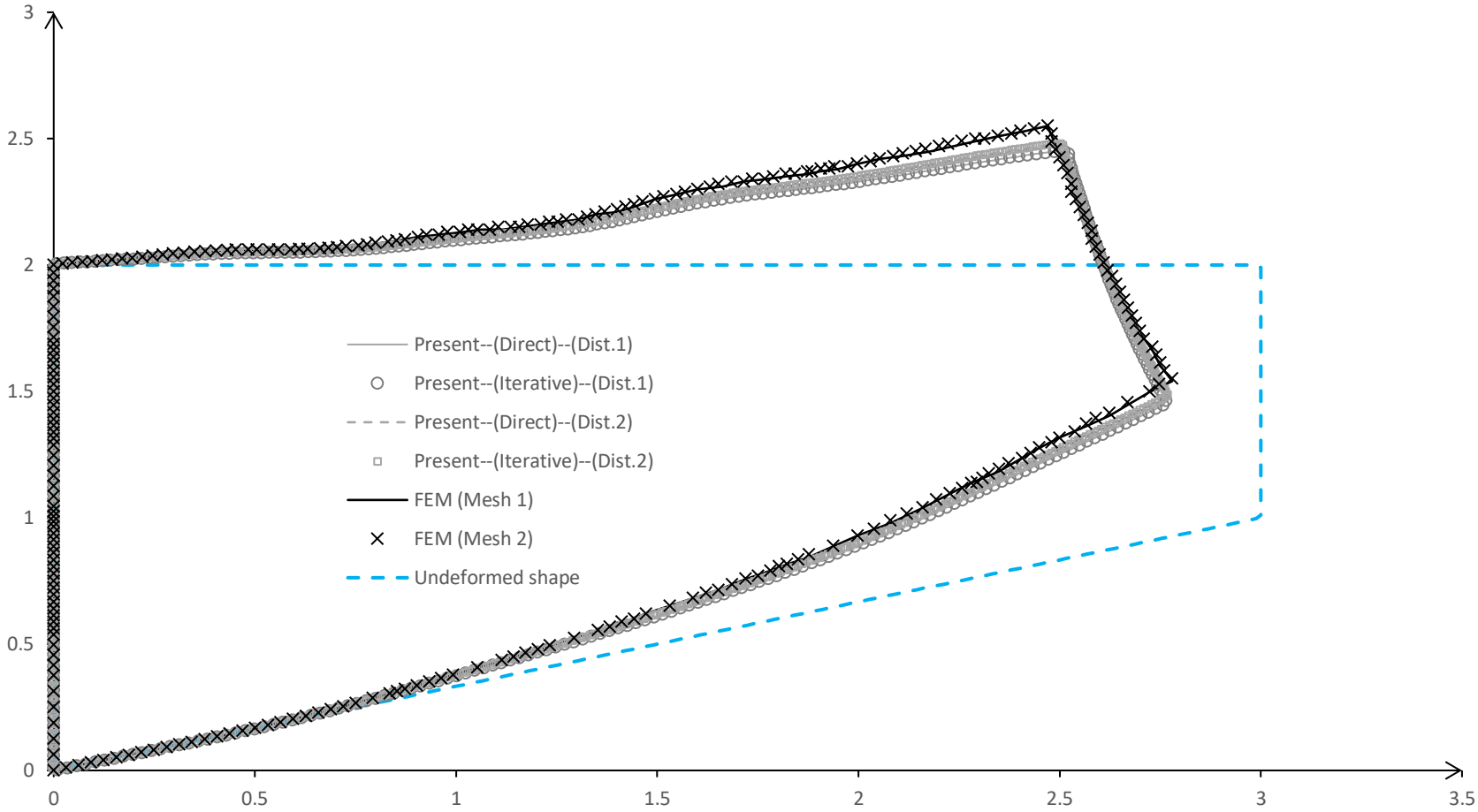

Fig.(3.33): The deformed shape in example 3.8.

3.7.5.Bar with inhomogeneities

The bar containing array of inhomogeneities shown in Fig.(3.34) is considered in this example. The purpose of this example is to compare the difference in computational time between the direct approach and iterative approach with respect to that of the FEM. The bar contains 1729 circular inhomogeneities. The material properties of the matrix are $E_o=10^6$ N/m^2 and $\nu=0$, and for the inhomogeneities is $E=\alpha E_o$, where α takes values between 0 to 0.8.

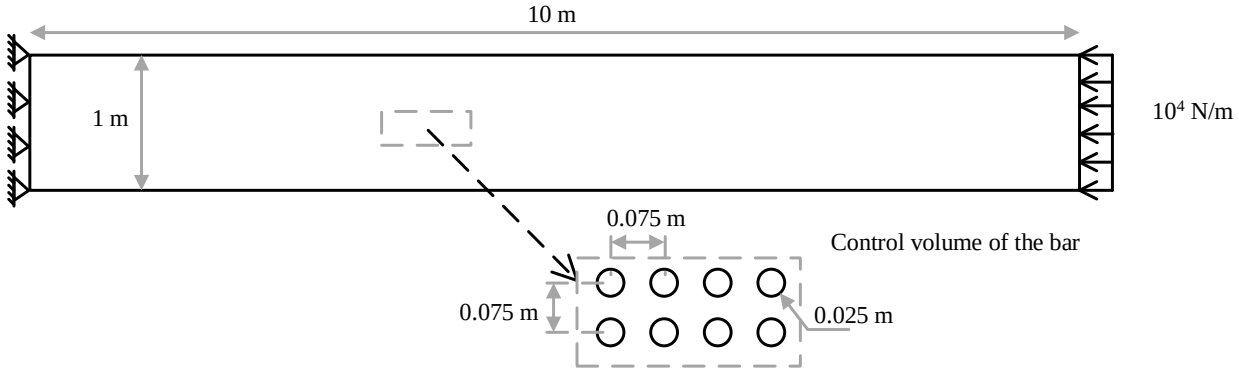

Fig.(3.34): The bar in example 3.9.

The problem is solved using the present formulation using 240 FSM points (100 points on the long sides and 20 points in the short ones). Also, it is solved using the FEM using 256000 four-noded quadratic finite elements (FE) for sake of comparison. Figure (3.35) demonstrates the used FE mesh for the shown control volume in Fig.(3.34). It has to be noted that in case of voids ($\alpha=0$), the number of the used FE is decreased to 145344 elements.

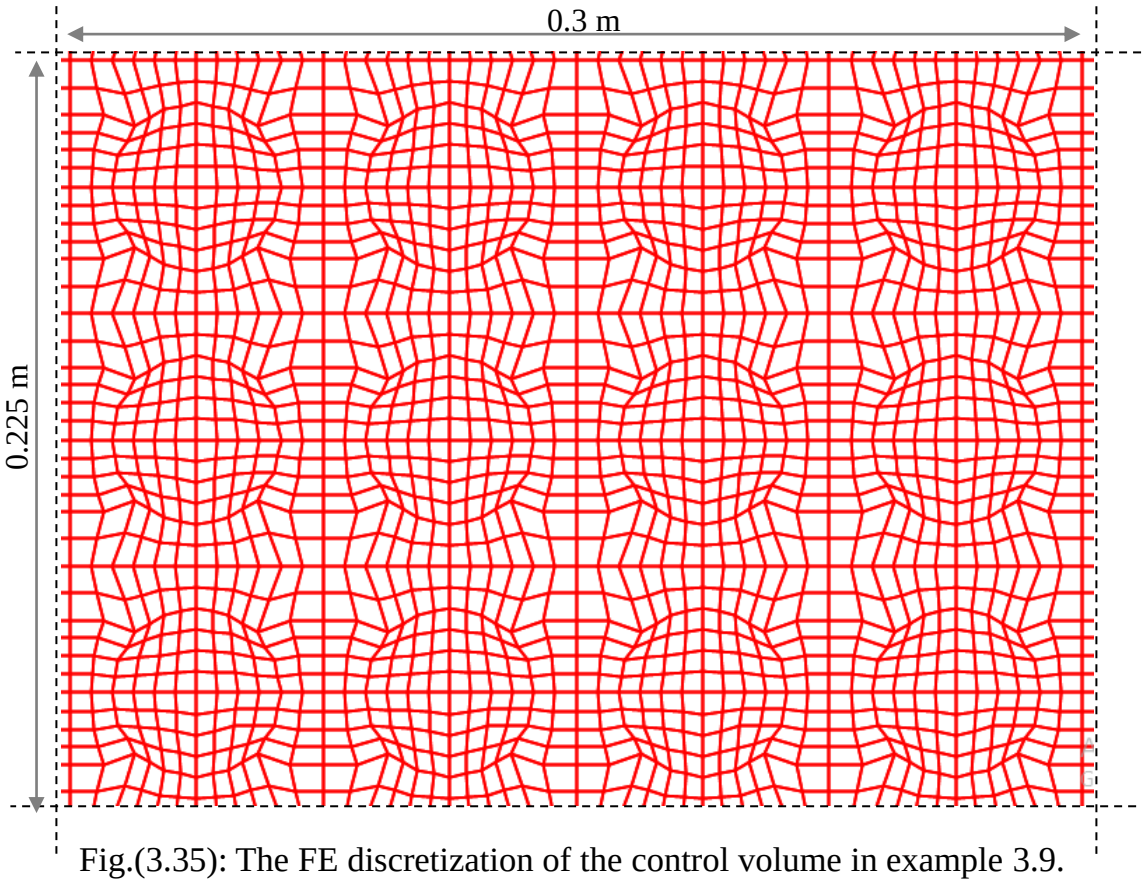

Fig.(3.35): The FE discretization of the control volume in example 3.9.

Figure (3.36) demonstrates the bar tip displacement for different α cases for both direct and iterative approaches together with the corresponding FEM results.

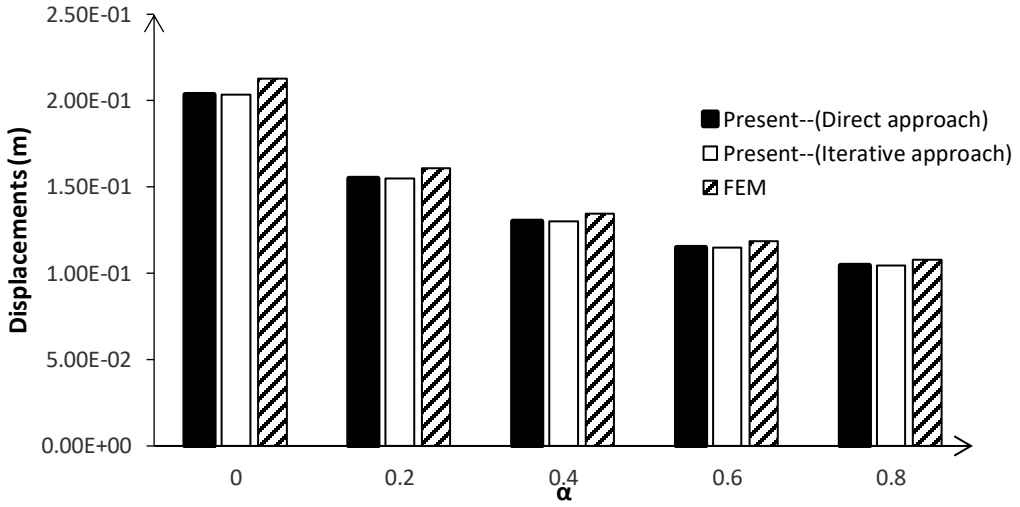

Fig.(3.36): The bar tip displacement for example 3.9.

It is clear form Fig.(3.36) that the results of the present formulation agree well with the results of the FEM. Figure (3.37), demonstrates the elapsed time of calculation. It has to be noted that such values are computed using Intel(R) Core(TM) i7-2630QM CPU@ 2.00 GHz computer.

The shown results of the FEM are obtained using commercial package with GPU computing technology. It can be seen that the results of the present formulation (which do not employ parallel computing) is comparable to the FEM. Therefore, considering the present formulation with GPU or multicore will improve the elapsed time dramatically.

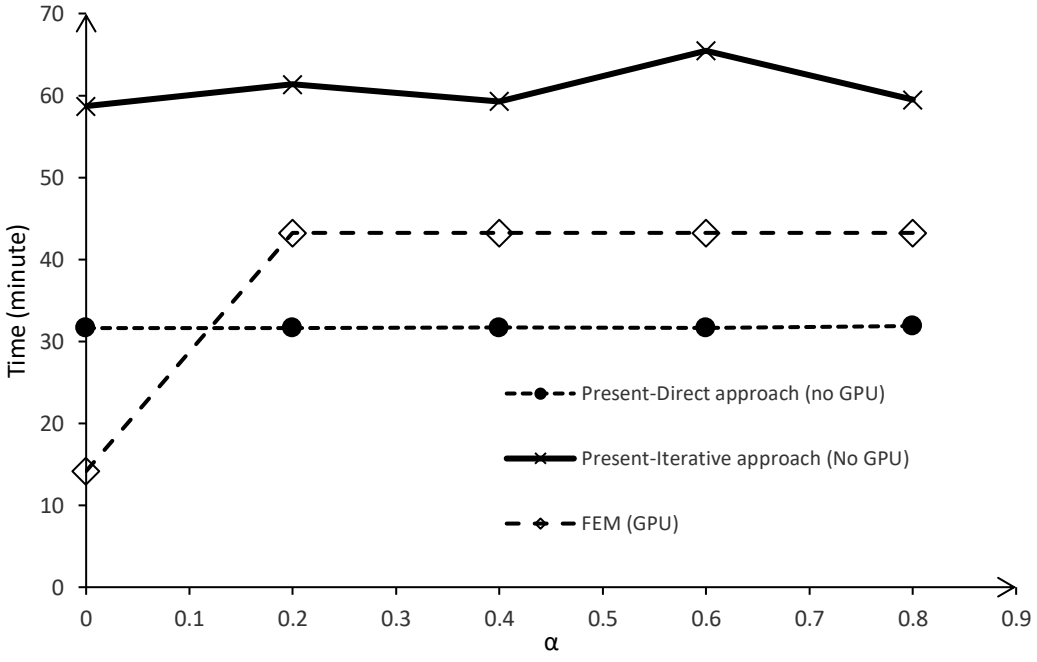

Fig.(3.37): Elapsed time of computation in example 3.9.

3.8. Conclusions

In this chapter, the FSM as a meshless technique is coupled with the Eshelby's equivalent inclusion theory to model the inhomogeneity problem. Here, no domain discretization was needed as the analytical solutions for circular inclusions were presented. Also, only FSM points were distributed on the boundary to solve the problem. Although constant distribution of sources was used and also constant eigenstrain was assumed in the equivalent inclusion, the results demonstrated good agreement with those of analytical solutions, the DBIEM and the FEM as demonstrated in the numerical examples (Sec.3.7). Two alternative techniques were presented for the solution, i.e. direct and iterative. It was demonstrated that the computation time of the present formulation without parallel computing is comparable to that of the FEM with GPU computational core. This concludes that implementing parallel computing to the present formulation will speed it up dramatically making it positioned for practical applications in materials.

Chapter 4: Damage simulation in Direct BIE

4.1. Introduction

In this chapter a new explicit boundary element modeling for the nonlocal damage is introduced. Despite the damage occurred inside the domain, the problem boundary is only discretized. The change in the material properties due to damage is introduced by coupling Eshelby's equivalent inclusion theory [16,19,20,42] with the direct boundary element equations. At any arbitrary point when the internal strain exceeds the threshold strain, an equivalent inclusion is inserted with a prescribed eigenstrain to model the damaged material property due to damage level, making the damage be represented explicitly. A finite-element like stiffness matrix is formulated from the proposed coupled integral equations. Such a stiffness is obtained in a condensed form on the problem boundary directly. The new system of equations is nonlinear as material properties are changed with the problem deformation. This system is solved using the load control secant algorithm [48]. It has to be noted that, in the present formulation, no prior knowledge of the damage locations is required. Some examples are solved to verify the proposed formulation. Also, a parametric study on the parameters affecting the results (number of boundary elements, inclusion diameter, inclusion pattern, residual *tolerance* and maximum number of iterations) is done.

4.2. Boundary integral equation formulation

The displacement boundary integral equation for 2D elasticity containing (*NOI*) non-homogeneities or equivalent inclusions (see Fig.(4.1)) is [19,20]:

$$c_{ij}(\xi)u_j(\xi) = \int_{\Gamma} U_{ij}^{*}(\xi, x)t_j(\mathrm{x})d\Gamma(\mathrm{x}) - \int_{\Gamma} T_{ij}^{*}(\xi, \mathrm{x})u_j(\mathrm{x})d\Gamma(\mathrm{x}) + \sum_{\mathrm{I}=1}^{\mathrm{I}=NOI} \varepsilon_{jk}^{o}(\mathrm{x}_I) \int_{\Omega_{\mathrm{I}}} \sigma_{ijk}^{*}(\xi, \mathrm{x}_I)\mathrm{d}\Omega_{\mathrm{I}}(\mathrm{x}_I) \tag{4.1}$$

In this chapter, the introduced circular inclusions are considered to be small in size, hence the domain integral in Eq. (4.1) is computed as follows:

$$\sum_{I=1}^{I=NOI} \varepsilon_{jk}^{o}(\mathrm{x}_I) \int_{\Omega_{\mathrm{I}}} \sigma_{ijk}^{*}(\xi, \mathrm{x}_I)\mathrm{d}\Omega_{\mathrm{I}}(\mathrm{x}_I) = \sum_{I=1}^{I=NOI} \varepsilon_{jk}^{o}(\mathrm{x}_I)\sigma_{ijk}^{*}(\xi, \mathrm{x}_I)\mathrm{A}_I \tag{4.2}$$

Where, A_I is the area of inclusion number *I*.

The boundary integral equation for the strains as in chapter 2:

$$\varepsilon_{im}(\xi) = \int_{\Gamma} U_{ijm}^{*}(\xi, \mathrm{x})t_j(\mathrm{x})d\Gamma(\mathrm{x}) - \int_{\Gamma} T_{ijm}^{*}(\xi, \mathrm{x})u_j(\mathrm{x})d\Gamma(\mathrm{x}) + f_{im}(\xi) \tag{4.3}$$

The new kernels U_{ijm}^{*} and T_{ijm}^{*} are as given in chapter 2. When the strain $\varepsilon_{im}(\xi)$ is calculated outside the inclusion i.e. $\xi \notin \Omega_{\mathrm{I}}$, $f_{im}(\xi)$ could be computed as follows:

$$f_{im}(\xi) = \sum_{I=1}^{I=NOI} \varepsilon_{jk}^{o}(\mathrm{x}_I) \int_{\Omega_{\mathrm{I}}} O_{imjk}^{*}(\xi, \mathrm{x})\mathrm{d}\Omega_{\mathrm{I}}(\mathrm{x}) \tag{4.4}$$

The expression of the new kernel $O_{imjk}^{*}(\xi, \mathrm{x})$ is also as given in chapter 2. Similar to Eq. (4.1) the domain integral in Eq. (4.4) is computed as follows:

$$f_{im}(\xi) = \sum_{I=1}^{I=NOI} \varepsilon_{jk}^{o}(\mathrm{x}_I)O_{imjk}^{*}(\xi, \mathrm{x})\mathrm{A}_I \tag{4.5}$$

On the other hand, when the strain $\varepsilon_{im}(\xi)$ is calculated at the center of the inclusion i.e. ($\xi \in \Omega_I$), the term $f_{im}(\xi)$ could be computed as follows [7]:

$$f_{im}(\xi) = \frac{1}{8(1-\nu)}[(6-8\upsilon)\varepsilon^{o}_{im} - (1-4\upsilon)\varepsilon^{o}_{ll}\delta_{im}] \tag{4.6}$$

Where, ν and δ_{im} are Poisson's ratio of the domain and the Kronecker delta symbol, respectively.

For the matrix $[ek]$ (see Eq.(2.52)) it will be approximated by eliminating the inclusion-inclusion interaction.

$[ek]_{3\times3}$ is defined for one inclusion as follows:

$$[ek] = \begin{bmatrix} C_1 - S_{1111} & -2S_{1112} & -C_2 - S_{1122} \\ -S_{1211} & \frac{1}{B} - 2S_{1212} & -S_{1222} \\ -C_1 - S_{2211} & -2S_{2212} & C_2 - S_{2222} \end{bmatrix} \tag{4.7}$$

in which, C_1, C_2, B, A and C are as given in chapter 2 Eqs.(2.47-2.51)

4.3. The proposed nonlinear matrix equations

The basic idea of this chapter is to represent the domain stiffness degradation during loading by inserting virtual inclusions at damaged places. Then the non-homogeneous problem is converted to homogeneous one via Eshelby's eigenstrains. These eigenstrain values are varying during loading resulting in a nonlinear behavior of equations.

In this section the BIE (recall section 4.2) is rewritten in a form to facilitate applying the proposed idea. The discretization is carried out on the problem boundary, the domain is covered by investigation points (see Fig.(4.1)) at which the strain is calculated and checked to decide whether the material is damaged or

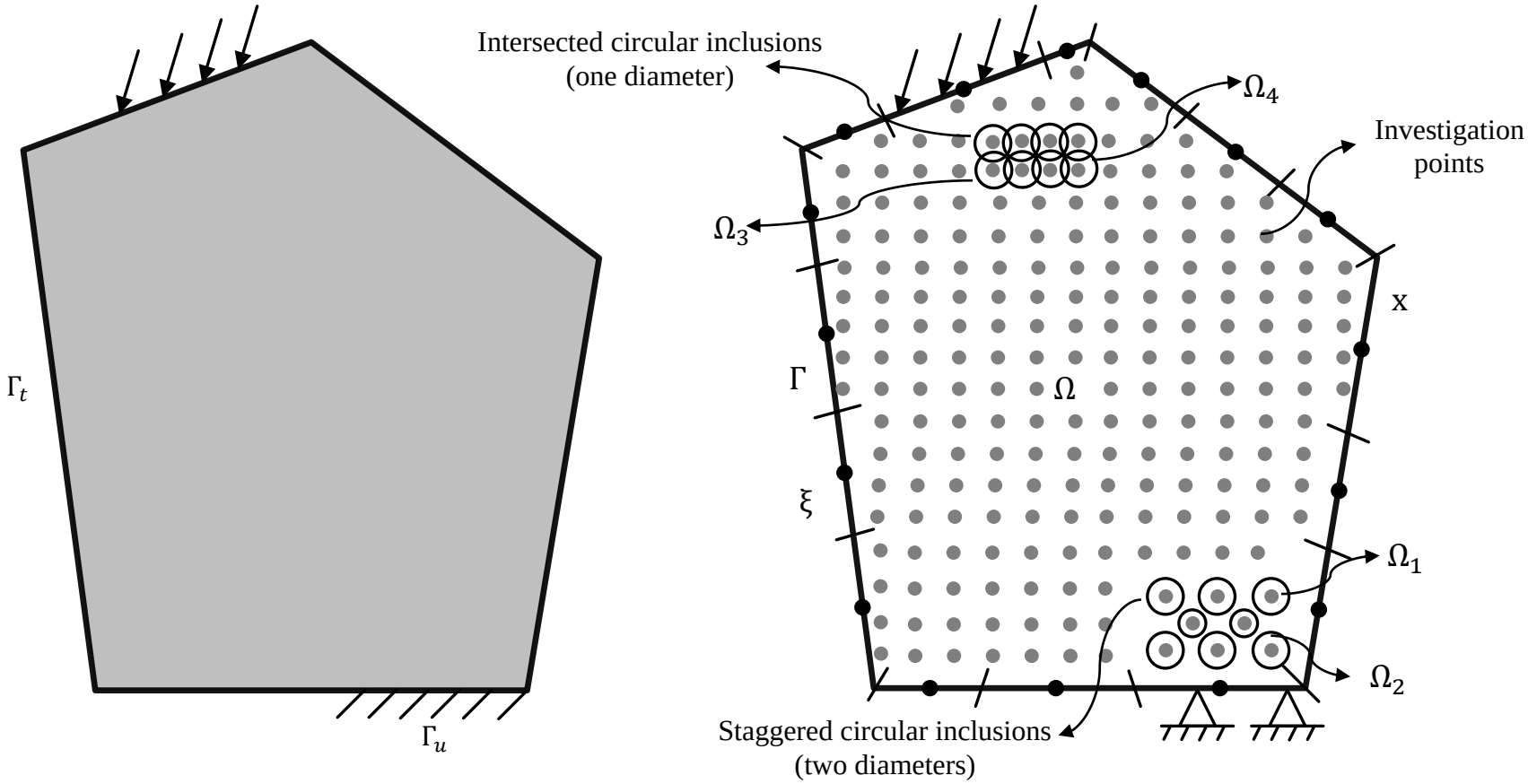

a) Actual problem

b) Discretized problem

Fig.(4.1): The actual and the discretized problems.

not. If an investigation point is damaged, a small virtual circular inclusion is inserted.

The problem is discretized into *N* boundary nodes, *NE* boundary elements (without losing the generality, quadratic boundary elements are used). At a certain damage level with a number of inclusions indicated as *NOI*, Eq. (4.1) could be rewritten in a matrix form as follows:

$$\begin{aligned}\left[G_{ij}(\xi,\mathrm{x})\right]_{2N\times 6NE}\left\{t_j(\mathrm{x})\right\}_{6NE\times 1}-\left[H_{ij}(\xi,\mathrm{x})\right]_{2N\times 2N}\left\{u_j(\mathrm{x})\right\}_{2N\times 1}\\ +\left[B_{ijk}(\xi,\mathrm{x})\right]_{2N\times 3NOI}\left\{\varepsilon^{o}_{jk}\right\}_{3NOI\times 1}=\{0\}_{2N\times 1}\end{aligned} \tag{4.8}$$

Where $\left[G_{ij}\right]$, $\left[H_{ij}\right]$ and $\left[B_{ijk}\right]$ are well known influence matrices.

In a similar way, Eq. (4.3) could be rewritten in a matrix form (without the eigenstrain term) as follows:

$$\begin{aligned}\{\varepsilon_{im}(\xi)\}^{\text{applied}}_{3NOI\times 1}=\left[\bar{G}_{ijm}(\xi,\mathrm{x})\right]_{3NOI\times 6NE}\left\{t_j(\mathrm{x})\right\}_{6NE\times 1}\\ -\left[\bar{H}_{ijm}(\xi,\mathrm{x})\right]_{3NOI\times 2N}\left\{u_j(\mathrm{x})\right\}_{2N\times 1}\end{aligned} \tag{4.9}$$

Where $\left[\bar{G}_{ijm}\right]$ and $\left[\bar{H}_{ijm}\right]$ are the derivative of the influence matrices.

Substituting from Eq. (2.52) into Eq. (4.9), gives:

$$\begin{aligned}\{\varepsilon^{o}_{lk}\}_{3NOI\times 1}=[ek_{imlk}]^{-1}_{3NOI\times 3NOI}\left(\left[\bar{G}_{ijm}(\xi,\mathrm{x})\right]_{3NOI\times 6NE}\left\{t_j(\mathrm{x})\right\}_{6NE\times 1}\right.\\ \left.-\left[\bar{H}_{ijm}(\xi,\mathrm{x})\right]_{3NOI\times 2N}\left\{u_j(\mathrm{x})\right\}_{2N\times 1}\right)\end{aligned} \tag{4.10}$$

Substituting from Eq. (4.10) into Eq. (4.8) and rearrange, gives:

$$
\begin{aligned}
&([G_{il}(\xi,\mathrm{x})]_{2N\times 6NE} \\
&+\left[B_{ijk}(\xi,\mathrm{x})\right]_{2N\times 3NOI}\left[ek_{qmjk}\right]^{-1}_{3NOI\times 3NOI}\left[\bar{G}_{qlm}(\xi,\mathrm{x})\right]_{3NOI\times 6NE}\Big) \\
&\left\{t_j(\mathrm{x})\right\}_{6NE\times 1}-([H_{il}(\xi,\mathrm{x})]_{2N\times 2N}+\left[B_{ijk}(\xi,\mathrm{x})\right]_{2N\times 3NOI} \\
&\left[ek_{qmjk}\right]^{-1}_{3NOI\times 3NOI}\left[\bar{H}_{qlm}(\xi,\mathrm{x})\right]_{3NOI\times 2N}\Big)\left\{u_j(\mathrm{x})\right\}_{2N\times 1}=\{0\}_{2N\times 1}
\end{aligned}
\tag{4.11}
$$

Introducing the following transformation matrix [L]:

$$
L_{ij}(\mathrm{x})=\int_{\Gamma}\phi_i^T(\mathrm{x})\phi_j(\mathrm{x})d\Gamma(\mathrm{x}) \tag{4.12}
$$

which transforms the traction vector to concentrated load vector [3] where, ϕ is a set of relevant shape functions. Multiplying Eq. (4.12) by Eq. (4.11) and rearrange, it gives:

$$
\{F_i(\mathrm{x})\}_{2N\times 1}-\left[K_{ij}(\xi,\mathrm{x})\right]_{2N\times 2N}\left\{u_j(\mathrm{x})\right\}_{2N\times 1}=\{0\}_{2N\times 1} \tag{4.13}
$$

where,

$\{F_i(\mathrm{x})\}_{2N}$ is the equivalent force vector and is given by:

$$
\{F_i(\mathrm{x})\}_{2N\times 1}=\left[L_{ij}(\mathrm{x})\right]_{2N\times 6NE}\left\{t_j(\mathrm{x})\right\}_{6NE\times 1} \tag{4.14}
$$

and $\left[K_{ij}(\xi,\mathrm{x})\right]_{2N\times 2N}$ is the equivalent stiffness matrix and is given by:

$$
\begin{aligned}
&\left[K_{jl}(\xi,\mathrm{x})\right]_{2N\times 2N}=\left[L_{jl}\right]_{2N\times 6NE}([G_{il}(\xi,\mathrm{x})]_{2N\times 6NE}+\left[B_{ijk}(\xi,\mathrm{x})\right]_{2N\times 3NOI} \\
&\left[ek_{qmjk}\right]^{-1}_{3NOI\times 3NOI}\left[\bar{G}_{qlm}(\xi,\mathrm{x})\right]_{3NOI\times 6NE}\Big)^{-1} \\
&([H_{il}(\xi,\mathrm{x})]_{2N\times 2N}+\left[B_{ijk}(\xi,\mathrm{x})\right]_{2N\times 3NOI}
\end{aligned}
\tag{4.15}
$$

$$\left[ek_{qmjk}\right]^{-1}_{3NOI\times 3NOI}\left[\bar{H}_{qlm}(\xi,\mathrm{x})\right]_{3NOI\times 2N}\Big)$$

It can be seen that despite the existence of damage inside the domain, Eq. (4.13) represents stiffness equation similar to that of the FEM with a boundary-only discretization. This equation could simulate the damage and could be solved in a similar way to that of the FEM. Consequently, using Eq. (4.10) the eigenstrain at the inclusions could be computed. Hence, using Eq. (4.3) the strain at the internal points could be computed.

4.4. The proposed incremental iterative approach

Tracing a problem damage requires the solution of Eq. (4.13) which is a nonlinear set of equations. In this chapter the secant algorithm [48] is used for its solution.

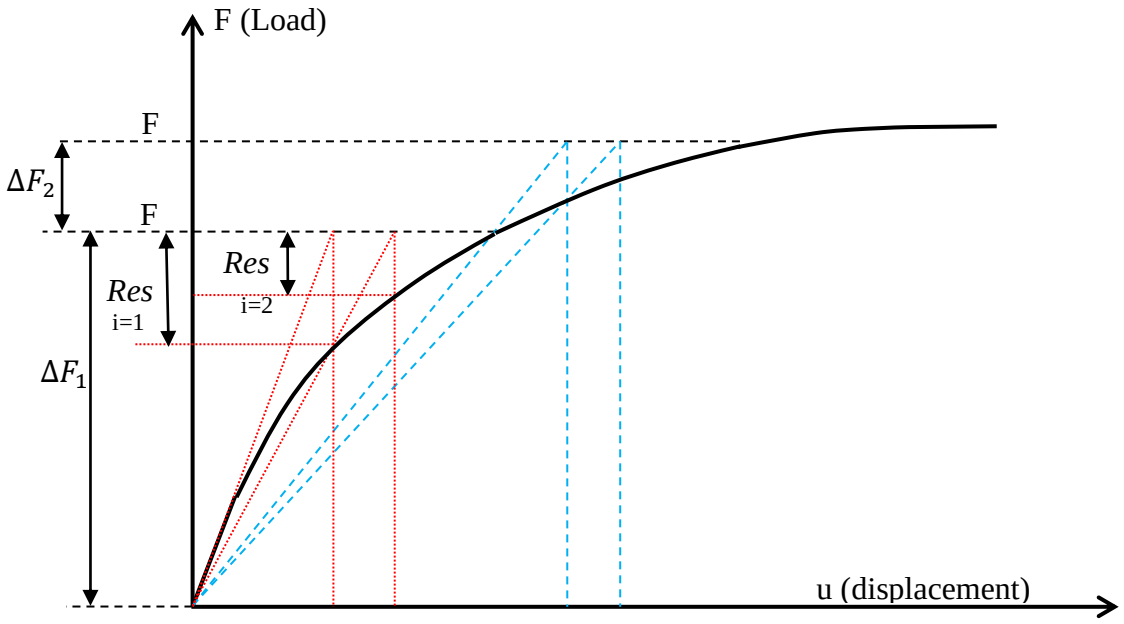

Fig.(4.2): A load-displacement curve showing the secant algorithm.

Consider the nonlinear load-displacement curve shown in Fig.(4.1), the solution procedure is described as follows (given that the counter (*i*) represents the current number of the nonlinear iterations):

1. Discretize the boundary of the problem into elements.
2. Define the investigation points to cover the overall problem domain.
3. Divide the total load into increments.
4. At each load increment (j), the applied load $\{F\}_j^{\text{applied}}$ is computed as follows:

$$\{F\}_j^{\text{applied}} = \{F\}_{j-1}^{\text{applied}} + \{\Delta F\} \tag{4.16}$$

Where, $\{\Delta F\}$ is the load increment.

5. Use Eq. (4.13) to compute the unknown displacement $\{u_t\}$.

$$\{F\}_j^{\text{applied}} = [K]_j\{u_t\}_j \tag{4.17}$$

6. Compute the strain Eq. (4.9) and the equivalent strain Eq. (2.57) according to the used damage model (see Appendix B) at all investigation points.
7. Compute the maximum value of the equivalent strain ε_{max}^* of the undamaged investigation points.
8. In this step the value of the occurred damage is computed via one of three ways:

- Way 1 (Damage is computed based on local strains):

In case of $\varepsilon_{max}^* > \varepsilon_D$ (where ε_D is the threshold strain, see Appendix B) insert a small virtual circular inclusion at this investigation point, with a Young's modulus equals to:

$$E_{new} = (1 - D)E_o \tag{4.18}$$

Where, E_o is Young's modulus of the undamaged problem, *D* is the scalar damage variable representing the ratio of the area damaged in the material (*D* is calculated according to the assumed damage model, see Appendix B).

- Way 2 (Damage is computed based on nonlocal strains):

The nonlocal strain at each investigation point is computed by considering all the points inside a circle of radius equals the interaction radius R. Hence, the average of all strains computed at all points inside this circle is computed (recall Fig.(4.1)). The maximum equivalent strain ε^*_{max} is computed at the undamaged investigation points.

In case of $\varepsilon^*_{max} > \varepsilon_D$, a small equivalent circular inclusion is inserted at this investigation point. The damage variable is computed at the inserted inclusion and for other previously damaged points (if any). modified Young's modulus due to damage is computed in a similar way as Eq.(4.18):

- Way 3 (Damage is computed based on nonlocal damage):

The maximum equivalent strain ε^*_{max} is computed at all undamaged investigation points. In case of $\varepsilon^*_{max} > \varepsilon_D$, a small equivalent circular inclusion is inserted at this investigation point. The damage variable is then computed at the inserted inclusion and for other previously damage points (if any). The nonlocal damage is computed for the damaged points and for all points inside the circle of radius R (recall Fig. (1)), then the modified Young's modulus due to damage is computed in a similar way as Eq.(4.18).

In case there are two points having the same ε^*_{max} (i.e. cases of symmetric problems) two virtual inclusions are placed simultaneously with the same Young's modulus as in Eq.(4.18). Otherwise, if $\varepsilon^*_{max} < \varepsilon_D$ and there is no damage at all investigation points, the load is increased (another load increment is added) in other words, jump to step 4.

9. Compute the updated stiffness $[K]_j^{(i)}$(by rebuilding Eq. (4.15)) and compute the updated force vector as follows:

$$\{F\}_j^{(i)} = [K]_j^{(i)}\{u_t\}_j^{(i-1)} \tag{4.19}$$

10. Compute the force residual vector $\{Res\}$ due to the change in the problem stiffness resulting from the occurred damage, as follows:

$$\{Res\} = \{F\}_j^{\text{applied}} - \{F\}_j^{(i)} \tag{4.20}$$

11. Compute the maximum value of $\{Res\}$ to be denoted by Res_max. In case of Res_max > *tolerance* (it has to be noted that the *tolerance* is going to be chosen in the examples in section 4.6, and its effect will be demonstrated), continue to step 12 otherwise jump to step 16.
12. Compute the change in displacement $\{\Delta u\}_j^{(i)}$ due to the residual force vector $\{Res\}$, and the change in strain $\{\Delta\varepsilon\}_j^{(i)}$ from Eq. (4.3):

$$\{\Delta u\}_j^{(i)} = \left([K]_j^{(i)}\right)^{-1}\{Res_j\} \tag{4.21}$$

13. Compute the total displacement $\{u_t\}_j^{(i)}$, and total strain $\{\varepsilon_t\}_j^{(i)}$ at each damaged point, as follows:

$$\{u_t\}_j^{(i)} = \{u_t\}_j^{(i-1)} + \{\Delta u\}_j^{(i)} \tag{4.22}$$

$$\{\varepsilon_t\}_j^{(i)} = \{\varepsilon_t\}_j^{(i-1)} + \{\Delta\varepsilon\}_j^{(i)} \tag{4.23}$$

14. Modify the damage variable according to the modified total strain in Eq.(4.23) and then compute the modified Young's modulus from Eq.(4.18).

15. Repeat steps from step 9 until the numerical value of the maximum force residual Res_max is within the chosen *tolerance*. In other words, jump to step 9.
16. Check the undamaged points: if there is no other point with $\varepsilon^* > \varepsilon_D$, increase the applied load by $\{\Delta F\}$ (apply another load increment) and repeat from step 4, otherwise if there is other point with $\varepsilon^* > \varepsilon_D$ jump to step8.
17. In case the number of iterations (*NI*) reaches its maximum value (NI_{max}, a chosen number will be demonstrated in the examples in section 4.6) for the secant algorithm and Res_max > *tolerance*, decrease the load increment, in other words, use one half of the load increment (*j*): and repeat the load increment starting from step 4.

$$\{\Delta F\}_j = \frac{1}{2}\{\Delta F\}_j \tag{4.24}$$

Hence, repeat steps starting from step 4.

This procedure is repeated until the problem reaches a stable damage pattern under a certain load or reaches numerical instability, regardless, increasing the number of nonlinear iterations or increasing the used *tolerance* level. Figure (4.3) demonstrates a flow chart that summarizes the above procedures.

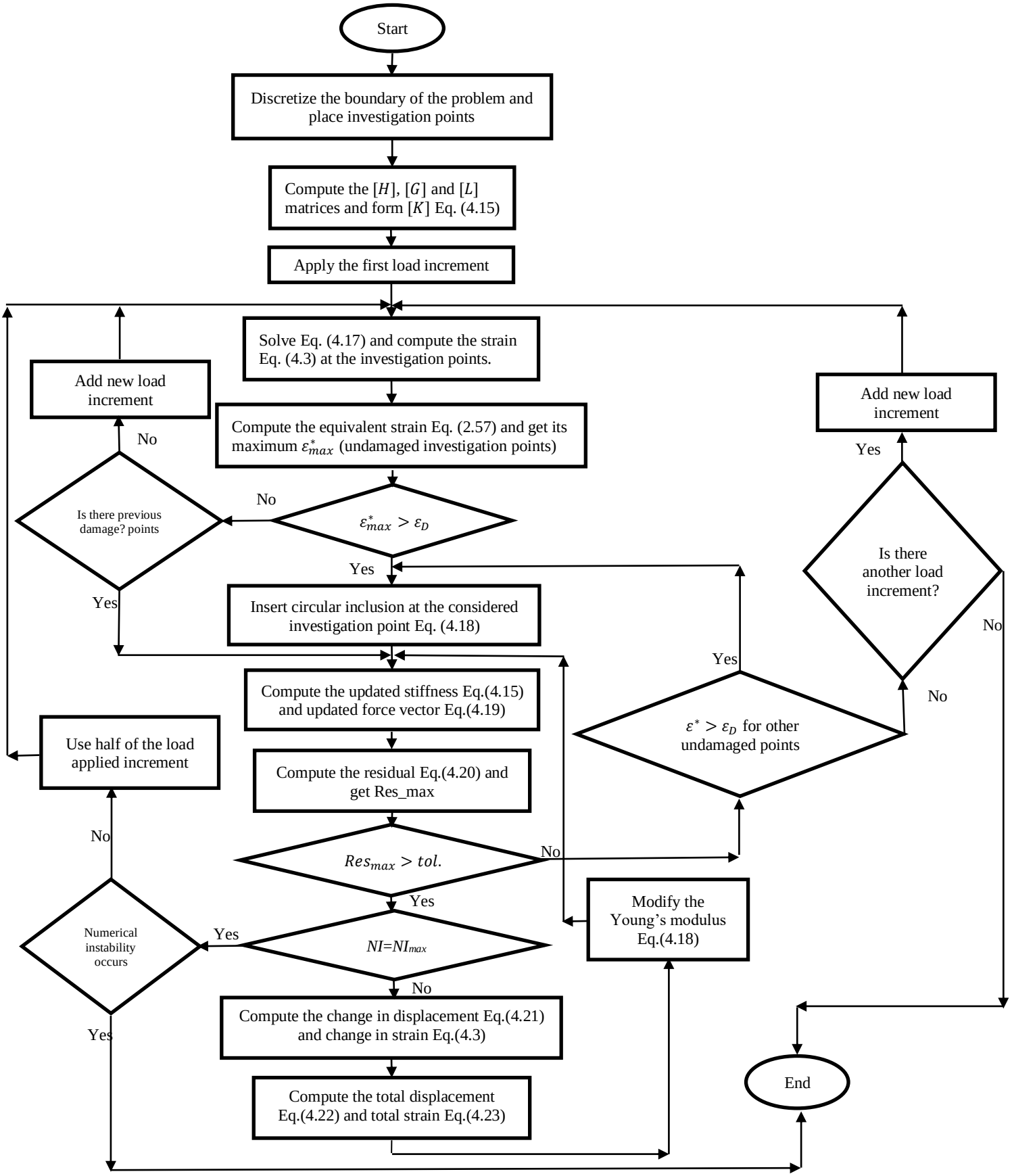

Fig.(4.3): Flow chart of the proposed incremental-iterative approach.

4.5. Visualizing the damage patterns

A Matlab code is done by the author to visualize the damage pattern. In this code the coordinates of the center of the inclusions are entered with the radius defined and the corresponding damage variable. The program draws a circle at the given points with a color corresponding to the damage variable value.

```
%A program to draw Damage pattern
disp('A program to draw Damage pattern')
NON=input('Enter number of nodes: ');
NOI=input('Enter number of inclusions: ');
clear nodalcoor;clear IDa;
nodalcoor=load('coor.txt');
IDa=load('Dcoor.txt');
plot(nodalcoor(:,1),nodalcoor(:,2),'k')
Xmax=max(nodalcoor(:,1));
Ymax=max(nodalcoor(:,2));
hold on
for i=1:NOI
        if IDa(i,4)>=0 && IDa(i,4)<0.2 %blue
            filledCircle([IDa(i,1),IDa(i,2)],IDa(i,3),1000,'b');
            hold on
        elseif IDa(i,4)>=0.2 && IDa(i,4)<0.3 %cyan
            filledCircle([IDa(i,1),IDa(i,2)],IDa(i,3),1000,'c');
            hold on
        elseif IDa(i,4)>=0.3 && IDa(i,4)<0.6 %green
            filledCircle([IDa(i,1),IDa(i,2)],IDa(i,3),1000,'g');
            hold on
        elseif IDa(i,4)>=0.6 && IDa(i,4)<0.8 %yellow
            filledCircle([IDa(i,1),IDa(i,2)],IDa(i,3),1000,'y');
            hold on
        elseif IDa(i,4)>=0.8 && IDa(i,4)<0.9 %orange
            filledCircle([IDa(i,1),IDa(i,2)],IDa(i,3),1000,[ 0.9100
0.4100 0.1700]); %%%%%%%%%%%%%
            hold on
        elseif IDa(i,4)>=0.9 && IDa(i,4)<=1 %red
            filledCircle([IDa(i,1),IDa(i,2)],IDa(i,3),1000,'r');
            hold on
        end
end
pbaspect([Xmax,Ymax,1])
hold off
```

4.6. Numerical examples

In this section, three numerical examples are solved to investigate the validity of the proposed formulation (the first is solved using local approach and the other two are solved using local and nonlocal approaches). It has to be noted that the allowable maximum number of nonlinear iterations is set to be 50 (otherwise, it will be stated) as such number is found to be enough to trace all nonlinear steps. Throughout the numerical examples different parameters are considered for:

1. Boundary discretizations.
2. The inclusion pattern (intersected or staggered as demonstrated in Fig.(4.1)).
3. Inclusion diameter.
4. The residual *tolerance* level.
5. Maximum number on nonlinear iterations.

4.6.1 Fixed-Fixed beam

This problem is as shown in Fig.(4.4) and was previously solved by Pituba and Lacerda [50] using the FEM. Mazars damage model is used (see the appendix B). The material properties of the beam are E_o=2.47×10^{10} N/m^2, ν=0.2, a=0.7 and b=8000 and ε_D=0.00067. The beam thickness is 0.2 m.

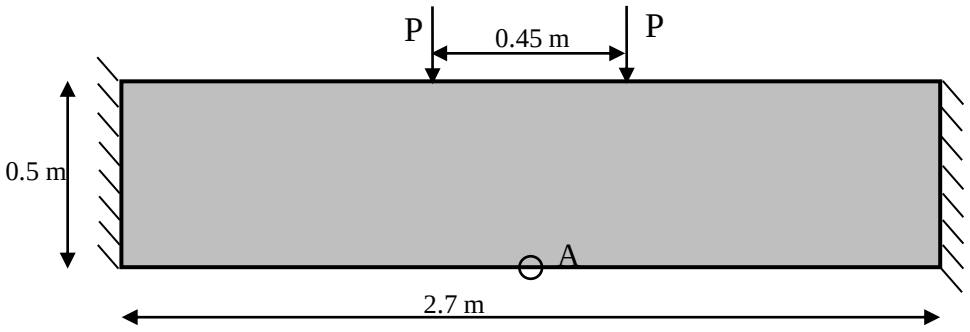

Fig.(4.4): Dimensions of the fixed-fixed beam in example 4.6.1.

The problem is solved with local damage approach using 17 boundary elements and with two investigation points patterns to allow inserting intersected or staggered inclusions. For intersected pattern a spacing of 0.078 m is used. For the staggered pattern a spacing of 0.0196 m is used. The problem is solved with a sufficient *tolerance* level of a value within the range of 0.1% to 1% of the applied load at each increment without any change in the results. The *tolerance* level is increased near the failure to allow tracking further steps in the nonlinear load-displacement curve as shown in Fig.(4.5).

The used inclusions are of diameter 0.11 m for the intersected pattern. Two diameters are used for the staggered pattern, they are 0.0302 m and 0.02 m.

The computed nonlinear load-displacement curve at the point A (see Fig.(4.4)) is plotted in Fig.(4.5) together with the results of Pituba and Lacerda [50].

The results in Pituba and Lacerda [50] are presented using finite elements discretizations of 0.11 mm. It can be seen from Fig.(4.5) that the results of the proposed model are in good agreement with the previously published results of Pituba and Lacerda [50].

It can be seen that for the case of intersected pattern, numerical instability is detected at a load of 60.8 kN. Hence the *tolerance* is increased to from 1% to 3% to reach a load level of 62.1 kN then increased to 5% to reach a load level of 63.6 kN. Hence, failure is detected at load level of 63.6 kN. In case of staggered pattern, the *tolerance* range from 0.1% to 1% was enough to trace all the nonlinear curve to failure. Figure (4.6) demonstrates the predicted damage patterns for the used two patterns (intersected and staggered) at different load levels.

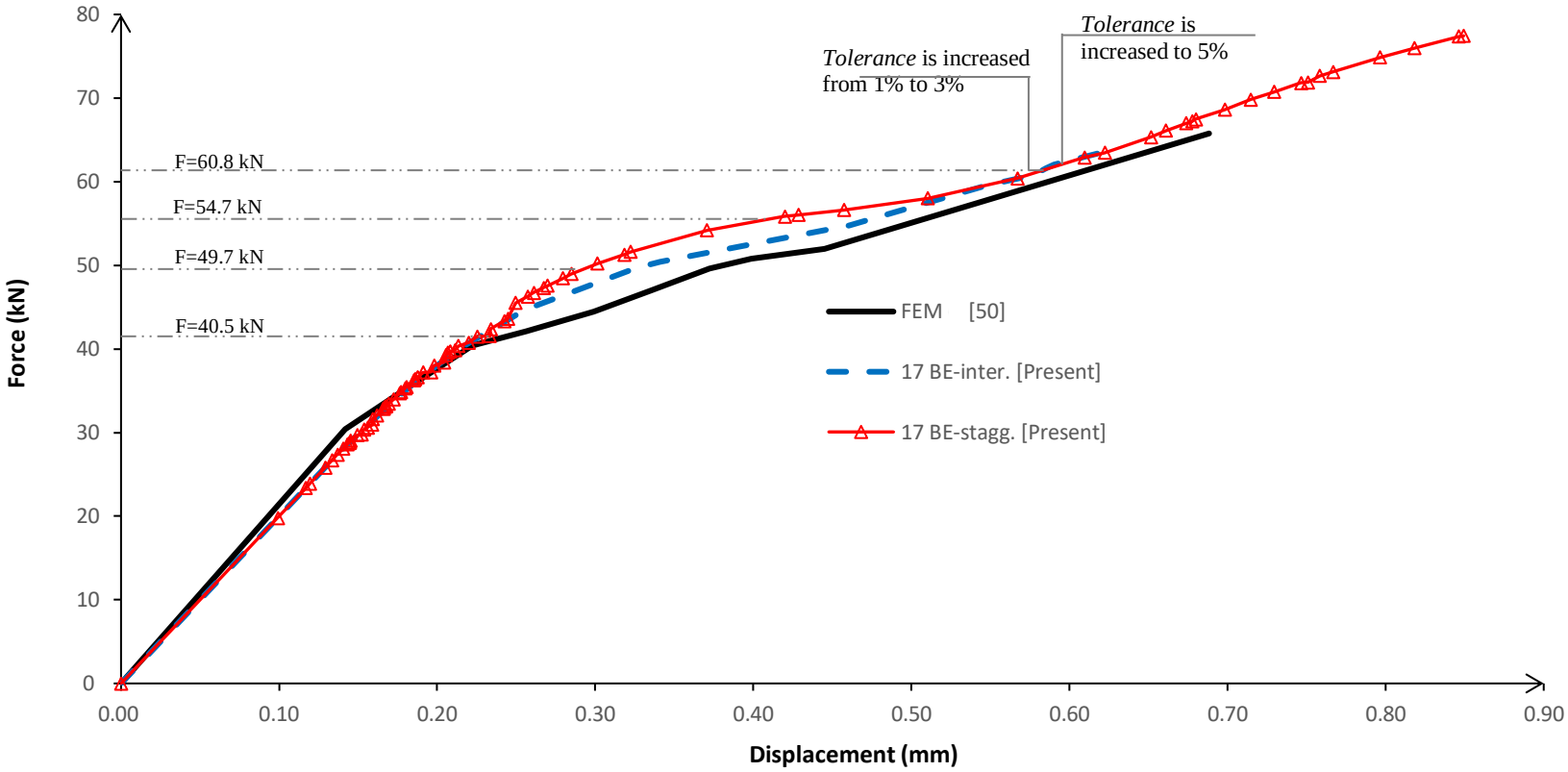

Fig.(4.5): The computed nonlinear load-displacement curve for example 4.6.1.

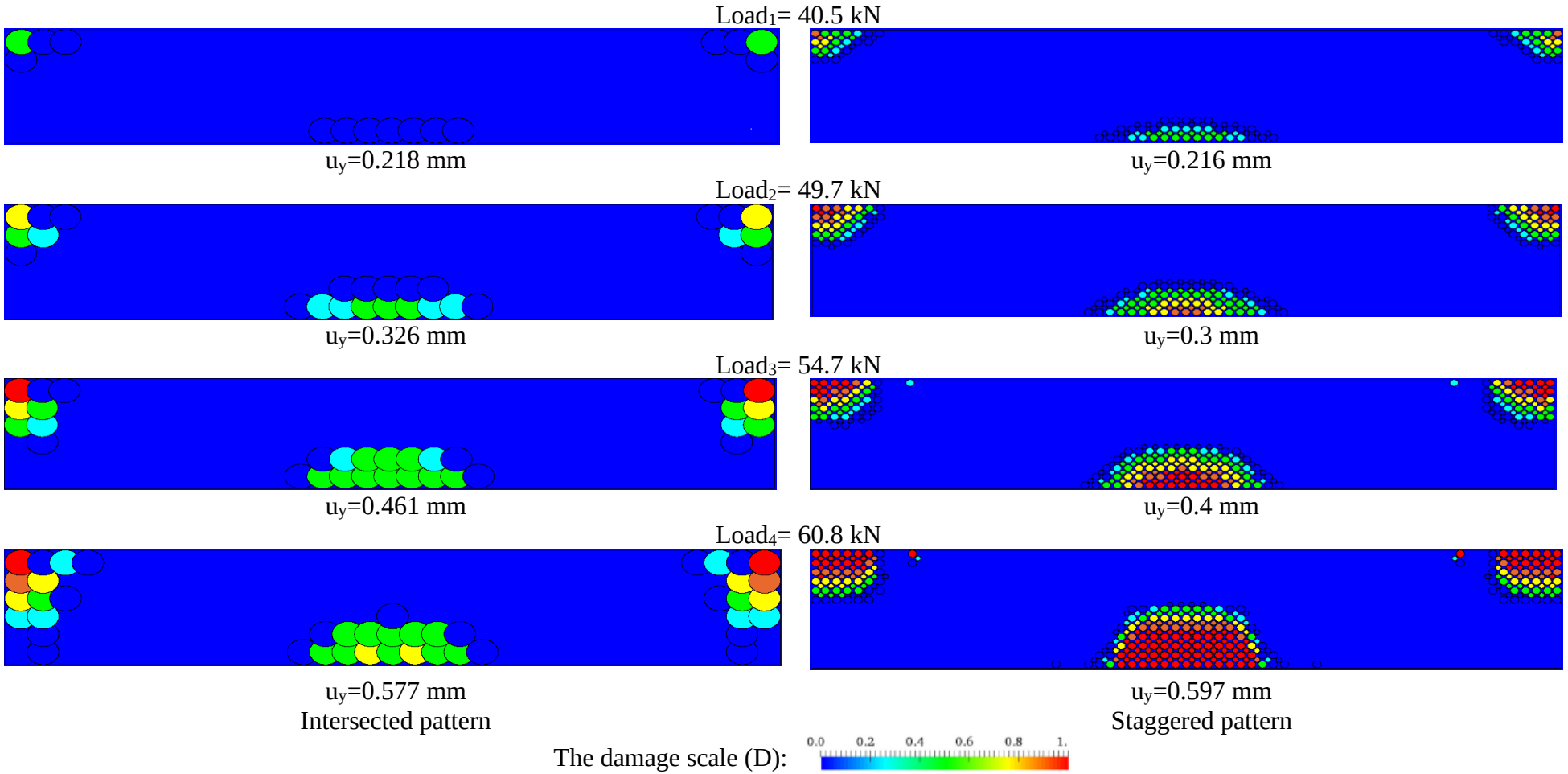

Fig.(4.6): The predicted damage patterns for example 4.6.1.

The problem is solved again with different inclusion diameters. For the intersected case, two diameters are considered, i.e. 0.16 m and 0.078 m. This will produce double and half the inclusion size used before. For the staggered case, the considered diameters are (0.0427 m, 0.0283 m) and (0.0214 m, 0.0142 m) for the double and the one-half inclusion size. In this example the analysis is carried out with fixed *tolerance* level of 1%.

The load-displacement curve is shown in Figs. (4.7 and 4.8) for the intersected and staggered cases, respectively. It can be seen from the figures that there is a compatibility between the developed method results with those of the finite element having the same size. However, change of inclusion size could slightly affect the results in a similar way as the FEM, which is mentioned previously in [25] for local damage models.

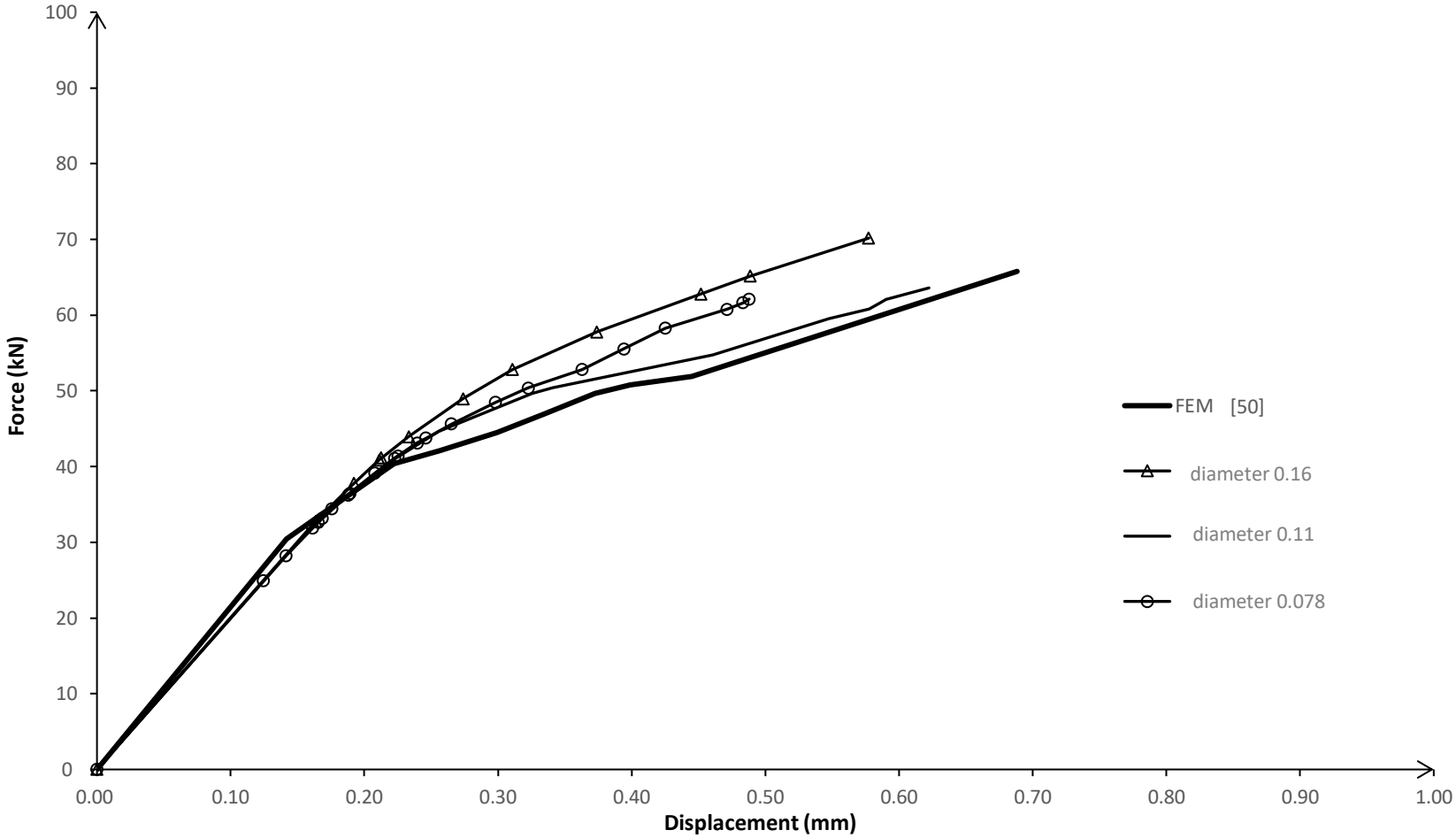

Fig.(4.7): The load-displacement curve for example 4.6.1 with intersected inclusion patterns.

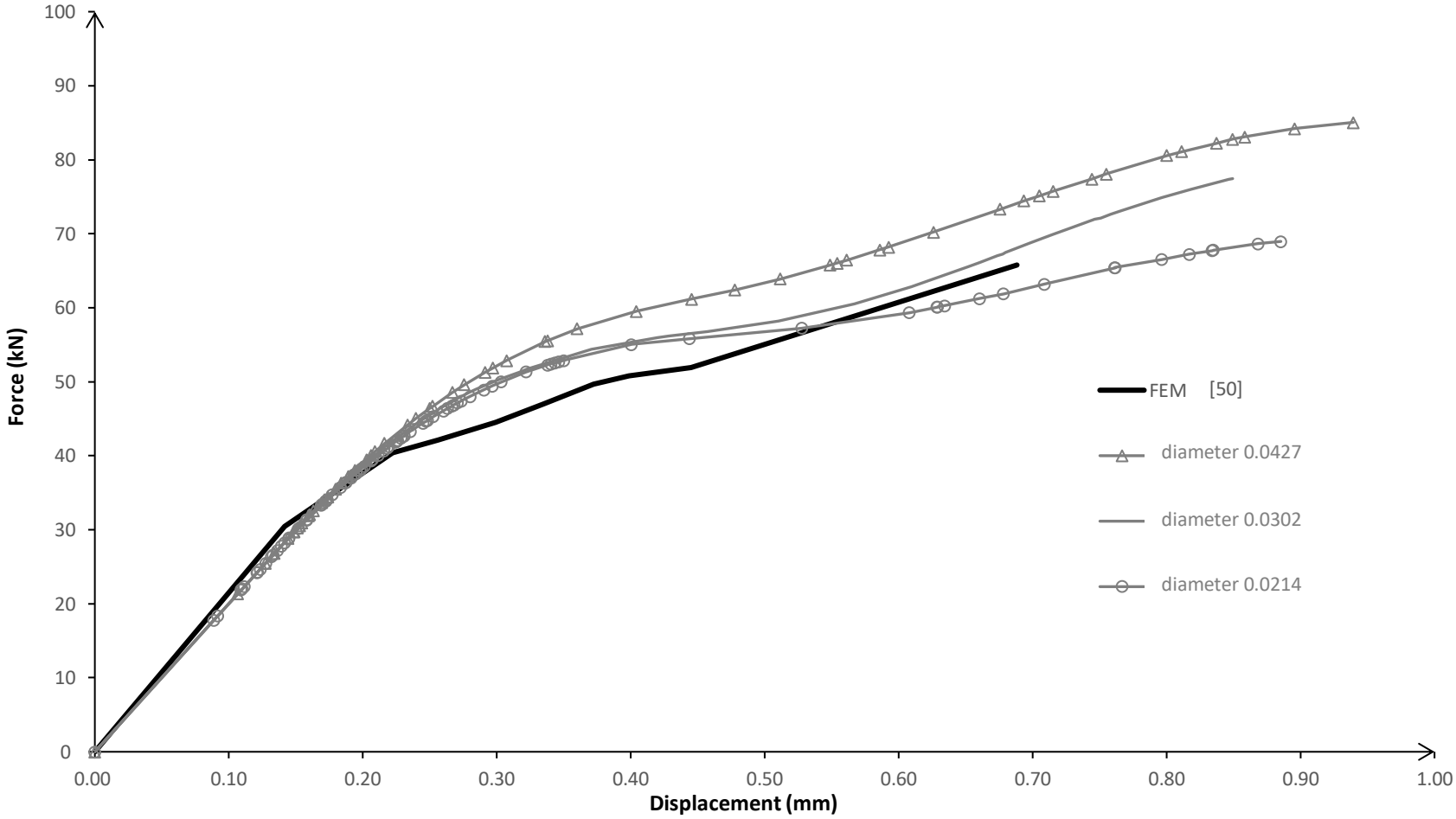

Fig.(4.8): The load-displacement curve for example 4.6.1 with staggered inclusion patterns.

4.6.2 Simply supported beam

In this example, a simply supported beam under concentrated load shown in Fig.(4.9) is solved. This example was previously solved by Jirasek [25] using the FEM and reconsidered by Zhang *et al.* [64] using the SBFEM. The material properties are E_o= 20850428446 N/m^2 and ν =0.2. The parameters of the damage model (as in appendix B) are $\varepsilon_D = 0.00009$ and $\varepsilon_f = 0.005$, and the interaction radius $R = 8$ mm.

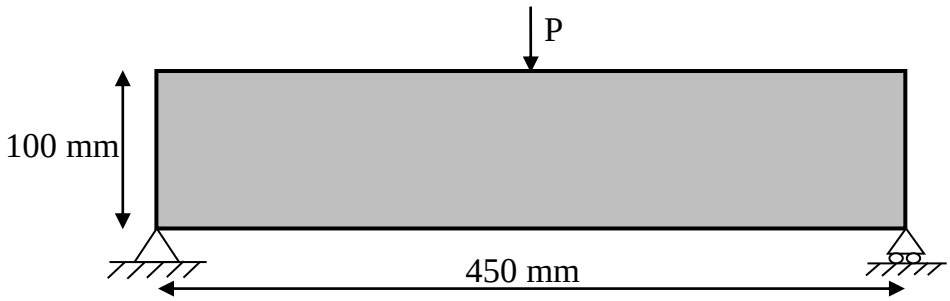

Fig.(4.9): Dimensions of the simply supported beam in examples 4.6.2.

The problem is discretized into 47 boundary elements. Intersected inclusion pattern is used (see Fig.(4.1)) with diameter of 5 mm.

The load-displacement curves for the presented formulation using local (L) and nonlocal (NL) (strain and damage) cases are demonstrated in Fig.(4.10). Table (4.1) demonstrates the load level at which instability occurs with the corresponding adjusted *tolerance* level. It should be noted that the *tolerance* level is increased with the load level.

The previous results of Jirasek [25] are also plotted on Fig.(4.10) for the sake of verification. As shown in Fig.(4.10), the case of nonlocal (using strain or damage) can well trace the nonlinear curve in more efficient way than that of the local case. The predicted damage patterns (contour maps) are demonstrated in Fig.(4.11) for the local and nonlocal models at various load steps (recall Fig.(6.10)), also the damaged areas (inclusions) are demonstrated in Fig.(4.12).

Damage patterns obtained from [64], are also presented in Figs.(4.11 and 4.12) for the sake of verification. It can be seen that in the local case, the damage is localized in some points whereas in the nonlocal cases the damage is more smooth.

Table 4.1 : Adjusted *tolerance* at different load levels in example 4.6.2.

Load level (N)			Adjusted *tolerance* level
Local	Nonlocal (average strain)	Nonlocal (average damage)	
4670.00	4880.00	4880.00	1%
4857.90	5200.00	5132.36	3%
4933.71	5270.00	5257.36	5%
4946.76	5319.20		6%
4966.21	5328.47	5382.36	7%
4989.13	5341.23		8%
	5355.34		9%
5030.00	5370.09		13%
	5384.62		15%

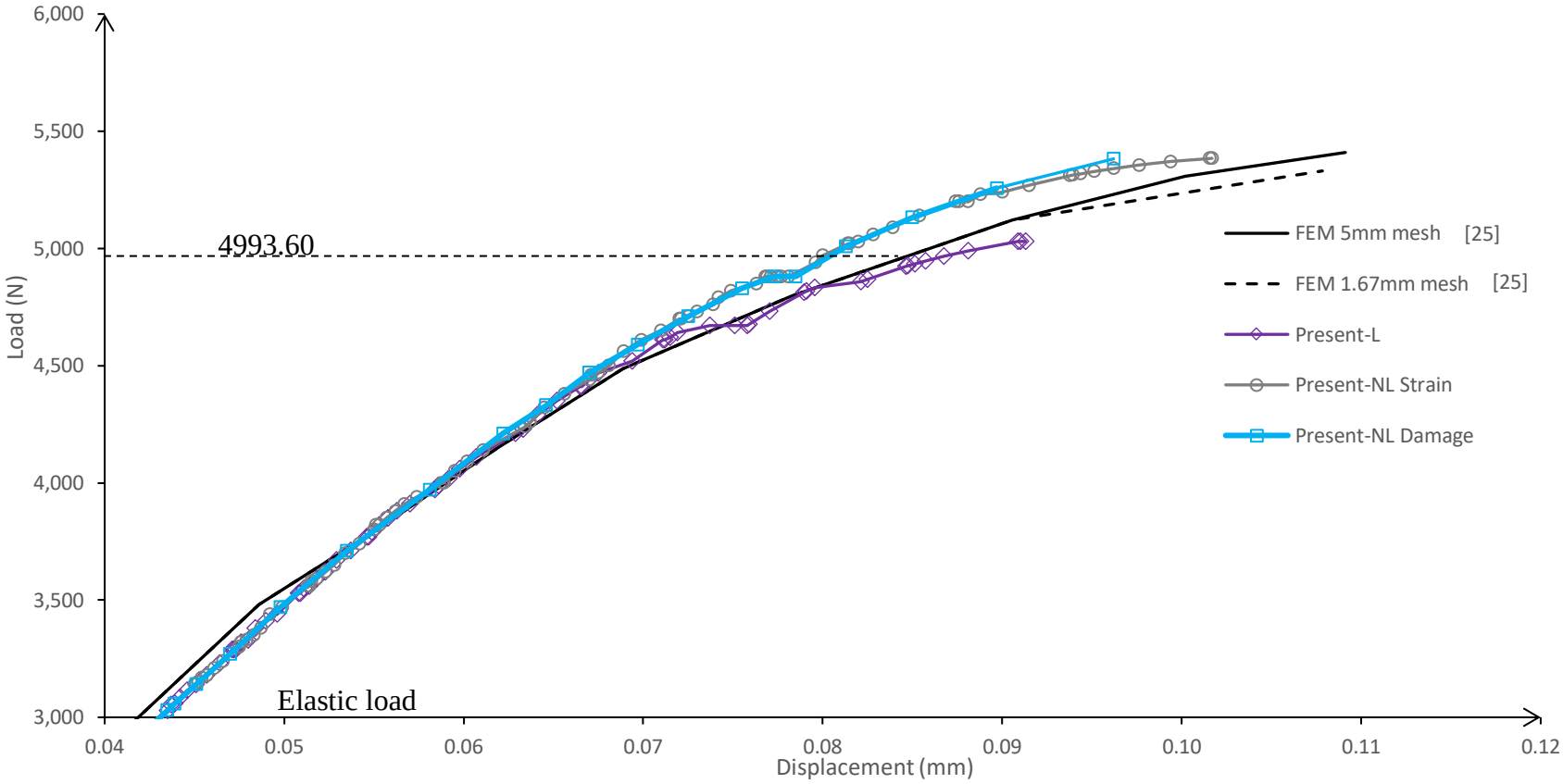

Fig.(4.10): Load-displacement curve for example 4.6.2.

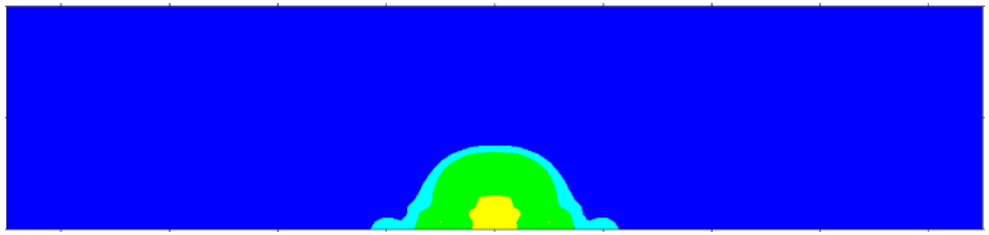

Present Local u_y=0.091 mm

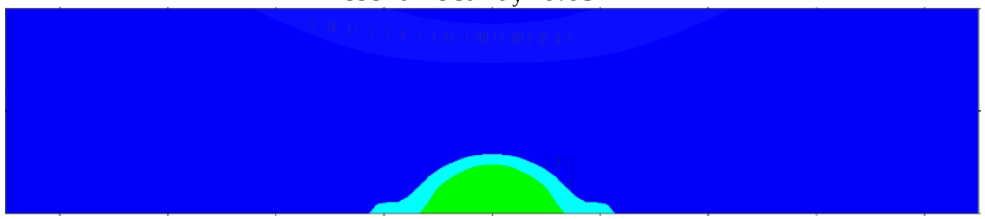

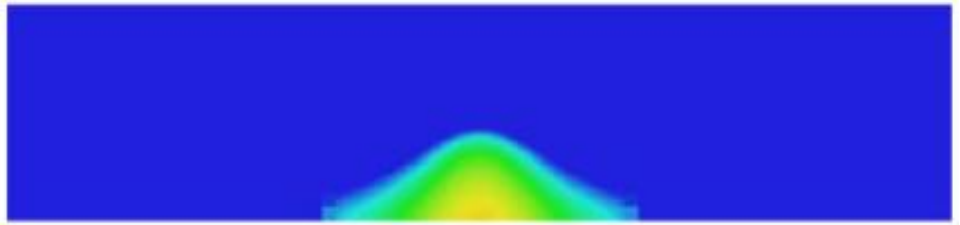

Present Non-Local Strain u_y=0.082 mm

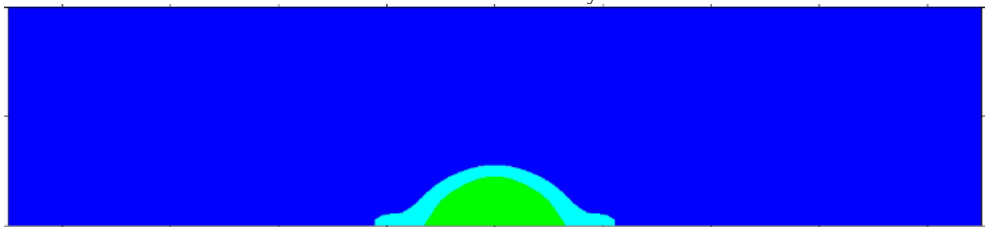

Present Non-Local Damage u_y=0.081 mm

Reference [64] u_y=0.090 mm

The damage scale (D):

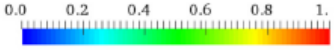

Fig.(4.11): The predicted damage contour map for example 4.6.2 at load level of 4993.60 N.

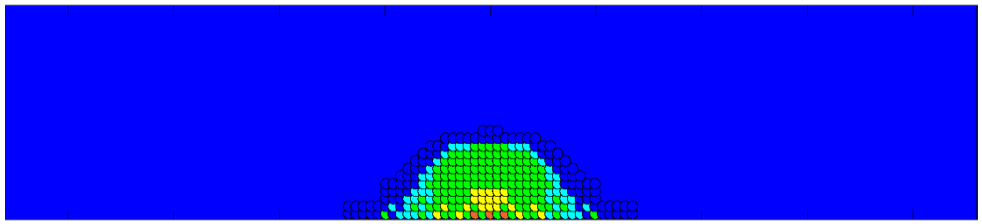

Present Local u_y=0.091 mm

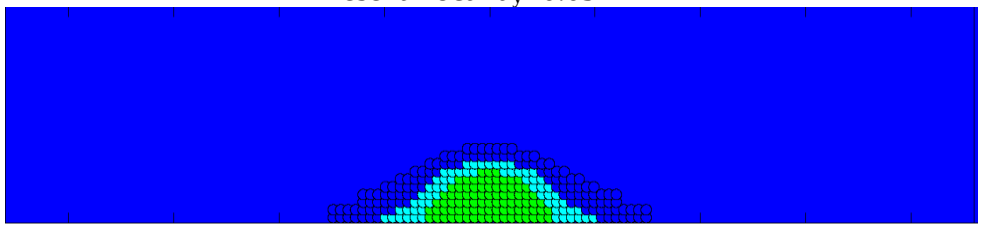

Present NL Strain u_y=0.082 mm

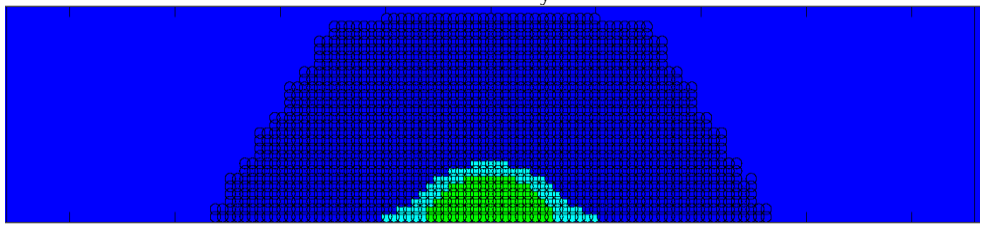

Present NL Damage u_y=0.081 mm

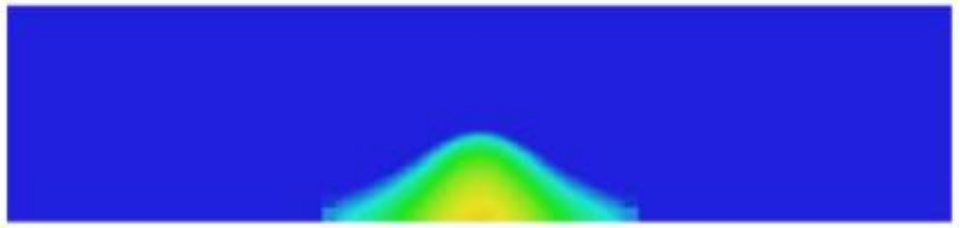

Reference [64] u_y=0.090 mm

The damage scale (D):

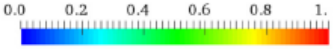

Fig.(4.12): The predicted damaged areas (inclusions) for example 4.6.2 at load level of 4993.60 N

4.6.3 Simply supported beam with a notch

In this example, a simply supported beam with a middle notch, and subjected to concentrated load, shown in Fig.(4.13) is solved. The problem was previously considered by Jirasek [25] using the FEM and by Zhang *et al.* [64] using the SBFEM. The material properties are E_o= 2×10^{10} N/m^2 and ν =0.2. The parameters of the damage model (as in appendix B) are $\varepsilon_D = 0.00009$ and $\varepsilon_f = 0.007$, and the interaction radius $R = 4$ mm.

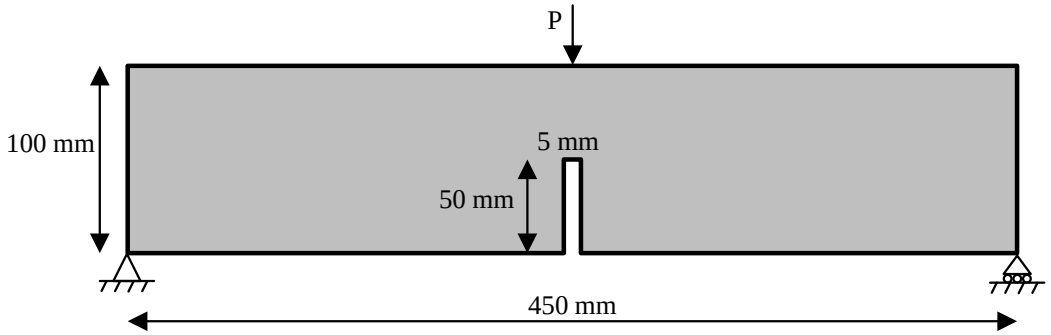

Fig.(4.13): Dimensions of the notched simply supported beam in example 4.6.3.

The problem is discretized into 68 boundary elements. Staggered inclusion pattern is used (see Fig.(4.1)) with two diameters of 2.5 and 1.75 mm.

The load-displacement curves for the presented formulation using local (L) and nonlocal (NL) (strain and damage) cases are demonstrated in Fig.(4.14). Table (4.2) demonstrates the load level at which instability occurs with the corresponding adjusted *tolerance* level.

The previous results of Jirasek [25] are also plotted on Fig.(4.14) together with experimental results [25,58] for the sake of verification. As shown in Fig.(4.14), the case of nonlocal (using strain or damage) can well trace the nonlinear curve in more efficient way than that of the local case. The predicted damage patterns (contour maps) are demonstrated in Figs.(4.15,4.17) for the local and nonlocal models at various load steps (recall Fig. (4.14)). Damage patterns obtained from

[64] are also demonstrated in Figs. (4.15 - 4.18) for the sake of verification, also the damaged areas are demonstrated in Figs. (4.16 and 4.18). The shown figures demonstrated the good agreement with the results of reference [58].

Table 4.2 : Adjusted *tolerance* at different load levels in example 4.6.3.

<table>
<tr><td colspan="3">Load level (N)</td><td rowspan="2">Adjusted tolerance level</td></tr>
<tr><td>Local</td><td>Nonlocal (average strain)</td><td>Nonlocal (average damage)</td></tr>
<tr><td>1094.00</td><td rowspan="2">942.03</td><td rowspan="2">1281.99</td><td>1%</td></tr>
<tr><td rowspan="3">1155.00</td><td>3%</td></tr>
<tr><td>1182.55</td><td rowspan="3">1313.24</td><td>5%</td></tr>
<tr><td rowspan="2">1279.00</td><td>6%</td></tr>
<tr><td>1169.22</td><td>7%</td></tr>
</table>

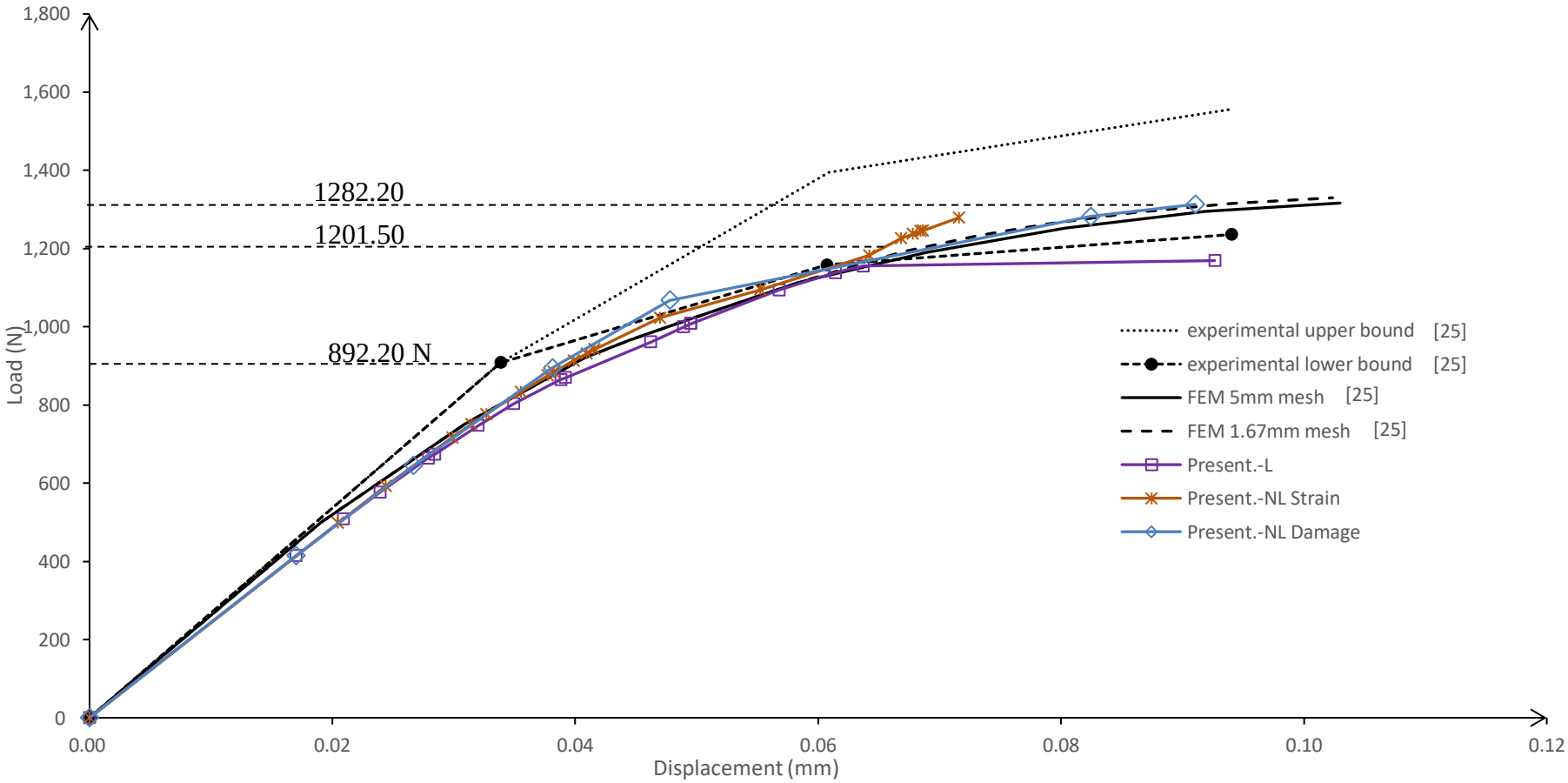

Fig.(4.14): Load-displacement curve for example 4.6.3.

Load level= 892.20 N

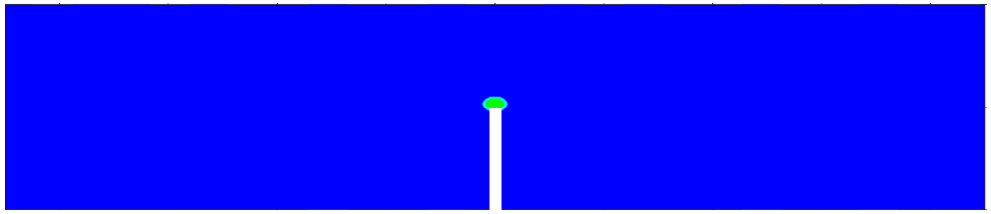

u_y=0.038 mm

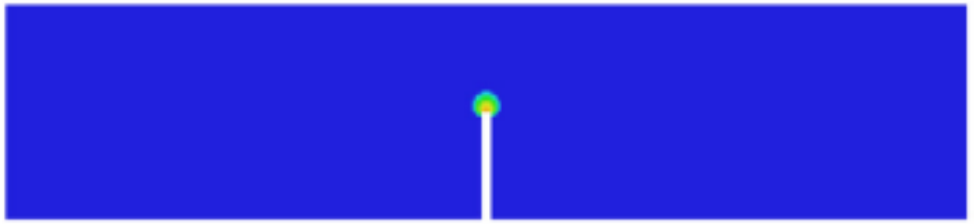

u_y=0.040 mm

Load level= 1201.50 N

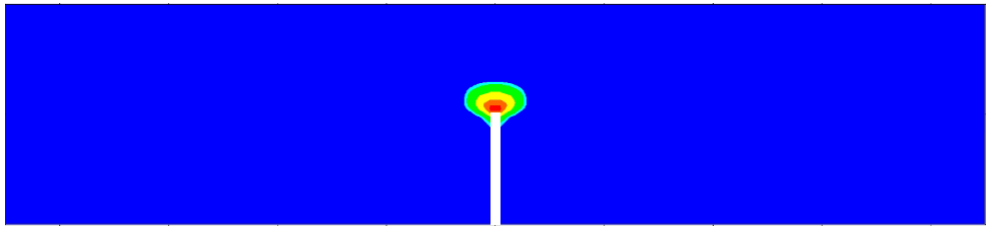

u_y=0.065 mm

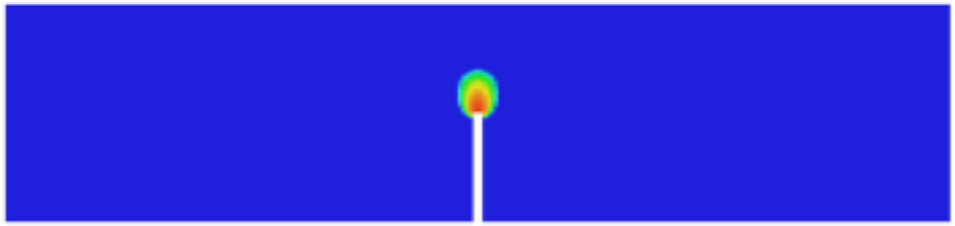

u_y=0.070 mm

Load level= 1282.20 N

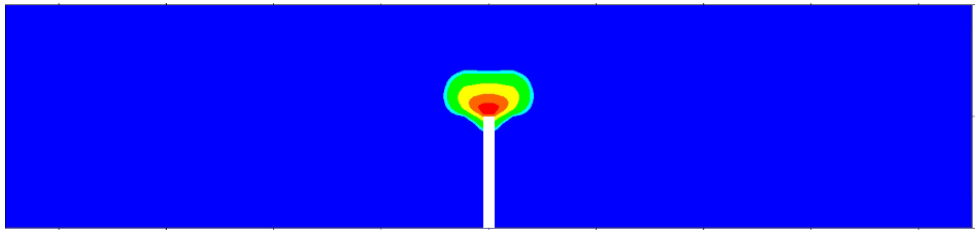

u_y=0.088 mm
Present solution

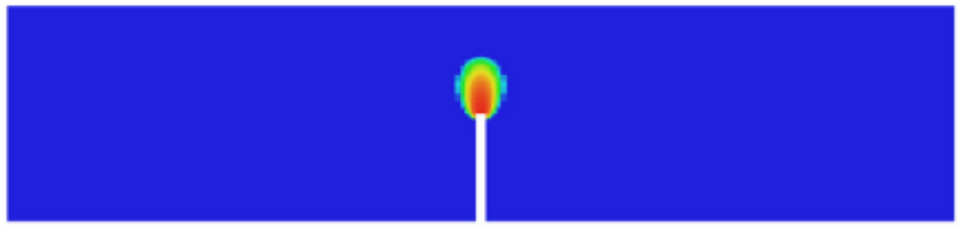

u_y=0.098 mm
Reference [64]

The damage scale (D): 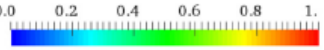

Fig.(4.15): The predicted damage contour map (Nonlocal damage) for example 4.6.3.

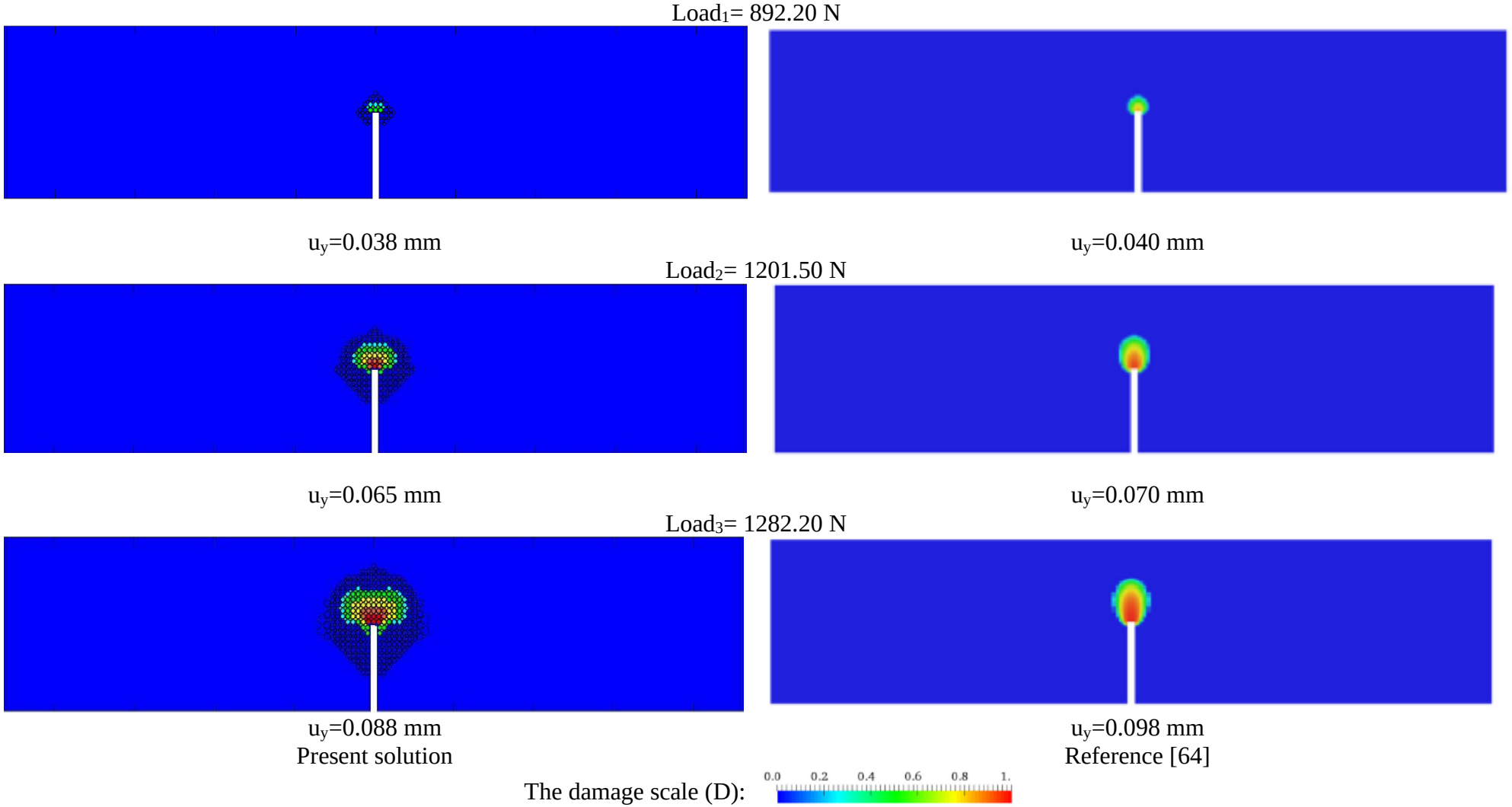

Fig.(4.16): The predicted damaged areas (inclusions) (Nonlocal damage) for example 4.6.3.

Load level = 892.20 N

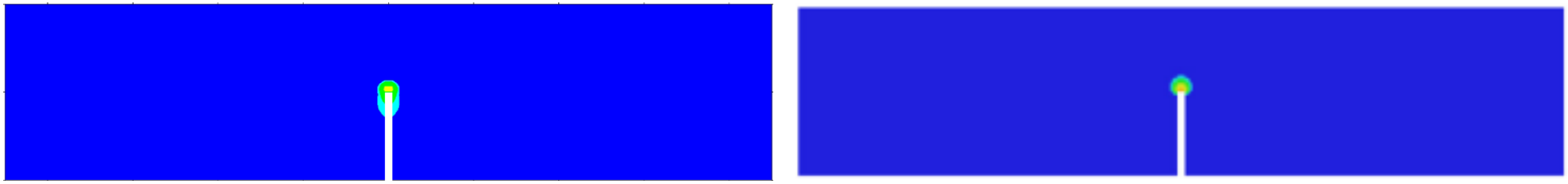

u_y=0.039 mm

u_y=0.040 mm

Load level = 1201.50 N

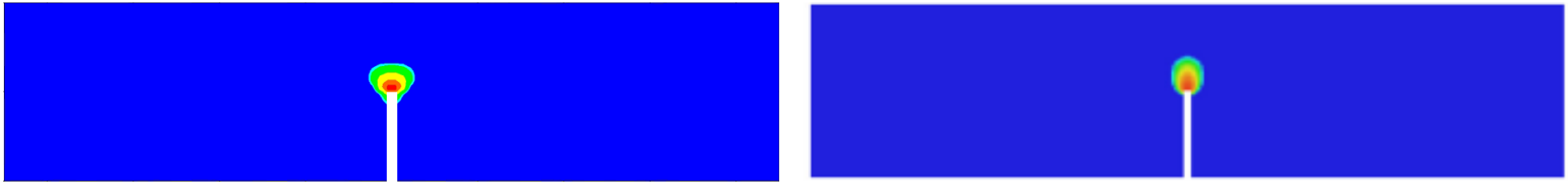

u_y=0.065 mm
Present solution

u_y=0.070 mm
Reference [64]

The damage scale (D): 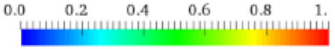

Fig.(4.17): The predicted damage contour map (Nonlocal strain) for example 4.6.3.

Load level = 892.2 N

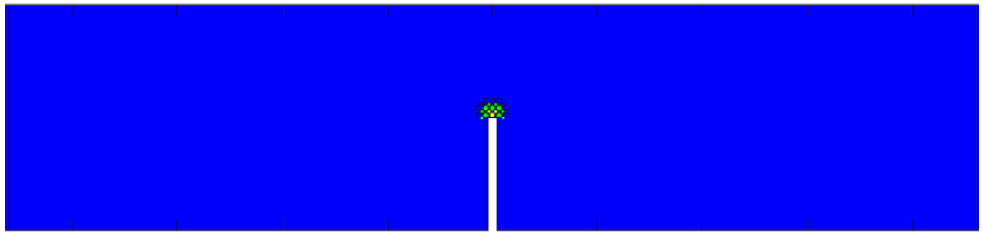

u_y=0.039 mm

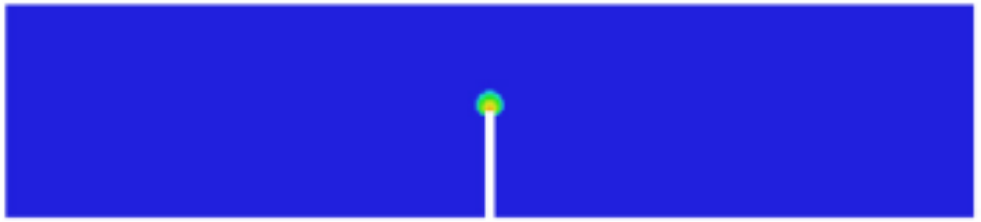

u_y=0.040 mm

Load level = 1201.5 N

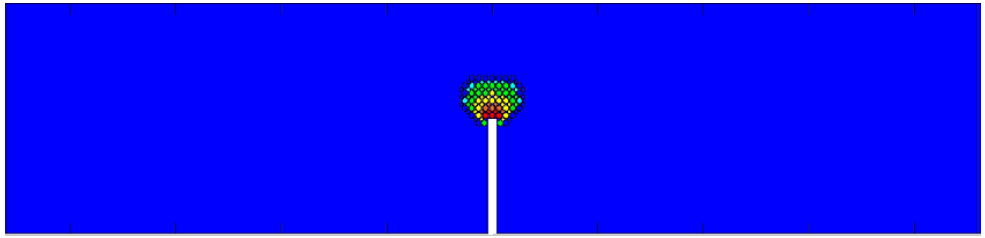

u_y=0.065 mm
Present solution

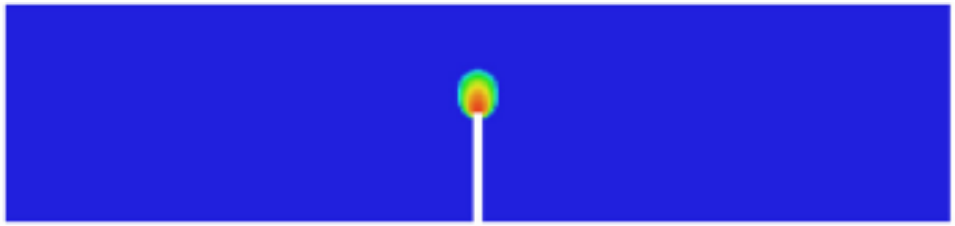

u_y=0.070 mm
Reference [64]

The damage scale (D):

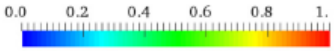

Fig.(4.18): The predicted damaged areas (inclusions) (Nonlocal strain) for example 4.6.3.

4.7. Numerical discussion

In this section the influence of parameters that affect the solution is discussed. The two previously solved examples 4.6.2 and 4.6.3 are re-considered herein by varying the following parameters:

1. Boundary discretization
2. Inclusion pattern
3. Inclusion diameter
4. The residual *tolerance* level.
5. Maximum number of nonlinear iterations

4.7.1.Boundary discretization

In this section different boundary discretizations are considered, i.e. 17 & 47 boundary elements are considered for example 4.6.2, and 38 & 68 boundary elements are considered for example 4.6.3.

Figures (4.19 and 4.20) demonstrates the load-displacement curves for examples (4.6.2) and (4.6.3) for local and nonlocal models, respectively. It can be seen that problems having stress concentrations need more boundary discretiztion.

4.7.2.Inclusion pattern

In this section different inclusion patterns are considered, i.e. staggered and intersected (recall Fig.(4.1)). Figures (4.21 and 4.22) demonestrate the load-displacement curves for examples (4.6.2) and (4.6.3), respectively. It can be seen from these figures that the used pattern affects the load-displacement curve. Therefore, in general, for a certain problem it is recommended to carry out the analysis using the two inclusion patterns (or in general more than one

pattern). Hence, the modeler can figure out the problem nonlinear behaviour based on the analyzed results.

4.7.3.Inclusion diameter

In this section different inclusion diameters are considered, in case of local and nonlocal models. For example (4.6.2) a diameter 2.5 mm (5 mm previously used) is used for the intersected pattern and, diameters (5 mm and 3.5 mm) and (2.5 mm and 1.75 mm) are used for the staggered pattern. For example (4.6.3) two diameters 1.2 mm and 0.84 mm (2.5 mm and 1.75 mm previously used) are used for the staggered pattern and, diameters 2.5 mm and 1.2 mm are used for the intersected pattern. The results are plotted in Figs.(4.23 and 4.24) for example (4.6.2) and in Figs.(4.25 and 4.26) for example (4.6.3). It can be seen that the results are affected by the decrease in inclusion diameter. Unlike the nonlocal models, such results are sensitive in the local damage model.

4.7.4.Residual *tolerance* level

Examples (4.6.2) and (4.6.3) are re-considered using constant different *tolerance* levels 1%, 3%, 6% and 10% to demonstrate the effect of the *tolerance* level on the results. Example (4.6.2) and example (4.6.3) are solved for the case of nonlocal strain and nonlocal damage, respectively. According to the load-displacement curve shown in Figs.(4.27 and 4.28), when starting the solution with a high *tolerance* level (for example 6%), the resulting curve is more stiff. As the high *tolerance* level allow jumping to another load step before developing the total nonlinear dispacement. So, it is recommended to start first with small *tolerance* level and then increases it gradualy if unstable results is detected. This exactly was demonestrated in the previous example sections in tables (4.1) and (4.2).

4.7.5.Maximum number of nonlinear iterations

The former two examples (4.6.2) and (4.6.3) are solved using NI_{max} equals 50. When instability in the results is detected such a number is increased to 100, 200, and 500. However, such an increase does not affect the solution. Hence, it is decided to increase the *tolerance* level instead (as presented in the former subsection).

4.6.4 Conclusions

In this chapter a new explicit boundary element modeling for the nonlocal damage was introduced. The solution requires boundary only discretization. If the strain exceeds the threshold strain at any point, an equivalent inclusion is placed to simulate its damage. The Eshelby's theory was coupled with the direct boundary integral equations to model the introduced equivalent inclusions. A finite-element like stiffness matrix is formulated and obtained directly in a condensed form along the problem boundary. In the developed approach there is no need for a prior knowledge for the damage zone in the problem. The present formulation is a boundary-only formulation and stretches the BEM to another era in nonlinear applications. The proposed idea was implemented in a detailed incremental-iterative load control procedure via computer code.

It was observed in this chapter that if instability was detected increasing the *tolerance* gradually can trace the load-displacement curve. It was also recommended that a modeler should analyze the relevant problem using more than one inclusion pattern to be able to accurately predict the problem nonlinear behavior.

The results of the examples demonstrated that the effect of discretization (either the boundary elements or the inclusion diameter) is decreased in the nonlocal approach than in the local one. Despite this observation, still this difference is

slightly more than the one occurred in the finite element method. This could be caused by the used circular inclusion type, which do not cover the overall damaged domain in both the intersected and the staggered patterns. Therefore, alternative types of inclusions (such as squares) should be furtherly investigated.
In this chapter the solution was obtained only for the raising part of the load-displacement curve, however it could be extended to model the falling part via using dispacement control or arclength algorithms.
In the following chapter a new family of FE will be used using the variational BIE as discussed in chapter 2 in order to simulate damage in more efficient way than the conventianal FE with respect to number of elements and the ability to use elemnts with arbitrary number of nodes which facilitates the modeling of the problem.

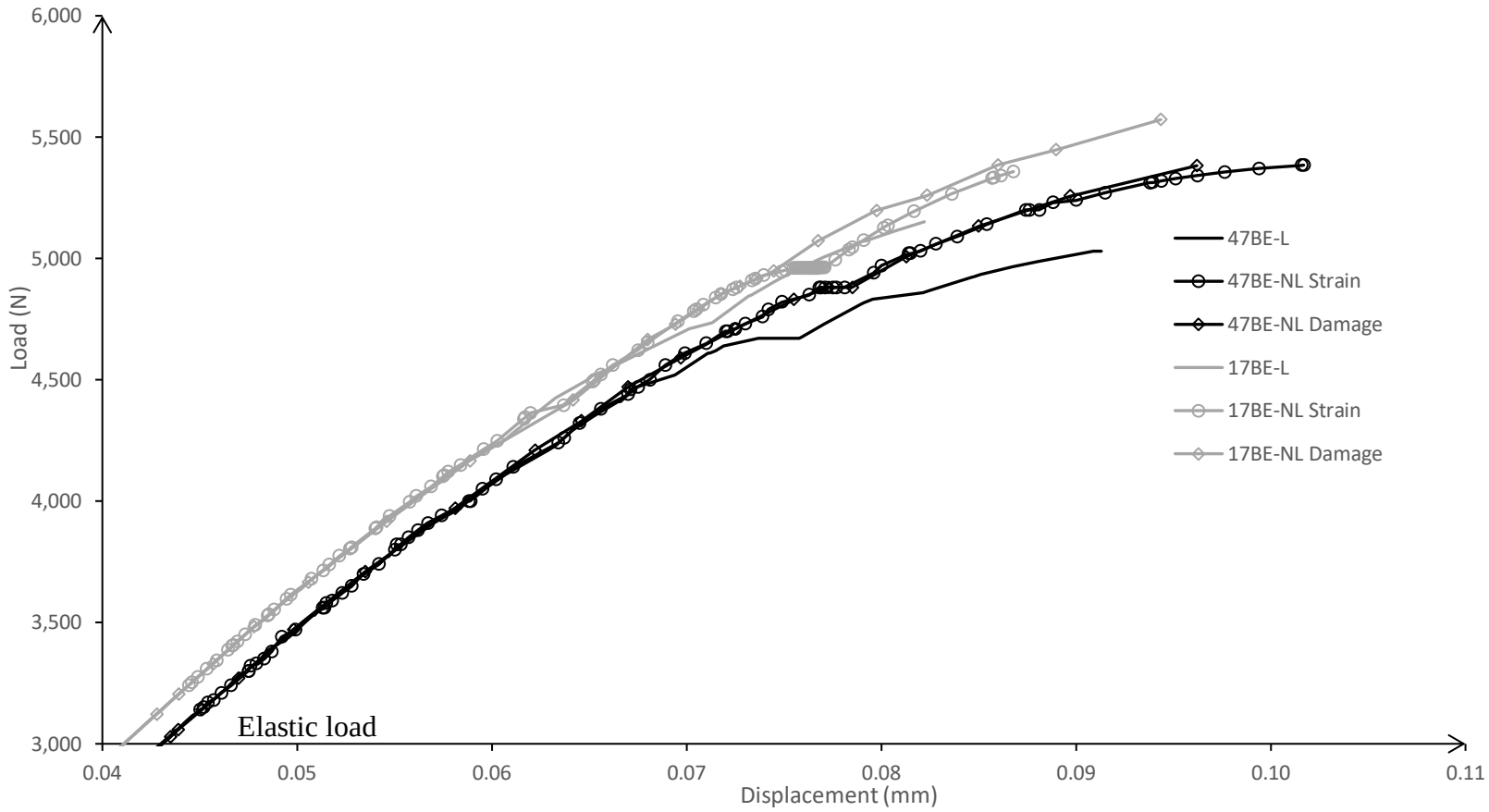

Fig.(4.19): Load-displacement curve for example 4.6.2 with different boundary discretizations.

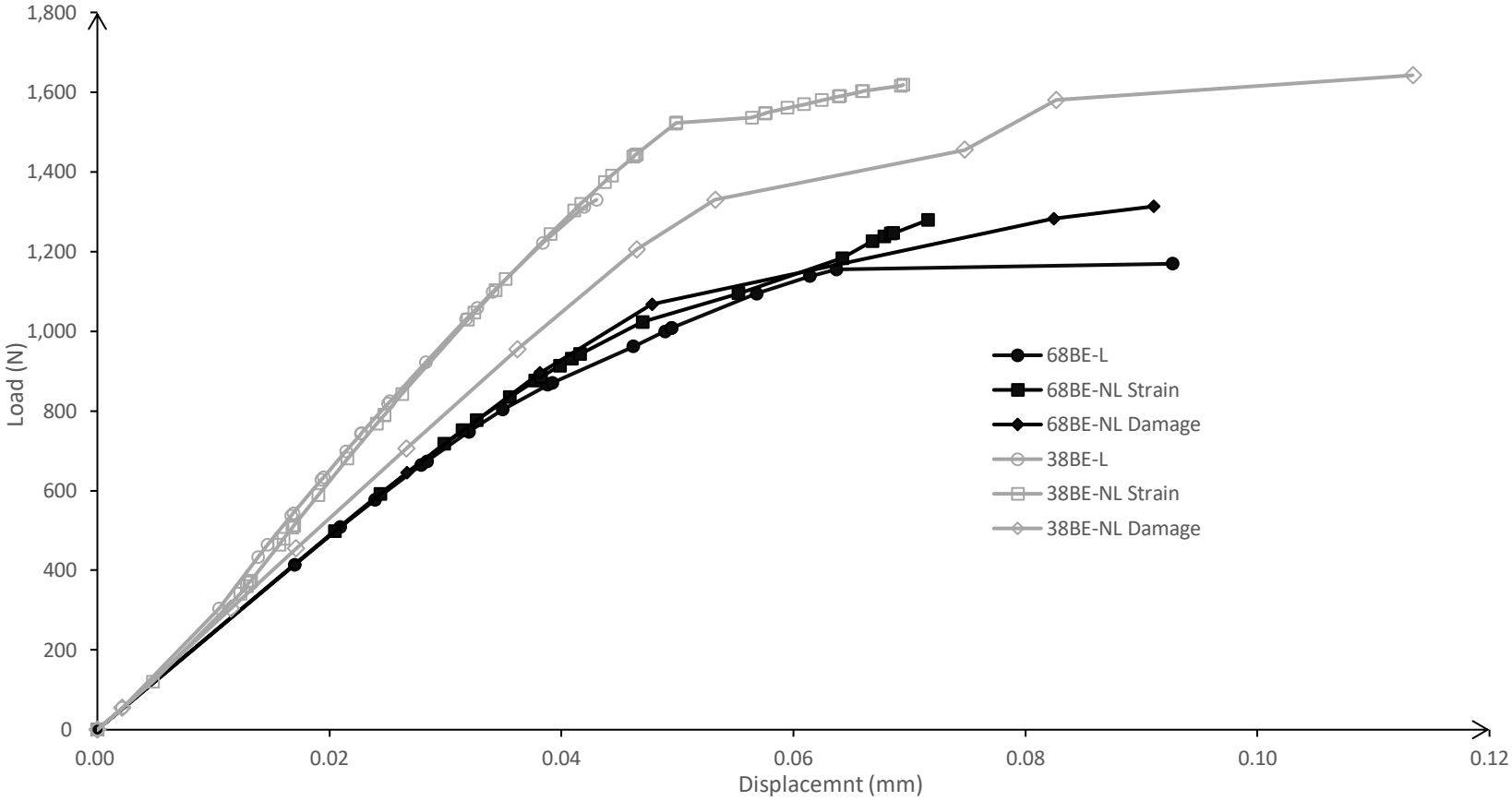

Fig.(4.20): Load-displacement curve for example 4.6.3 with different boundary discretizations.

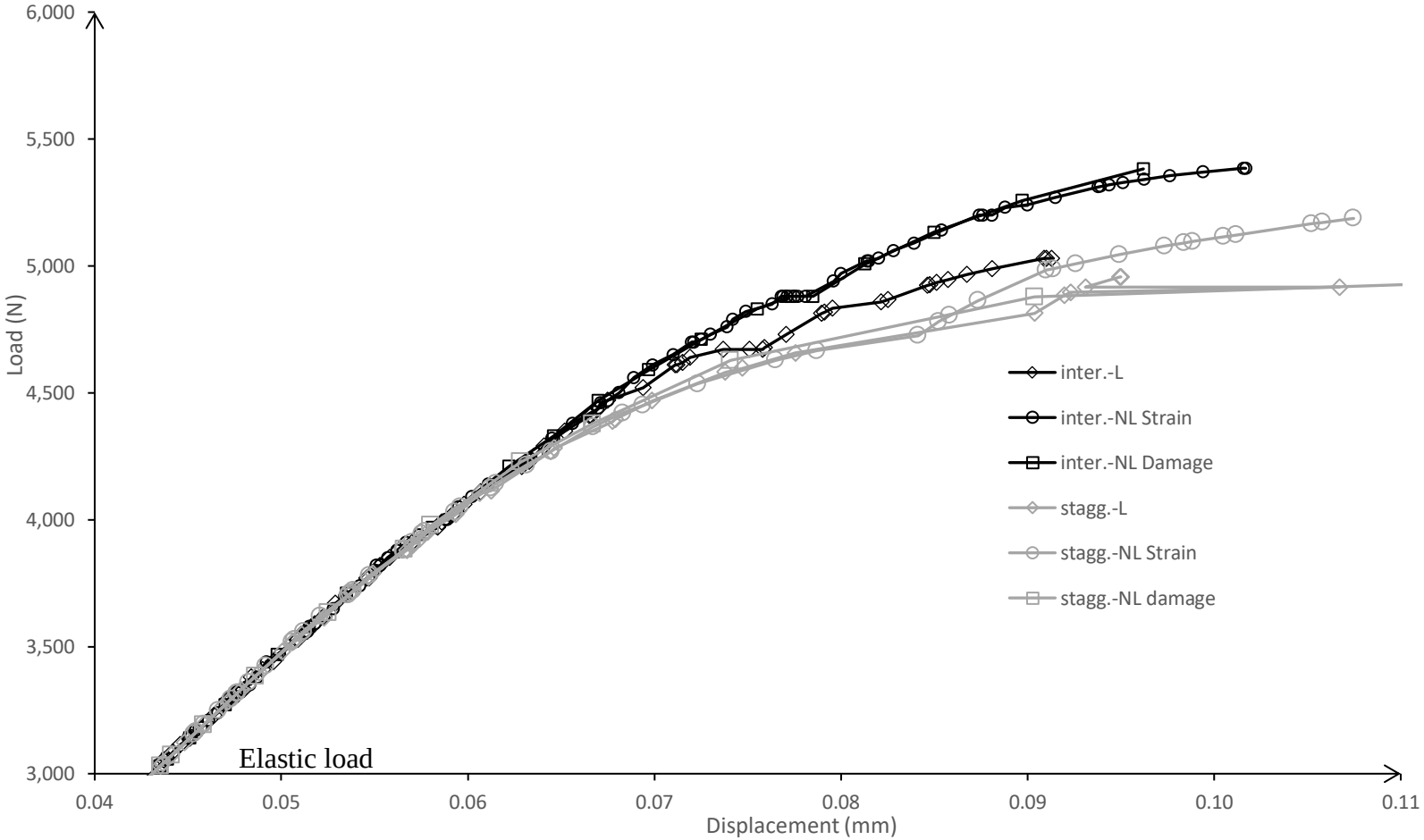

Fig.(4.21): Load-displacement curve for example 4.6.2 with different inclusion patterns.

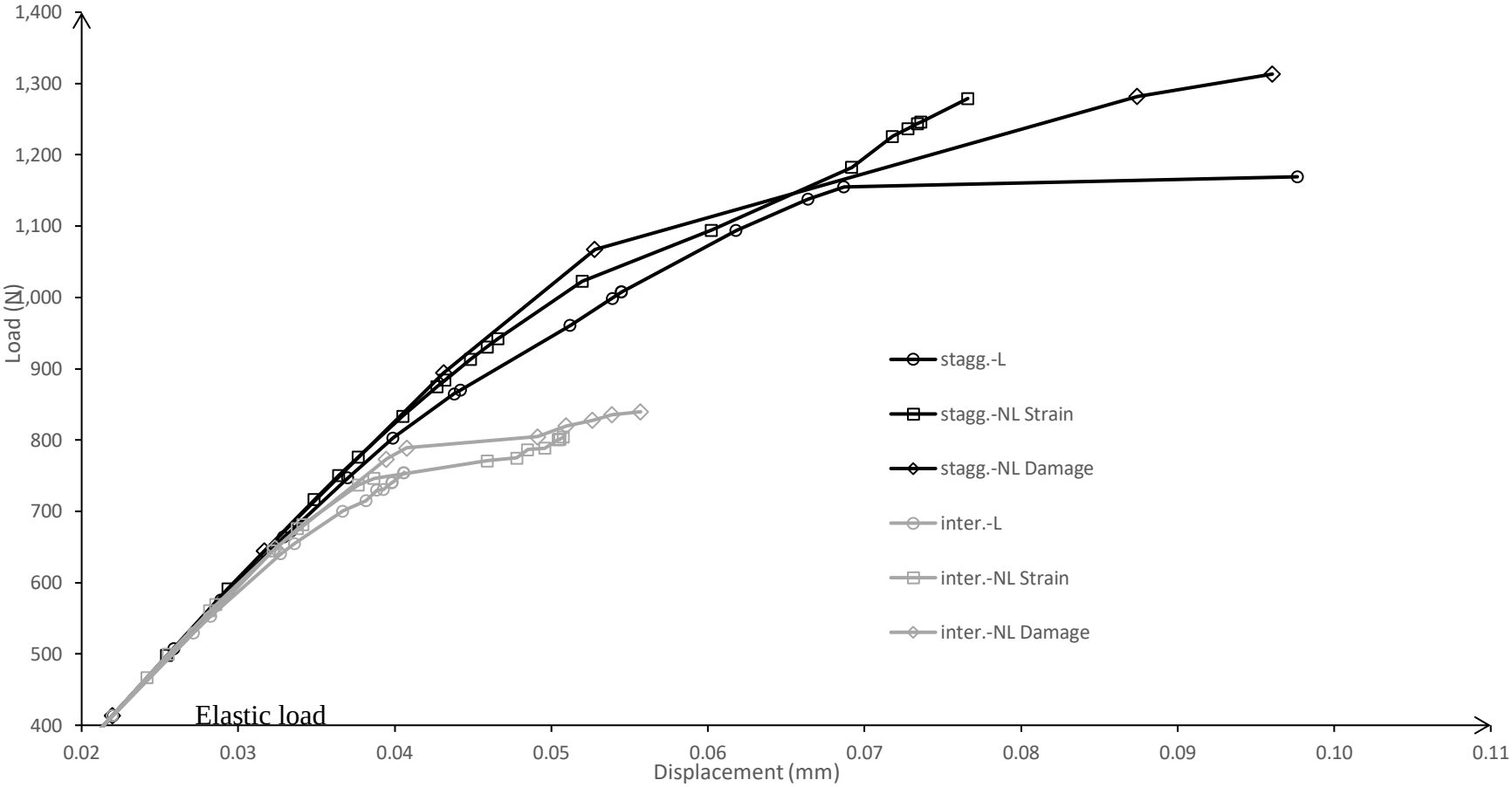

Fig.(4.22): Load-displacement curve for example 4.6.3 with different inclusion patterns.

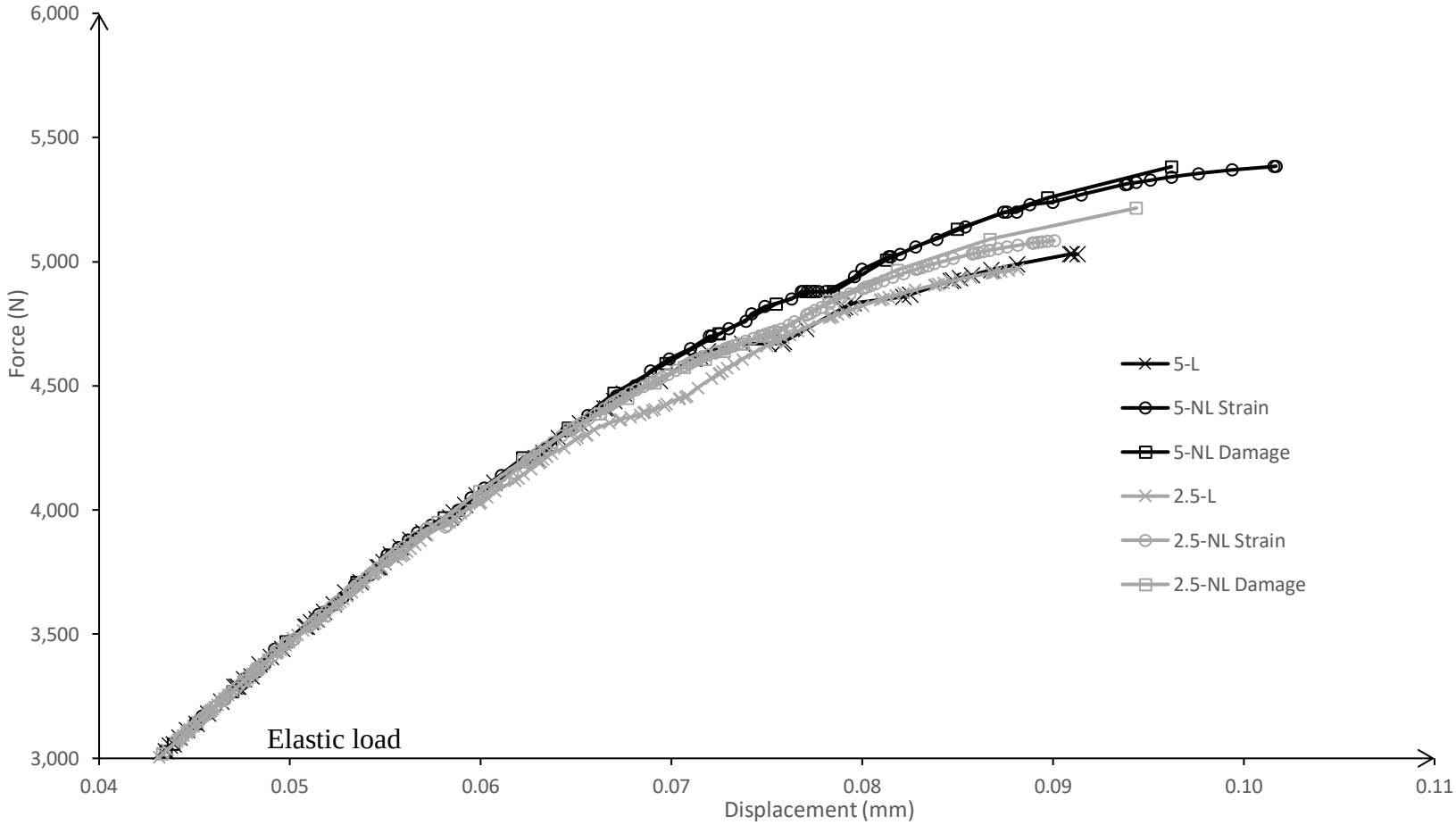

Fig.(4.23): Load-displacement curve for example 4.6.2 with different inclusion diameters (intersected case).

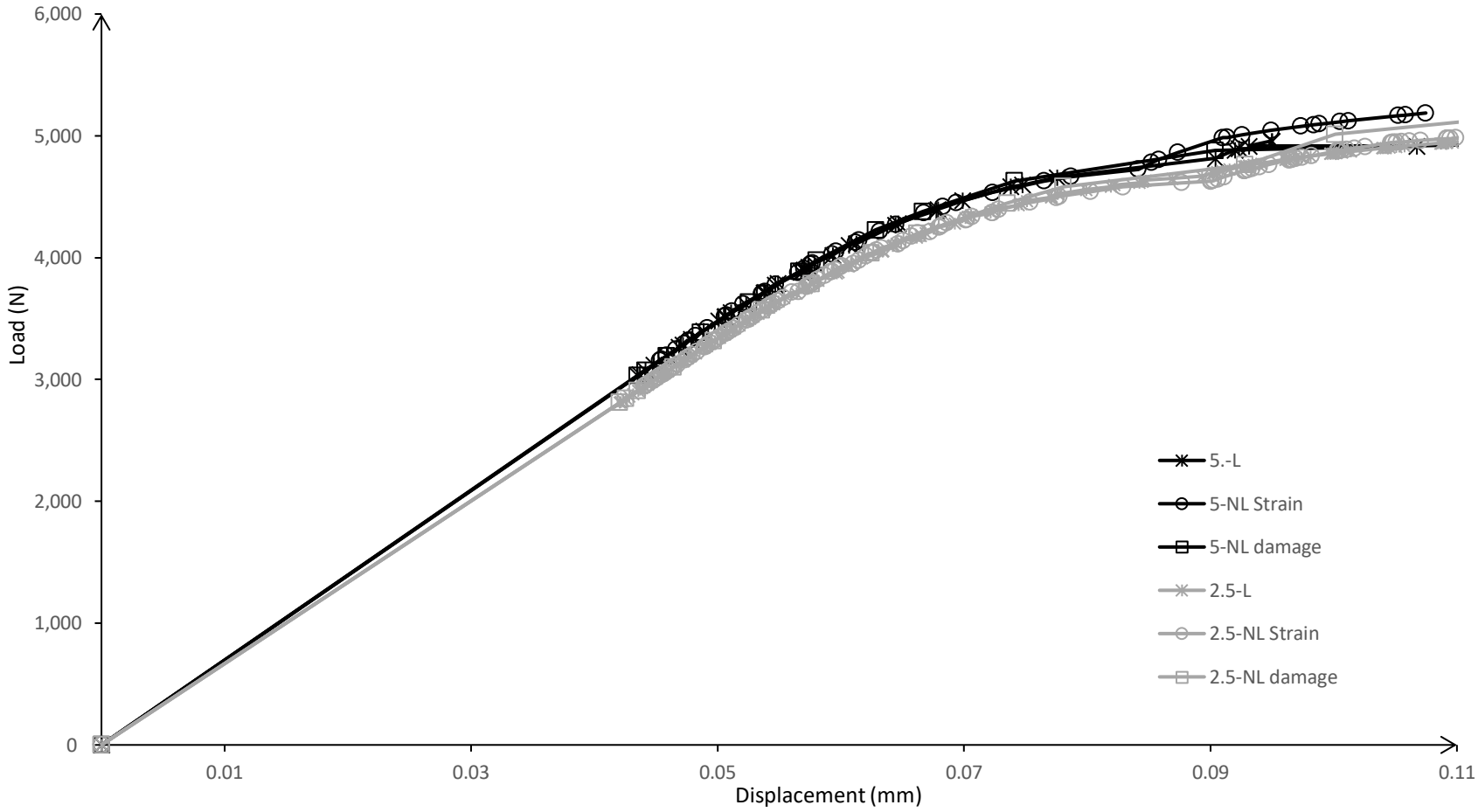

Fig.(4.24): Load-displacement curve for example 4.6.2 with different inclusion diameters (staggered case).

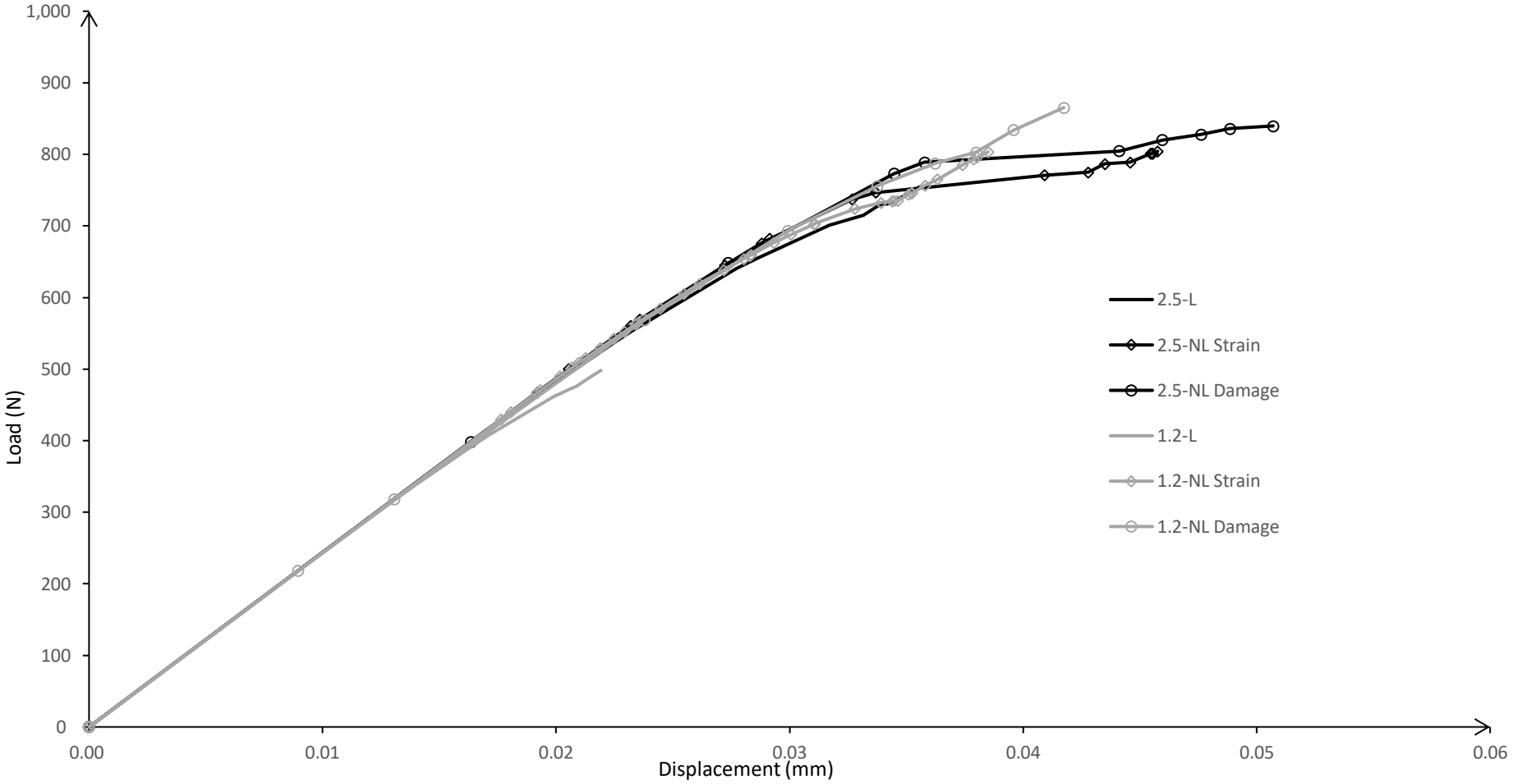

Fig.(4.25): Load-displacement curve for example 4.6.3 with different inclusion diameters (intersected case)

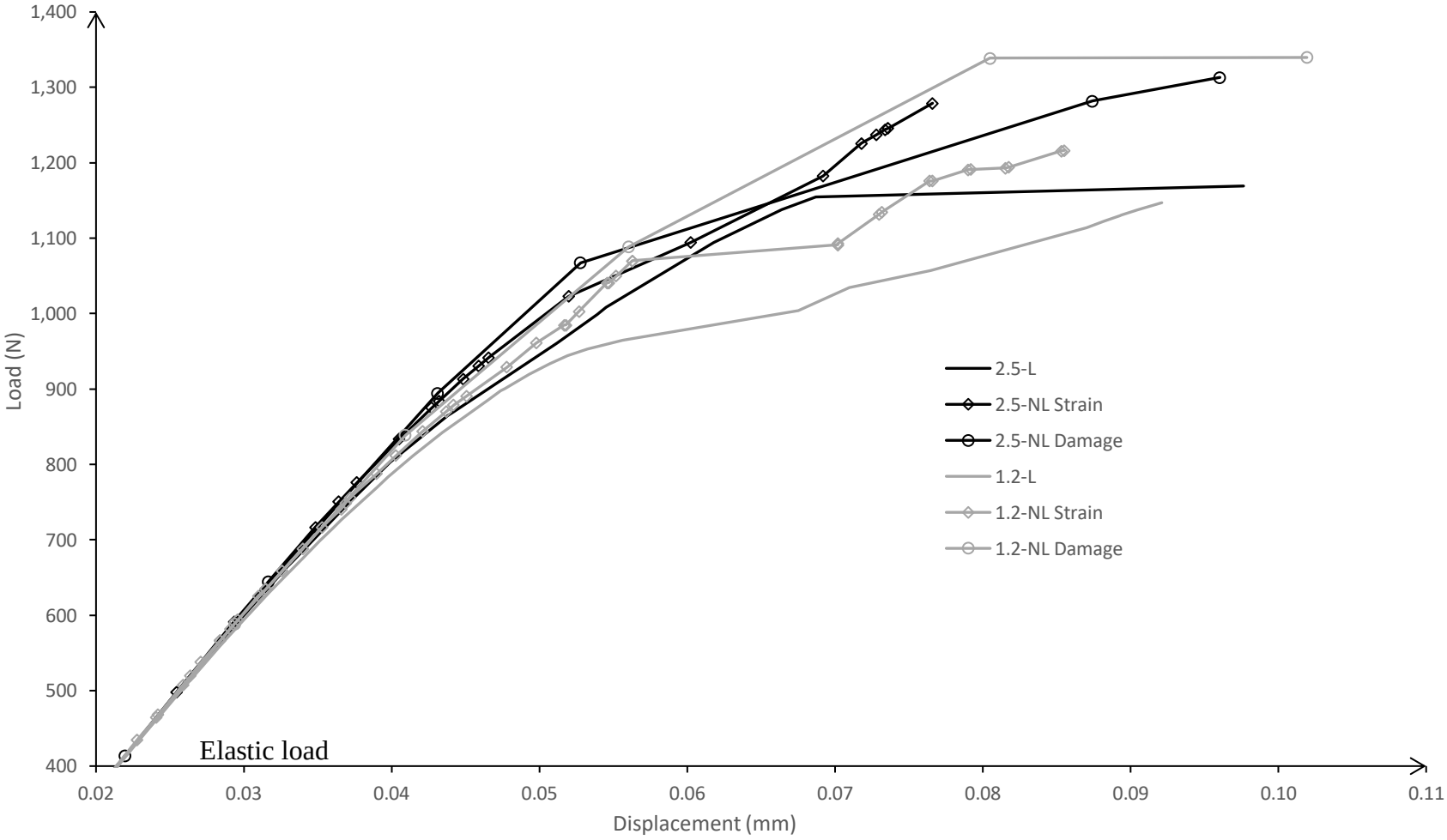

Fig.(4.26): Load-displacement curve for example 4.6.3 with different inclusion diameters (staggered case).

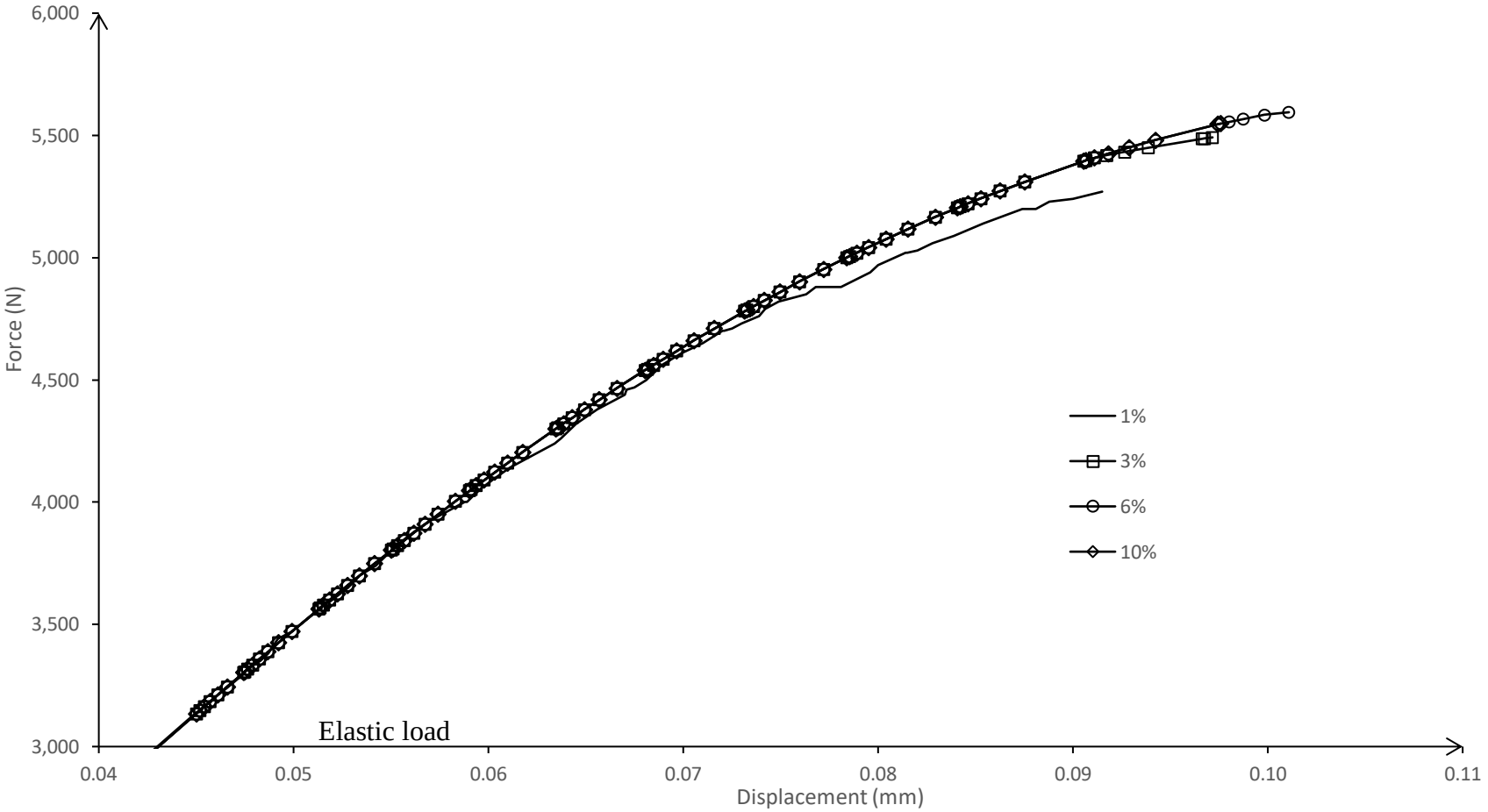

Fig.(4.27): Load-displacement curve for example 4.6.2 with different *tolerance* level.

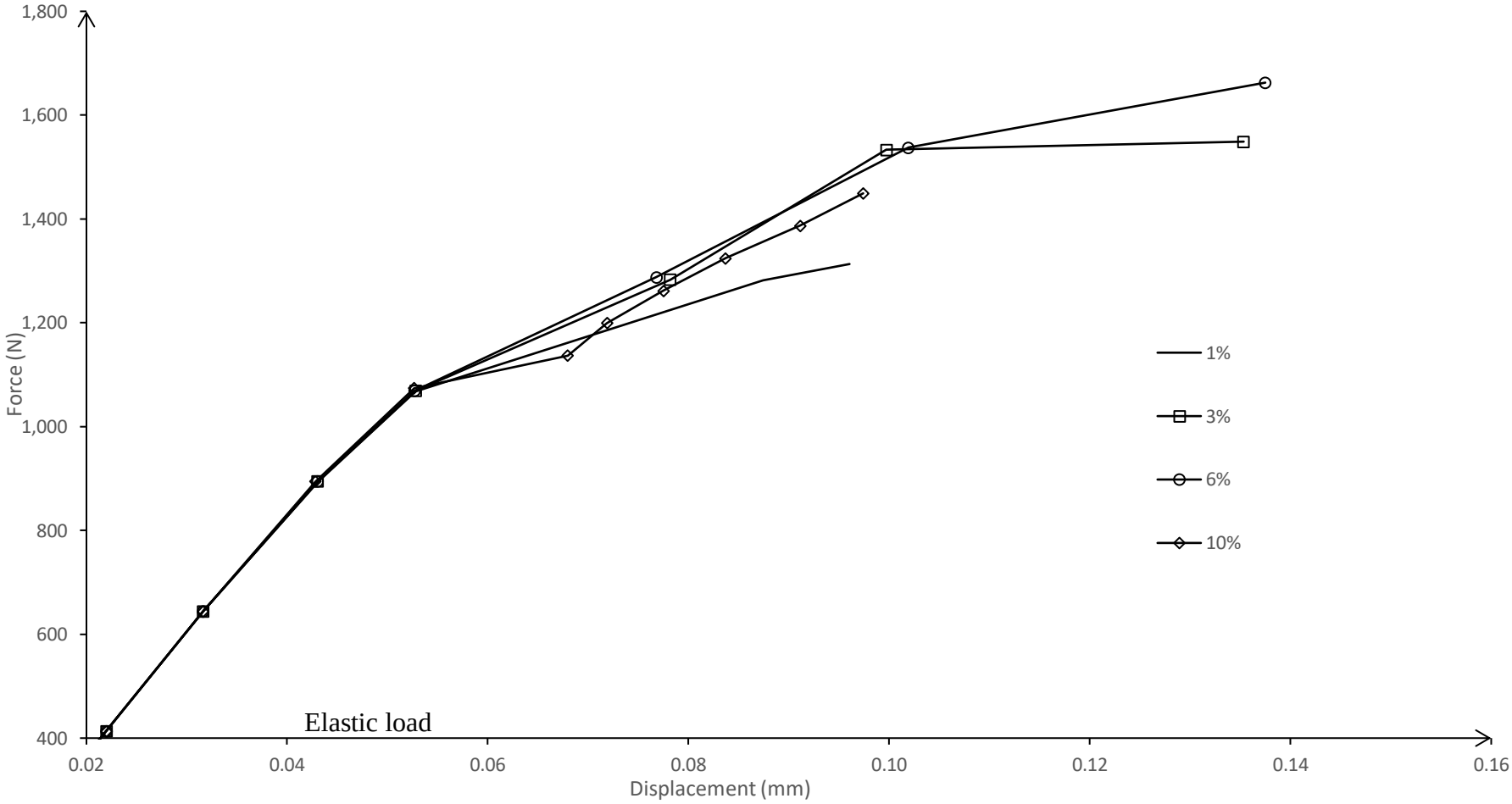

Fig.(4.28): Load-displacement curve for example 4.6.3 with different *tolerance* level.

Chapter 5: Damage simulation in Variational BIE

5.1. Introduction

In this chapter the VBIE is used to model damage. Using this formulation, a special type of finite element is used. This special type gives the ability to model the domain with lower number of degrees of freedom compared to the conventional FEM and create a symmetric stiffness. Three numerical examples are solved here to show the ability of the VBIE in modeling damage.

5.2. Special type of finite elements using VBIE

Using the VBIE described in chapter 2 special type of FE is used (Fundamental solution-based FE [59]). Instead of approximating the displacement on the boundary and inside the domain with interpolation function as in the conventional FE the displacement and traction are approximated on the boundary with interpolation functions, but inside the domain the displacement is calculated using the fundamental solution (recall Eq.(2.30, 2.31)). In this special type large size element can be used compared to the conventional FE.

In this work regular element is used i.e. the source points are placed outside the element as shown in Fig.(5.1). Of course, the location of the source points is obtained by trials. Without loss of generality quadratic boundary elements are used to model each FE.

On modeling damage only the part near the domain which is supposed to be damaged will be discretized with fine mesh and for the far part large discretization will be used.

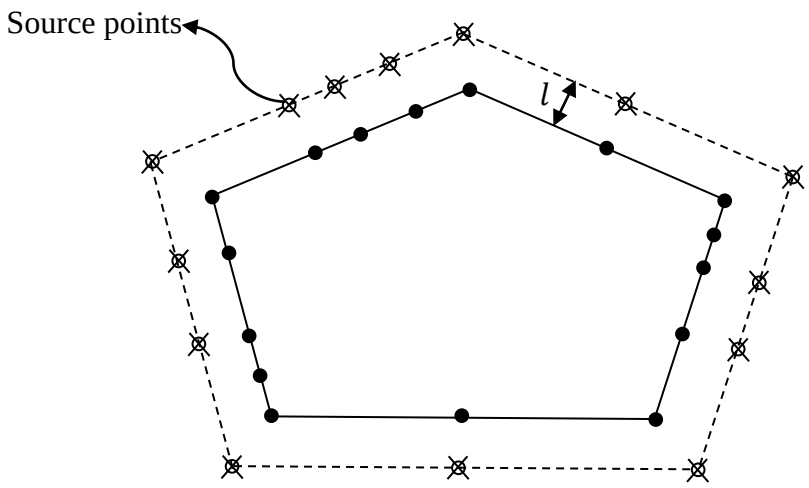

Fig.(5.1): Finite element according to the VBIE

5.3. Solution algorithm

Consider the nonlinear load-displacement curve shown in Fig.(4.2), the solution procedure is described as follows (given that the counter (*i*) represents the current number of the nonlinear iterations):

1. Discretize the domain of the problem into elements.
2. Define the internal points inside each element.
3. Divide the total load into increments.
4. At each load increment (j), the applied load $\{F\}_j^{\text{applied}}$ is computed as follows:

$$\{F\}_j^{\text{applied}} = \{F\}_{j-1}^{\text{applied}} + \{\Delta F\} \tag{5.1}$$

Where, $\{\Delta F\}$ is the load increment.

5. Use Eq. (2.37) to compute the unknown displacement $\{u_t\}$.

$$\{F\}_j^{\text{applied}} = [K]_j\{u_t\}_j \tag{5.2}$$

6. Compute the strain and the equivalent strain according to the used damage model (see Appendix B) at all internal points as follows:

$$\varepsilon_{jm}(y) = \sum_{k=1}^{k=N} \varepsilon^*_{ijm}(y, \xi_k)\psi_i(\xi_k) \tag{5.3}$$

7. Compute the maximum value of the equivalent strain ε^*_{max} of the undamaged elements.
8. In case of $\varepsilon^*_{max} > \varepsilon_D$ (where ε_D is the threshold strain, see Appendix B) modify the Young's modulus of the element to be:

$$E_{new} = (1 - D)E_o \tag{5.4}$$

Where, E_o is Young's modulus of the undamaged problem, *D* is the scalar damage variable representing the ratio of the area damaged in the material (*D* is calculated according to the assumed damage model, see Appendix B).

In case there are two points having the same ε^*_{max} (i.e. cases of symmetric problems) the same Young's modulus is assigned for the two elements as in Eq.(5.4). Otherwise, if $\varepsilon^*_{max} < \varepsilon_D$ and there is no damage at all elements, the load is increased (new load increment is added) in other words, jump to step 4.

9. Compute the updated stiffness $[K]_j^{(i)}$(by rebuilding Eq. (2.38)) and compute the updated force vector as follows:

$$\{F\}_j^{(i)} = [K]_j^{(i)}\{u_t\}_j^{(i-1)} \tag{5.5}$$

10. Compute the force residual vector $\{Res\}$ due to the change in the problem stiffness resulting from the occurred damage, as follows:

$$\{Res\} = \{F\}_j^{\text{applied}} - \{F\}_j^{(i)} \tag{5.6}$$

11. Compute the maximum value of $\{Res\}$ to be denoted by Res_max. In case of Res_max > *tolerance*, continue to step 12 otherwise jump to step 16.
12. Compute the change in displacement $\{\Delta u\}_j^{(i)}$ due to the residual force vector $\{Res\}$, and the change in strain $\{\Delta\varepsilon\}_j^{(i)}$ from Eq. (5.3):

$$\{\Delta u\}_j^{(i)} = \left([K]_j^{(i)}\right)^{-1}\{Res_j\} \tag{5.7}$$

13. Compute the total displacement $\{u_t\}_j^{(i)}$, and total strain $\{\varepsilon_t\}_j^{(i)}$ at each damaged point, as follows:

$$\{u_t\}_j^{(i)} = \{u_t\}_j^{(i-1)} + \{\Delta u\}_j^{(i)} \tag{5.8}$$

$$\{\varepsilon_t\}_j^{(i)} = \{\varepsilon_t\}_j^{(i-1)} + \{\Delta \varepsilon\}_j^{(i)} \tag{5.9}$$

14. Modify the damage variable according to the modified total strain in Eq.(5.9) and then compute the modified Young's modulus from Eq.(5.4).
15. Repeat steps from step 9 until the numerical value of the maximum force residual Res_max is within the chosen *tolerance*. In other words, jump to step 9.
16. Check the undamaged points: if there is no other point with $\varepsilon^* > \varepsilon_D$, increase the applied load by $\{\Delta F\}$ (apply another load increment) and repeat from step 4, otherwise if there is other point with $\varepsilon^* > \varepsilon_D$ jump to step8.
17. In case the number of iterations (*NI*) reaches its maximum value for the secant algorithm and Res_max > *tolerance*, decrease the load increment, in other words, use one half of the load increment (*j*): and repeat the load increment starting from step 4.

$$\{\Delta F\}_j = \frac{1}{2}\{\Delta F\}_j \tag{5.10}$$

Hence, repeat steps starting from step 4.

This procedure is repeated until the problem reaches a stable damage pattern under a certain load or reaches numerical instability, regardless, increasing the number of nonlinear iterations or increasing the used *tolerance* level.

5.4. Numerical examples

Three numerical examples are solved here to demonstrate the ability of the variational formulation to model damage with coarse mesh compared to that of the conventional finite element method. In the examples shown the tolerance used is 1% and the maximum number of iterations is 50. The location of the source points $l = 4m$. The number of internal points in each element is the number of nodes plus one

5.4.1.Simply supported beam

This problem as shown in Fig.(4.9) was previously solved by Jirasek [25] using the FEM. The damage model according to Jirasek [25] as mentioned in Appendix B is used. The material properties of the beam are E_o=21670724658 N/m^2, ν=0.2, ε_D=0.00012 and ε_f=0.007. The beam thickness is 100 mm.

Only half of the problem is solved due to symmetry. The problem is solved using 2 discretization, 201 element (mesh 1 with size 5 mm near the mid of the beam) and 697 element (mesh 2 with size 2.5 mm near the mid of the beam) as shown in Fig.(5.2 and 5.3). The number of internal points in each element is the number of nodes plus 1.

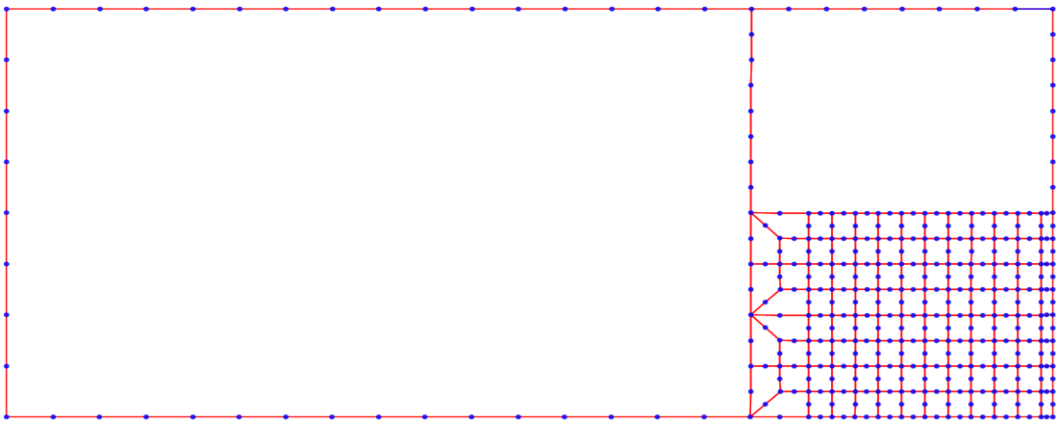

Fig.(5.2): Mesh1 of the domain of half of the problem in example 5.4.1.

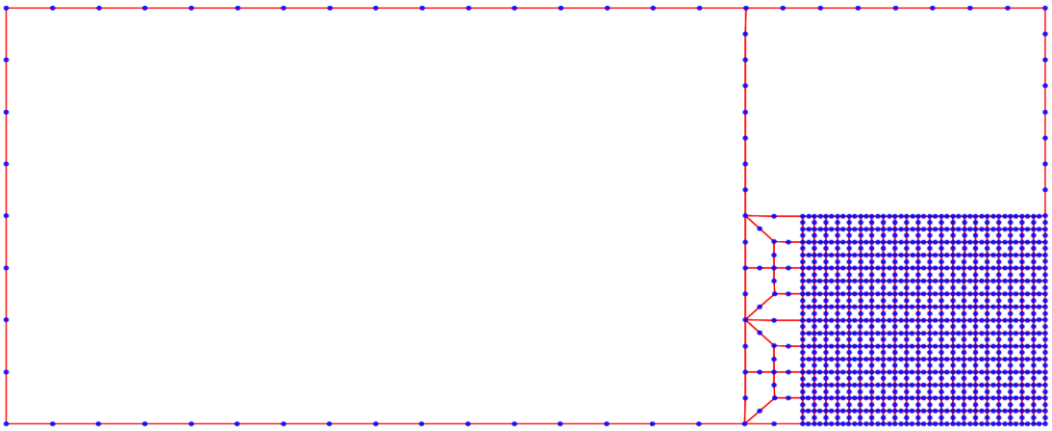

Fig.(5.3): Mesh 2 of the domain of half of the problem in example 5.4.1.

Figure (5.4) shows the load-displacement curve of the problem at the midpoint of the beam. The results are compared to that of Jirasek [25] at which the problem was solved using conventional finite element method with two meshes 15 mm and 5 mm. Good agreement with the results is shown, although course mesh is used compared to that of Jirasek [25], which shows the ability of the variational formulations to use large size elements with arbitrary number of nodes.

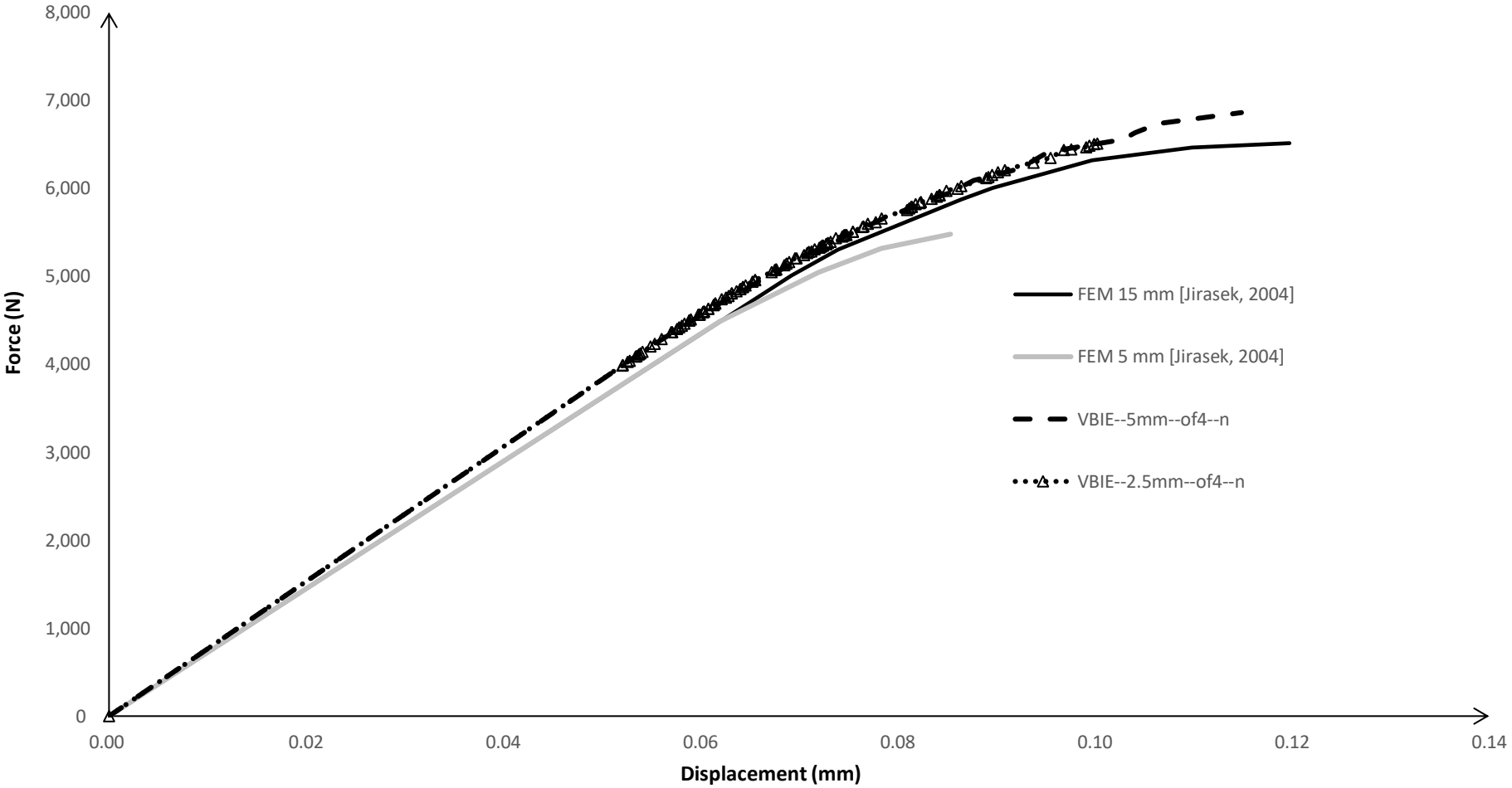

Fig.(5.4): Load-displacement curve of example 5.4.1.

5.4.2. Fixed-Fixed beam

This problem as shown in section 4.6.1 is solved here using the VBIE. The problem is discretized as shown in Fig.(5.5, 5.6) with two meshes.

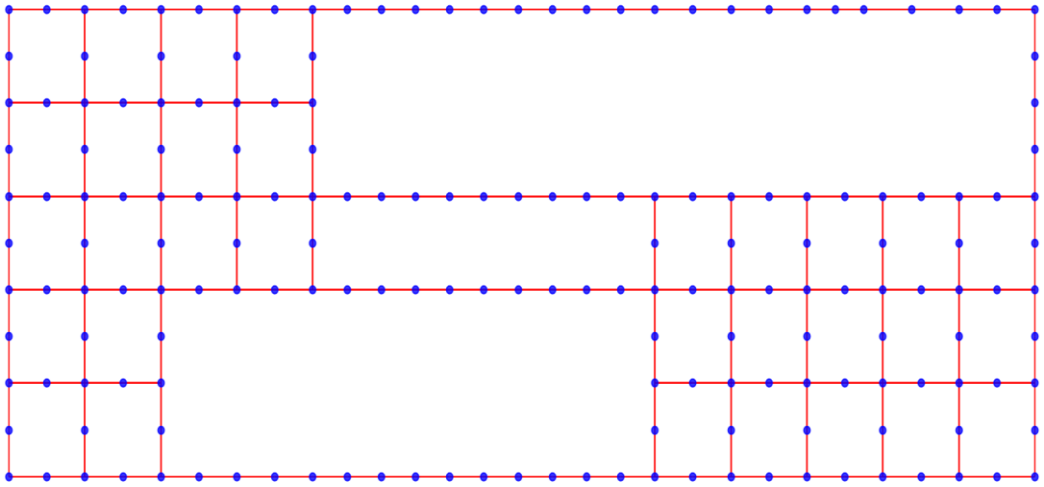

Fig.(5.5): Mesh 1 of the domain of half of the problem in example 5.4.2.

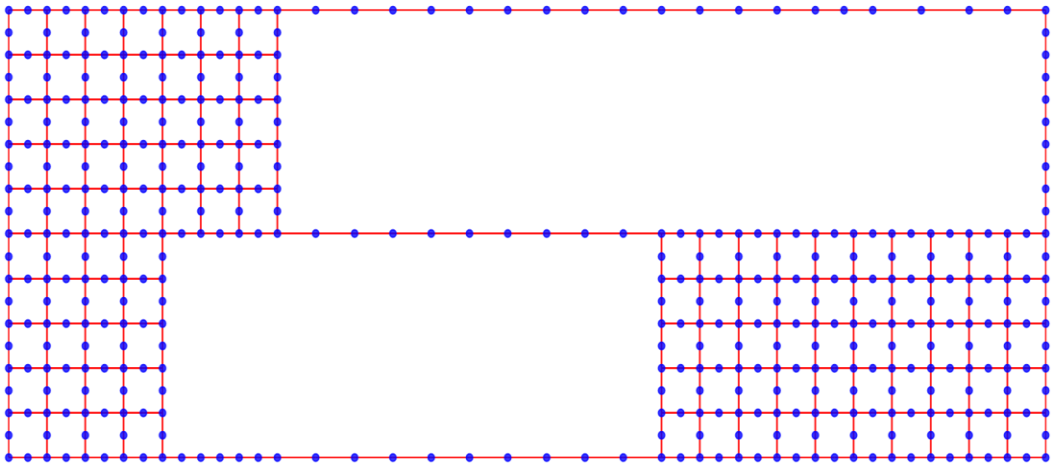

Fig.(5.6): Mesh 2 of the domain of half of the problem in example 5.4.2.

The load displacement curve at point A Fig.(4.4) is shown in Fig.(5.7) with the solution of Pituba [50]. Good agreement with the results of [50] is achieved.

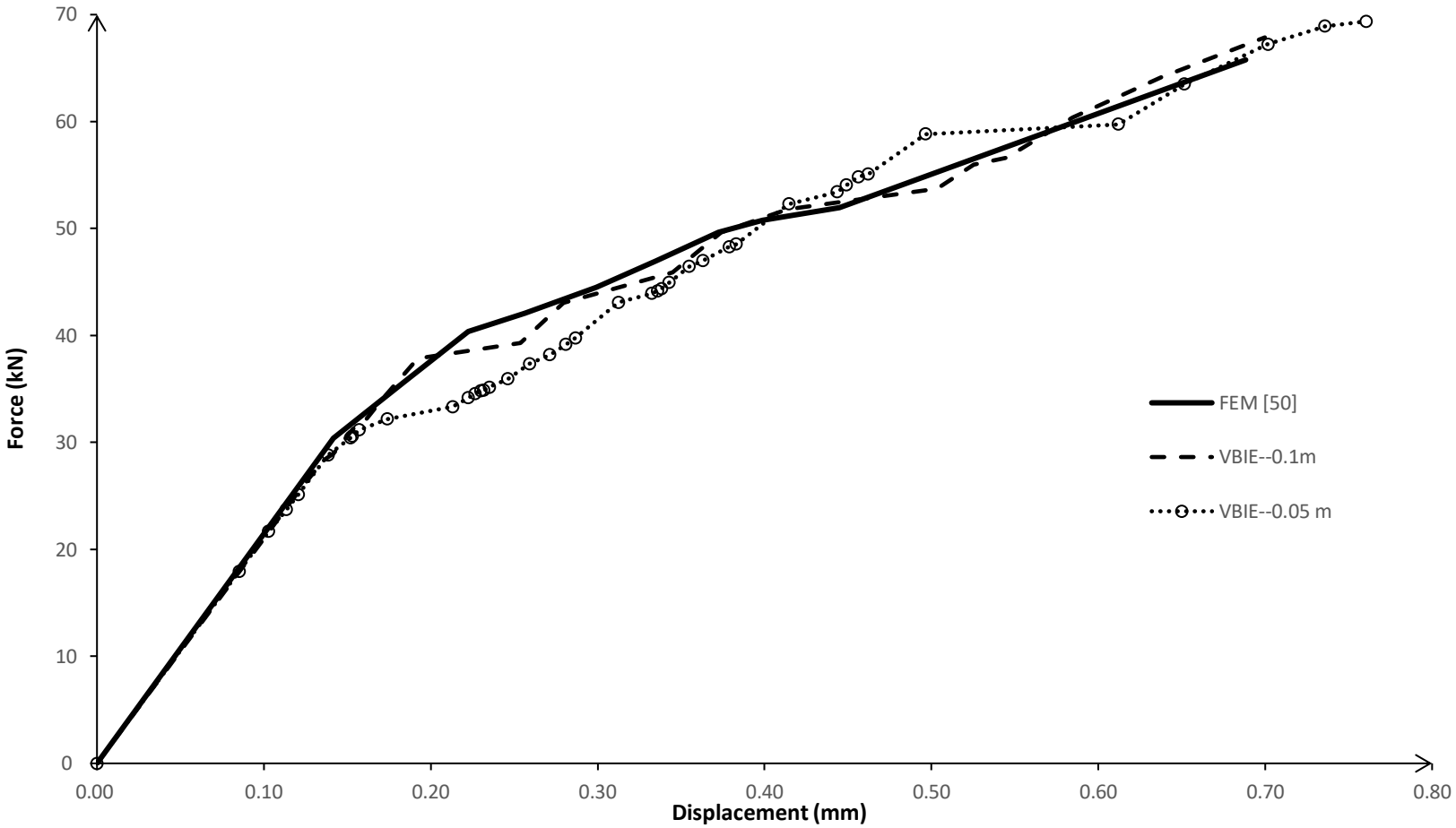

Fig.(5.7): Load-displacement curve of example 5.4.2.

5.4.3. Simple beam with notch

This problem shown in Fig.(4.13) was previously considered by Jirasek [25] experimentally and verified by FEM. The damage model according to Jirasek [25] as mentioned in Appendix B is used. The material properties of the beam are E_o=2×10^{10} N/m^2, ν=0.2, ε_D=0.00012 and ε_f=0.007. The beam thickness is 100 mm. The main purpose of this example is to demonstrate the stability of the proposed formulation to trace the damage in cases of stress concentrations.

Only half of the problem is solved due to symmetry. The problem solved using 2 discretization, 193 element (mesh 1) and 681 element (mesh 2) as shown in Fig.(5.8 and 5.9).

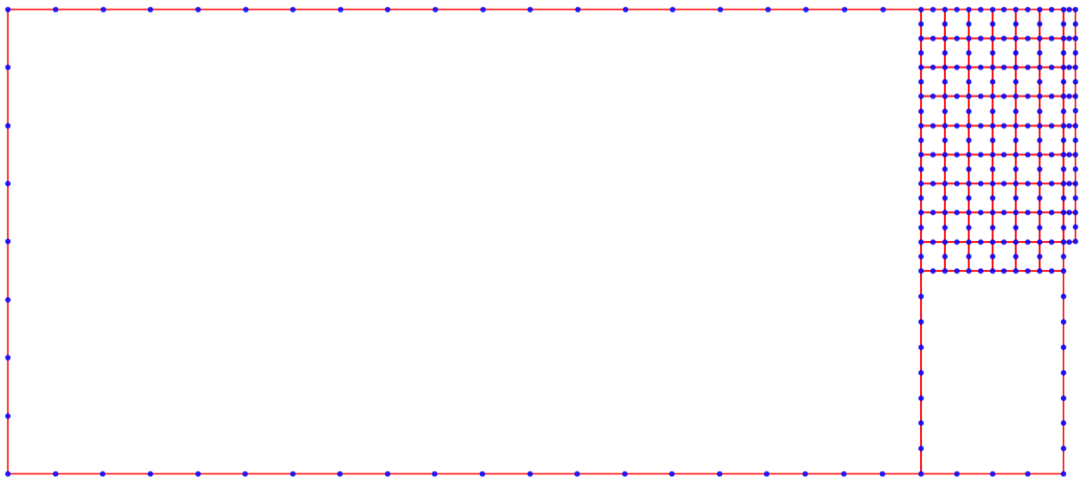

Fig.(5.8): Mesh 1 of the domain of half of the problem in example 5.4.3.

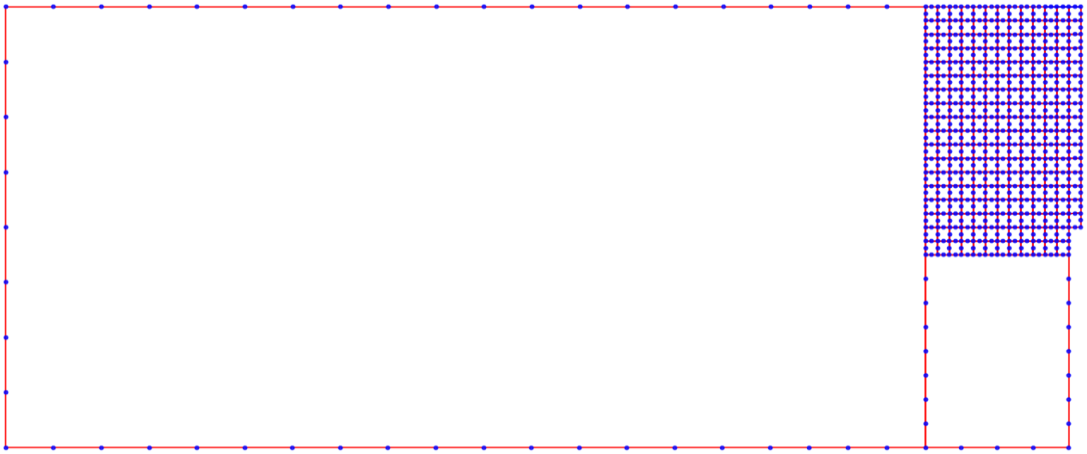

Fig.(5.9): Mesh 2 of the domain of half of the problem in example 5.4.3.

Figure (5.10) shows the load-displacement curve of the problem at the midpoint of the beam. The results are compared to that of Jirasek [25] at which the problem was solved using conventional finite element method with two meshes 5 mm and 1.67 mm, also experimental results for the problem are shown. Good agreement with the results is shown, although course mesh is used compared to that of Jirasek [25], which shows the ability of the variational formulations to use large size elements with arbitrary number of nodes

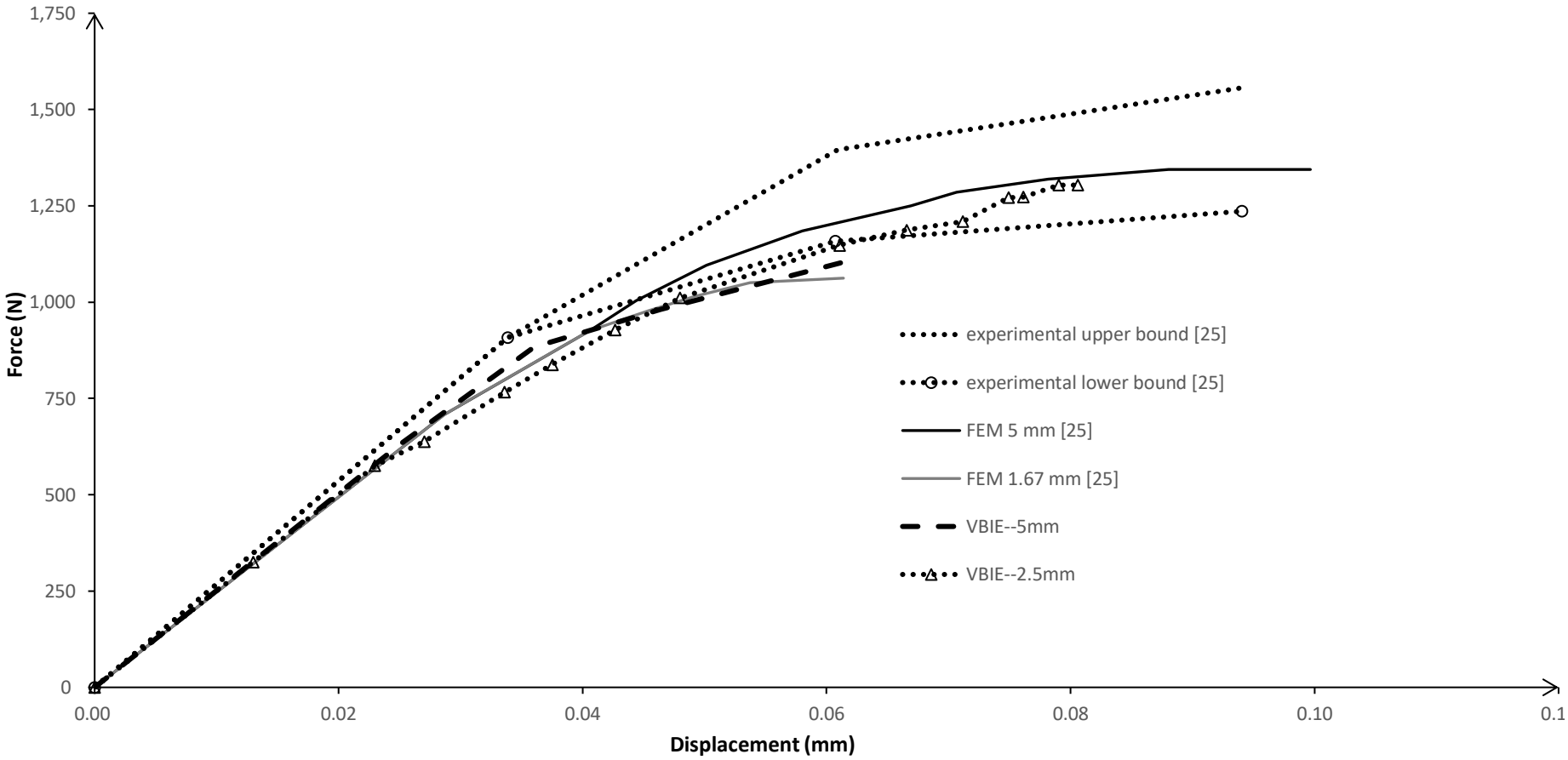

Fig.(5.10): Load-displacement curve of example 5.4.3.

5.5. Conclusions

It was shown in this chapter the ability of the variational formulation to model the damage with good accuracy despite using large size elements compared with the conventional finite element method.

Chapter 6: Summary and Future work

6.1. Summary

In this Thesis:

Eshelby's theory for equivalent inclusions was coupled with the indirect boundary integral equation (as a meshless technique) to solve problems with inhomogeneity for the first time using the indirect boundary integral equations.

Eshelby's theory coupled with the direct boundary integral equation was used to model damage where a finite-element like stiffness matrix is formed for the damaged problems obtained directly on the boundary in a condensed form.

The variational formulation for 2D elasticity has been used to model damage where the advantage of using coarse finite element compared to the conventional finite element was shown.

6.2. Future work

1- Our algorithm for the damage can be modified to use the displacement control or the arc length technique to be able to trace the snap through and snap back curves.
2- Use of inclusions with other shapes than the circle to be able to improve the modelling of the damaged areas (or the inhomogeneous parts).
3- Use adaptive techniques for the VBIE formulation.

Appendix A

Eshelby tensor for interior ($i = j$) and exterior point ($i \neq j$) [3,24,30]:

For $i = j$:

$$S_{qlmn}^{ii} = \frac{1}{8(1-\nu)}(3-4\nu)\left(\delta_{qm}\delta_{ln} + \delta_{qn}\delta_{lm}\right) + (4\nu-1)\delta_{ql}\delta_{mn} \tag{A.1}$$

For $i \neq j$:

$$\begin{aligned} S_{qlmn}^{ij} = \frac{\rho^2}{8(1-\nu)}\{&(\rho^2+4\nu-2)\delta_{ql}\delta_{mn} \\ &+ (\rho^2-4\nu+2)\left(\delta_{qm}\delta_{ln} + \delta_{qn}\delta_{lm}\right) + 4(1-\rho^2)\delta_{ql}r_{,m}r_{,n} \\ &+ 4(1-2\nu-\rho^2)\delta_{mn}r_{,i}r_{,j} \\ &+ 4(\nu-\rho^2)\left(\delta_{qm}r_{,l}r_{,n} + \delta_{lm}r_{,q}r_{,n} + \delta_{qn}r_{,l}r_{,m} + \delta_{ln}r_{,q}r_{,m}\right) \\ &+ 8(3\rho^2-2)r_{,q}r_{,l}r_{,m}r_{,n}\} \end{aligned} \tag{A.2}$$

Where,

$$\rho = \frac{R}{\sqrt{x^2+y^2}} \tag{A.3}$$

The expression of Q for interior ($i = j$) and exterior point ($i \neq j$) [24,61]:

For $i = j$:

$$\begin{aligned} Q_{mql}^{ii} = \frac{1}{8(1-\nu)}\Big(&-\left(\delta_{mq}x_l + \delta_{ml}x_q + \delta_{ql}x_m\right) + 4\nu\delta_{ql}x_m \\ &+ 4(1-\nu)\left(\delta_{mq}x_l + \delta_{ml}x_q\right)\Big) \end{aligned} \tag{A.4}$$

For $i \neq j$:

$$\begin{aligned} Q_{mql}^{ij} = \frac{\rho^2}{8(1-\nu)}\{&(\rho^2-2)\left(\delta_{mq}x_l + \delta_{ml}x_q + \delta_{ql}x_m\right) + 4r(1-\rho^2)r_{,q}r_{,l}r_{,m} \\ &+ 4\nu\delta_{ql}x_m + 4(1-\nu)\left(\delta_{mq}x_l + \delta_{ml}x_q\right)\} \end{aligned} \tag{A.5}$$

Appendix B

There are two damage models used herein, the first is the Jacky Mazars's damage model [37,38] which is used for concrete and defines the local damage as follows:

$$D(\varepsilon^*) = \begin{cases} 1 - \left[\dfrac{\varepsilon_D(1-a)}{\varepsilon^*} + \dfrac{a}{exp\big(b(\varepsilon^* - \varepsilon_D)\big)}\right] & if\ \varepsilon^* \geq \varepsilon_D \\ 0 & if\ \varepsilon^* < \varepsilon_D \end{cases} \quad \text{(B.1)}$$

Where, ε_D is the threshold strain, a, b, are material constants obtained experimentally.

The second damage model is according to [25,64] and define the local damage as follows:

$$D(\varepsilon^*) = \begin{cases} 1 - \dfrac{\varepsilon_D}{\varepsilon^*} exp\left(-\dfrac{\varepsilon^* - \varepsilon_D}{\varepsilon_f - \varepsilon_D}\right) & if\ \varepsilon^* \geq \varepsilon_D \\ 0 & if\ \varepsilon^* < \varepsilon_D \end{cases} \quad \text{(B.2)}$$

Where, ε_f is a material constant defined in [25,64].

It has to be noted that Poisson's ratio is assumed to be unchanged due to the occurred damage.

Appendix C

The analytical solution for stresses for Kirch problem is [58]:

$$\sigma_{xx}(r,\theta) = \sigma_o \left[1 - \frac{R^2}{r^2}\left(\frac{3}{2}cos2\theta + cos4\theta\right) + \frac{3R^2}{2r^2}cos4\theta\right] \quad \text{(C.1)}$$

$$\sigma_{xy}(r,\theta) = \sigma_o \left[-\frac{R^2}{r^2}\left(\frac{1}{2}sin2\theta + sin4\theta\right) + \frac{3R^2}{2r^2}sin4\theta\right] \quad \text{(C.2)}$$

$$\sigma_{yy}(r,\theta) = \sigma_o \left[-\frac{R^2}{r^2}\left(\frac{1}{2}cos2\theta - cos4\theta\right) - \frac{3R^2}{2r^2}cos4\theta\right] \quad \text{(C.3)}$$

in which, R and r are as define in Fig.(4.4).

REFERENCES

[1] Bažant Z P. Instability, ductility, and size effect in strain-softening concrete. J. Eng. Mech. Div. 1976; **102**(2): 331–44.

[2] Bažant Z P and Pijaudier-Cabot G. Nonlocal continuum damage, localization instability and convergence. J. Appl. Mech. 1988; **55**: 287-293.

[3] Becker A.A. Boundary element method in Engineering. A complete course, Mc-Graw-Hill, 1992.

[4] Belytschko T, Lu YY , Gu L . Element-free Galerkin methods. Int J Numer Methods Eng 1994; **37**(2):229–56.

[5] Botta A.S., Venturini W.S., Benallal A. A BEM implicit formulation applied to damage mechanics models. Transactions on Modelling and Simulation. 2003; **34**: 287–298.

[6] Botta A.S., Venturini W.S., Benallal A. BEM applied to damage models with emphasis on the localization and regularization techniques. Latin American Journal of Solids and Structures. 2005; **2**(1): 89–101.

[7] Brebbia C.A, Telles, J.C.F., Wrobel, L.C. Boundary elements techniques, Theory and Applications in Engineering. Springer-Verlag Berlin, Heidelberg, 1984.

[8] Carpinteri A., Scavia C. and Yang G.P. Microcracks propagation, coalescence and size effects in compression. Engineering Fracture Mechanics 1996; **54**: 335–347.

[9] Carpinteri A. and Yang G.P. The damage process in a finite-sized brittle specimen with interacting microcracks. Fatigue fracture Engineering Material structure 1997; **20**: 1105–1115.

[10] Cheng A., Hong Y. An overview of the method of fundamental solutions — Solvability, uniqueness, convergence, and stability. Engineering analysis with boundary elements 2020; **120**: 118–152.

[11] Comi C. and Perego U. Fracture energy based bi-dissipative damage model for concrete. International Journal of solids and structures 2001; **38**: 6427–6454.

[12] Crouch S.L. and Starfield A. M. Boundary element methods in solid mechanics with application in rock mechanics and geological engineering. George Allen and Unwin, London, 1983.

[13] De Borst R, Crisfield M. A., Remmers J.J.C., Verhoosel C. V. Nonlinear Finite Element Analysis of solids and structures. John Wiley & Sons Ltd, 2012.

[14] De Figueiredo T. G. B. A new boundary element formulation in engineering. In C. A. Brebbia and S. A. Orszag, editors, Lecture Notes in Engineering. Springer–Verlag, 1991.

[15] De Vree J.H.P., Brekelmans W.A.M., Van Gils, M.A.J. Comparison of nonlocal approaches in continuum damage mechanics. Computer and Structures. 1995; **55**(4): 581 – 588.

[16] Eshelby J.D. The determination of the elastic field of an ellipsoidal inclusion and related problem. Proceedings of the Royal Society of London. 1957; **A241**: 376–396.

[17] Garcia R., Florez-Lopez J., Cerrolaza M. A boundary element formulation for a class of non-local damage models. International Journal of solids and structures 1999; **36**: 3617–3638.

[18] Gurson A. L. Continuum Theory of Ductile Rupture by Void Nucleation and Growth: Part 1 — Yield Criteria and Flow Rules for Porous Ductile Media. GTRansaction ASME 1977; **99**: 2–15.

[19] Hang Ma, Li-wei Xia, Qin Qing Hua. Computational model for short-fiber composites with eigenstrain formulation for boundary integral equations. J. of applied Mathematics and Mechanics. 2008; **29**(6): 757–767.

[20] Hang Ma, Yan Cheng, Qin Qing Hua. Eigenstrain formulation of boundary integral equations for modeling particle-reinforced composites. J. Engineering analysis with boundary elements. 2009; **33**: 410–419.

[21] Hang Ma, Yan Cheng and Qin Qing Hua. Eigenstrain boundary integral equations with local Eshelby matrix for stress analysis of ellipsoidal particles. Math. Probl. Eng. 2014; 947205:1–10.

[22] Herding U. and Kuhn G. A field boundary element formulation for damage mechanics. Engineering Analysis with Boundary elements 1996; **18**: 137–147.

[23] Jin X., Keer L. M., Wang Q. A Closed-Form Solution for the Eshelby Tensor and the Elastic Field Outside an Elliptic Cylindrical Inclusion. ASME J. Appl. Mech. 2011; **78**(3): 031009.

[24] Jin X., Zhang X., Li Pu, Xu Z., Hu Y., Keer L. M. On the Displacement of a Two-Dimensional Eshelby Inclusion of Elliptic Cylindrical Shape. ASME J. Appl. Mech. 2017; **84**: 074501.

[25] Jirásek M. Non-local damage mechanics with application to concrete. Rev FrançGénie Civil. 2004; **8**(5,6): 683–707.

[26] Jirásek M. Non-local damage. Rev FrançGénie Civil 2007; **11**(7,8): 993–1021.

[27] Jirásek M. Non-local models for damage and fracture: comparison of approaches. International Journal of solids and structures 1998; **35**: 4133–4145.

[28] Kim S. An improved boundary distributed source method for two dimensional Laplace equations. Journal of Engineering Analysis with Boundary Elements 2013; **37**: 997–1003.

[29] Kothnur V. S., Mukherjee S., Mukherjee Yu Xie. Two-dimensional linear elasticity by the boundary node method. International Journal of Solids and Structures 1999; **36**: 1129–1147.

[30] Li S., Sauer R. and Wang G. A circular inclusion in a finite domain I. The Dirichlet-Eshelby problem. Acta Mechanics 2005; **179**: 67-90.

[31] Lin Feng-Bao, Yan Geng, Bazant Z.P. and Fangming Ding. Nonlocal strain softening model of quassi-brittle materials using boundary element method. Engineering Analysis with Boundary elements 2002; **26**: 417–424.

[32] Liu Y.J. A new boundary meshfree method with distributed sources. Journal of Engineering Analysis with Boundary Elements 2010; **34**: 914–919.

[33] Liu Q.G. and Sarler B. Improved non-singular method of fundamental solutions for two-dimensional isotropic elasticity problems with elastic/rigid inclusions or voids. Journal of Engineering Analysis with Boundary Elements 2016; **68**: 24–34.

[34] Mallardo V., Alessandri C. Arc-length procedures with BEM in physically nonlinear problems. Engineering Analysis with Boundary Elements. 2004; **28**: 547–559.

[35] Mallardo V. Integral equations and nonlocal damage theory: a numerical implementation using the BDEM. International Journal Fracture. 2009; **157**(1): 13–32.

[36] Markous N.A. Boundary mesh free method with distributed sources for 2D elasticity problems. Journal of Engineering Analysis with Boundary Elements 2019; **100**: 95–100.

[37] Mazars J. Mechanical damage and fracture of concrete structure. Proc. I.C.F.5, Cannes, France. 1981; 1499-1506.

[38] Mazars J. A description of micro- and macroscale damage of concrete structures. Engineering Fracture Mechanics. 1986; **25**(5): 729–737.

[39] McClintok F. A. Ductile rupture by the growth of holes. Journal of applied Mechanics 1968; **35**: 363–371.

[40] Mobasher M. E., Waisman H. Adaptive modeling of damage growth using a coupled FEM/BEM approach. International Journal for numerical methods in Engineering. 2016; **105**: 599–619.

[41] Mukherjee Yu Xie, Mukherjee S. The boundary node method for potential problems. Int J Numer Methods Eng 1997; **40**: 797–815.

[42] Mura, T. Micromechanics of Defects in Solids. Martinus Nijhoff publishers, 1987.

[43] Murakami S. Continuum Damage Mechanics: A Continuum Mechanics Approach to the Analysis of Damage and Fracture. Vol. 185. Springer: Berlin, 2012.

[44] Peerlings R. H. J., De Borst R., Brekelmans W. A. and De Vree J.H. R. Gradient enhanced damage for quasi-brittle materials. International Journal for numerical methods in Engineering 1996; **39**: 3391–3403.

[45] Peixoto R.G., Anacleto F.E.S., Ribeiro G.O., Pitangueira R.L.S and Penna S.S. A solution strategy for non-linear implicit BEM formulation using a unified constitutive modelling framework. Engineering Analysis with Boundary elements 2016; **64**: 295–310.

[46] Peixoto R.G., Ribeiro G.O., Pitangueira R.L.S and Penna S.S. The Strong Discontinuity Approach as a limit case of strain localization in the implicit BEM formulation. Engineering Analysis with Boundary elements 2017; **80**: 127–141.

[47] Peixoto R.G., Penna S.S., Pitangueira R.L.S., Ribeiro G.O. A non-local damage approach for the boundary element method. Applied Mathematical modelling 2019; **69**: 63–76.

[48] Pijaudier-Cabot G, and Jason Ludovic. Continuum damage modelling and some computational issues. Revue Francaise de Genie Civil. 2002; **6**: 991–1017.

[49] Pijaudier-Cabot G., and Bažant Z P. Nonlocal Damage Theory. J. Eng. Mech. Div. 1986; **113**(10): 1512-1533.

[50] Pituba J. J. C., Lacerda M. M. S. Simplified damage models applied in the numerical analysis of reinforced concrete structures. 2012.

[51] Rajgelj S., Amadio C., Nappi A. Application of Damage Mechanics Concepts to the Boundary Element Method. In Boundary Element Technology VII, ed. C. A. Brebbia & M. S. Ingber. Elsevier Applied Science. 1992; 617-634.

[52] Silva C. M., Castro L. M. S. S. Hybrid-mixed stress model for the nonlinear analysis of concrete structures. Computers and Structures. 2005; **83**: 2381–2394.

[53] Silva C. M., Castro L. M. S. S. Hybrid-mixed stress formulation using continuum damage models. Communications in Numerical Methods in Engineering. 2006; **22**: 605–617.

[54] Silva C. M., Castro L. M. S. S. Hybrid-displacement (Trefftz) formulation for softening materials. Computers and Structures. 2007; **85**: 1331–1342.

[55] Silva C. M., Castro L. M. S. S. Nonlocal damage theory in hybrid-displacement formulations. International Journal of Solids and Structures. 2009; **46**: 3516–3534.

[56] Silva C. M., Castro L. M. S. S. Continuum damage models with non-conventional finite element formulations. International Journal of Non-Linear Mechanics. 2010; **45**: 83–99.

[57] Sladek J., Sladek V., Bazant Z P. Non-local boundary integral formulation for softening damage. International Journal for numerical methods in Engineering 2003; **57**: 103–116.

[58] Timoshenko S, Goodier J, Abranson HN. Theory of Elasticity. J. Appl. Mech. 1970; **37**: 888.

[59] Wang H., Qin Qing Hua. Fundamental-solution-based hybrid FEM for plane elasticity with special elements. Computational Mechanics. 2011; **48**: 515–528.

[60] Wilczyfiski B. Shape optimization for stress reduction around single and interacting notches based on the fictitious stress method. J. Engineering analysis with boundary elements 1997; **19**: 117–128.

[61] Wu C., Yin H. The inclusion-based boundary element method (iBEM) for virtual experiments of elastic composites. J. Engineering analysis with boundary elements 2021; **124**: 245–258.

[62] Yan Fei, Jiang Quan, Bai Guo-Feng, Li Shao-Jun, Li Yun, Qiao Zhi-Bin. Dual reciprocity hybrid boundary node method for nonlinear problems. Engineering analysis with boundary elements 2019; **108**: 385–392.

[63] Yin H., Zhao Y. Introduction to the Micromechanics of Composite Materials. CRC press; 2016.

[64] Zhang Zihua, Liu Y., Dissanayake D. D., Saputra A. A., Song C. Nonlocal damage modelling by the scaled boundary finite element method. Engineering Analysis with Boundary elements. 2019; **99**: 29–45.

ARABIC SUMMARY

محتوى الرسـالة

الباب الأول : مقدمـة

يتضمن هذا الباب مراجعة على ما سبق بخصوص موضوع نمذجة التلف و نمذجة المسائل الغير المتجانسة.

الباب الثانى : الخلفية النظرية

يعرض هذا الباب مراجعة على اساليب الحل المختلفة في طريقة العناصرالحدودية (الطريقة المباشرة – الغير مباشرة و التغيريية). كذلك يتم توضيح نظرية اشيلبي للشوائب المكافئة و دمجها مع المعادلة التكاملية الحدودية المباشرة لحل المسائل الغير متجانسة. و كذلك يتم نوضيح المقصود بميكانيكا التلف كطريقة لدراسة الضعف في جساءة الوسط نتيجة التلف.

الباب الثالث : المعادلة التكاملية الحدودية الغير مباشرة فى وجود الأجزاء الغير متجانسة

يقدم هذا الباب حل المسائل ذات الأجزاء الغير متجانسة من خلال دمج طريقة الاجهادات التخيلية مع نظرية اشيلبي للشوائب الدخيلة المكافئة.

الباب الرابع : محاكة التلف فى المعادلة التكاملية الحدودية المباشرة

يقدم هذا الباب النموذج المقترح لمحاكاة التلف من خلال دمج نظرية اشيلبي للشوائب الدخيلة المكافئة مع المعادلة التكاملية الحدودية المباشرة مع حل بعض الأمثلة لتوضيح صلاحية الأسلوب المقترح لنمذجة التلف.

الباب الخامس : محاكة التلف فى المعادلة التكاملية الحدودية التغييرية

يقدم هذا الباب نمذجة التلف باستخدام طريقة العناصر الحدودية التغييرية حيث يتم الاستفادة من دقة الطريقة مقارنة بالعناصر المحدودة من خلال تقسيم الوسط بعناصر كبيرة نسبيا مقارنة بما يتم عمله في العناصر المحدودة.

الباب السادس: الخلاصة والاستنتاجات

يلخص هذا الباب ما تم انجازه في البحث و الأستنتاجات و كذلك الموضوعات المستقبلية.

ملخص الرسـالة

هذه الرسالة مقسمة الى ثلاثة اجزاء:

في الجزء الأول يتم دمج نظرية اشيلبي للشوائب الدخيلة المكافئة مع طريقة الاجهادات التخيلية – كطريقة لا تحتاج الى تقسيم – لعمل نمذجة للمسائل الغير متجانسة. طريقة الاجهادات التخيلية تعتبر احدى طرق العناصر الحدودية الغير مباشرة. المسئلة يتم حلها من خلال تقسيمها الى جزء متمم و جزء خاص. الجزء الخاص يتم الحصول عليه من خلال نظرية اشيلبي. و عليه الجزء المتمم تحصل عليه من خلال طريقة الاجهادات التخيلية. تم هنا استخدام الحل التحليلي لنمذجة الشوائب الدخيلة الدائرية التي استخدمناها في الحل. في هذه الطريقة لا يوجد نقسيم على حدوج المسئلة او داخلها. يتم حل المسئلة من خلال توزيع نقاط على حدود المسئلة و وضع نقط داخل حدود المسئلة في مركز الدوائر الممثلة للأجزاء الغير متجانسة. بالرغم من ان توزيع الاجهادات التخيلية على حدود المسئلة تم فرضها ثابت و كذلك توزيع الانفعال الذاتي داخل الشوائب الدخيلة المكافئة فان نتائج الأمثلة جيدة مقارنة مع طريقة المعادلات التكاملية الحدودية المباشرة و كذلك طريقة العناصر المحدودة كما هو مبين في الفصل الثالث.

في الجزء الثاني يتم عمل تمثيل جديد للتلف باستخدام الصيغة المباشرة للعناصر الحدودية. يتم دمج نظرية اشيلبي للشوائب الدخيلة المكافئة مع المعادلة التكاملية الحدودية المباشرة لنمذجة التغيير في خواص المادة نتيجة التلف, يتم الحصول على مصفوفة جساءة للوسط المعرض للتلف مثل التي نحصل عليها من العناصر المحدودة, مع العلم ان تلك المصفوفة يتم الحصول عليها مباشرة علي حدود الوسط. في تلك طريقة يتم تقسيم حدود الوسط فقط بالرغم من وجود اجزاء تالفة في الوسط. نظام المعادلات الغير خطي الناتج يتم حله باستخدام طريقة القاطع و يتم اعتبار الحمل هو المتحكم. العديد من المسائل تم حلها لتوضيح صلاحية الطريقة المقترحة كما هو مبين في الفصل الرابع.

في الجزء الثالث يتم مراجعة نموذج التلف في طريقة العناصرالمحدودة. يتم بعدها مناقشة المعادلة التكاملية الحدودية التغيرية حيث يتم عمل مصفوفة جساءة مكافئة لما يتم عملة في العناصر المحدودة و التي استخدمناها في نموذج التلف. المعادلة التكاملية الحدودية التغيرية تعطي القدرة لاستخدام

عناصرذات ابعاد كبيرة نسبيا مقارنة بالعناصر المحدودة التقليدية. تبين الأمثلة في الفصل الخامس ان نتائج الطريقة جيدة بالرغم من استخدام عناصر ذات الأبعاد الكبيرة.

نمذجة ميكانيكا التلف باستخدام شوائب اشيلبي الدخيلة

إعداد
مهندس / محمد أحمد كمال عبد الخالق أحمد سليمان

رسالة مقدمة إلى كلية الهندسة بشبرا ، جامعة بنها
كجزء من متطلبات الحصول على درجة دكتوراه الفلسفة
في الرياضيات الهندسية

يعتمد من لجنة الممتحنين: التوقيع

أ.د. محمد سعد متبولي ----------
أستاذ الرياضيات الهندسية (ممتحن خارجيا)
قسم الفيزياء و الرياضيات الهندسية
وكيل الكلية لشؤون الدراسات العليا
كلية الهندسة - جامعة الزقازيق

أ.د. مصطفى أحمد معوض عابدين ----------
أستاذ الميكانيكا الهندسية (ممتحن خارجيا)
رئيس قسم الرياضيات و الفيزيقا الهندسية
كلية الهندسة - جامعة القاهرة

أ.د. يوسف فوزى راشد ----------
أستاذ تحليل وميكانيكا الانشاءات (مشرف رئيسيا و مقررا)
قسم الهندسة الانشائية
كلية الهندسة - جامعة القاهرة

التاريخ :----------

كلية الهندسة بشبرا ، جامعة بنها
جمهورية مصر العربية
2021

نمذجة ميكانيكا التلف باستخدام شوائب اشيلبي الدخيلة

إعداد

مهندس / محمد أحمد كمال عبد الخالق أحمد سليمان

بكالوريوس الهندسة المدنية (مرتبة الشرف) 2005 – كلية الهندسة بشبرا- جامعة بنها

ماجستير في الرياضيات الهندسية 2015 – كلية الهندسة بشبرا – جامعة بنها

رسالة مقدمة إلى كلية الهندسة بشبرا ، جامعة بنها

كجزء من متطلبات الحصول على درجة دكتوراه الفلسفة

في الرياضيات الهندسية

تحت إشراف

أ.د. عبدالرحمن سعد (رحمه الله)

أستاذ الرياضيات الهندسية (متفرغ)

كلية الهندسة بشبرا

جامعة بنها

أ.د. يوسف فوزى راشد

أستاذ تحليل وميكانيكا الانشاءات

كلية الهندسة

جامعة القاهرة

د. طه حسين عبد الله أبوالنجا

مدرس بقسم الرياضيات و الفيزيقا الهندسية

كلية الهندسة بشبرا

جامعة بنها

د. أحمد فادي محمود فريد

مدرس بقسم الهندسة الانشائية

كلية الهندسة

جامعة القاهرة

كلية الهندسة بشبرا ، جامعة بنها

جمهورية مصر العربية

2021

نمذجة ميكانيكا التلف باستخدام شوائب اشيلبي الدخيلة

إعـداد
مهندس / محمد أحمد كمال عبد الخالق أحمد سليمان

رسـالة مقدمة إلى كلية الهندسـة بشبرا ، جامعة بنها
كجزء من متطلبات الحصـول على درجة دكتوراه الفلسفة
في الرياضيات الهندسية

كلية الهندسـة بشبرا ، جامعة بنها
جمهورية مصر العربية
2021